LBL-33313

A Search for Evidence of Nonlinear Elasticity in the Earth

Thomas M. Daley, John E. Peterson, Jr, and Thomas V. McEvilly

Earth Sciences Division
Lawrence Berkeley Laboratory
University of California
Berkeley, California 94720

December 1992

This work was supported by the Director, Office of Energy Research, Office of Basic Energy Sciences, Engineering and Geosciences Division, of the U.S. Department of Energy under Contract No. DE-AC03-76SF00098.

Introduction

When studying elastic wave propagation in the earth, a number of assumptions are usually made. Among the standard assumptions made in elastic wave theory is the linearity of rock material properties at the strain amplitudes of seismic waves. Stress and strain are assumed to be linearly related (Hooke's Law) so that elastic moduli (e.g. λ and μ) do not vary with the strains of the waves. If this linearity assumption is not true, there could be observable effects of nonlinearity in recorded seismic data, both natural source (earthquake) and man-made source. The theory of nonlinear elastic wave propagation has been known for over 40 years, with the original work in underwater acoustics and materials science (Hughes and Kelly, 1953, Jones and Kobett, 1963, Westervelt, 1963, Muir and Willette, 1972). This work continues, focused largely on materials more homogeneous than the earth and at strain levels generally larger than those of seismic waves.

Attempts to observe nonlinear elasticity in seismic wave propagation have been made in recent years (e.g. Beresnev, et. al. 1986, Johnson et. al. 1987, Bonner, 1989 Nikolaev, 1989). The sought-after nonlinear effects include harmonic distortion of a mono-frequency wave and nonlinear superposition of two waves of differing frequencies (leading to the generation of sum and difference frequencies). Most recent work has focused on laboratory measurements in rock samples, and there has been no definitive publication of nonlinear wave propagation in situ in rocks of the earth. Because LBL research has involved crustal seismic experiments over a wide range of scales (from ~10 m to ~10 km), there exists an excellent data base from which we can draw appropriate experimental data. In mid 1991, after reviewing the work of Johnson and Bonner and Shankland, we proceeded to use in-house data in a search for effects of nonlinear elasticity. The data sets selected include seismic reflection profiles from the Tehachapi Mountains area of California and seismic wave monitoring data from the Parkfield earthquake prediction experiment. In addition, we conducted one field experiment explicitly for detection of nonlinear wave propagation in conjunction with a previously planned Vertical Seismic Profile (VSP) at the Dept. of Energy's Nevada Test Site (NTS), and we analyzed a special data set acquired recently by Los Alamos National Lab (LANL) in West Texas in an attempt to verify nonlinear wave propagation during a seismic reflection profile. These data sets used Vibroseis energy sources which allowed analysis of time-separated frequency-domain data (as opposed to explosive energy sources which generate all frequencies simultaneously).

This report summarizes the results of our analysis of these data sets, which cover a range of scales and a variety of crustal materials. The nonlinear effects on which we focused our search are the generation of harmonic energy during propagation of a single wave-train, and the generation of difference-frequency energy during the interaction of two seismic waves. All experimental results here are from a complex system of one or more seismic sources, material along the propagation path, sensors, recording equipment, and data processing algorithms. Each part of this system may produce effects similar to nonlinear elastic wave propagation. Because of this, we seek multiple positive indications of material nonlinearity from various sources, receivers and recording equipment, as well as results which could be logically confined to the propagation material. Our analyses of the various studies are grouped by the two effects we looked for, variation of harmonic ratios, and generation of energy at a difference frequency.

Measurement of Harmonic Ratios

Introduction

For a seismic wave of fixed frequency, the changing ratio of harmonic amplitude to fundamental amplitude with distance can indicate nonlinear propagation. To determine what to expect of this ratio with distance, we consider two waves, A^a and A^b with differing frequencies, propagating in the x direction with initial amplitudes A^0_a and A^0_b;

$$A^a = A^0_a e^{-\alpha_a x} \qquad A^b = A^0_b e^{-\alpha_b x},$$

where α is exponential decay constant for a plane wane. The amplitude ratio of the two waves is

$$\frac{A_b}{A_a} = \frac{A^0_b}{A^0_a} \frac{e^{-\alpha_b x}}{e^{-\alpha_a x}}$$

$$= \frac{A^0_b}{A^0_a} e^{(\alpha_a - \alpha_b)x}$$

For attenuation independent of frequency, ($\alpha_a = \alpha_b$) and

$$\frac{A_b}{A_a} = \frac{A^0_b}{A^0_a}$$

and the amplitude ratio will be constant. Further, since

$$\alpha = \frac{\pi f}{Qv}$$

where Q is the seismic attenuation quality factor and v is wave velocity, Q is proportional to frequency. If Q is independent of frequency, then

$$\frac{\alpha_a}{\alpha_b} = \frac{f_a}{f_b}$$

and

$$\frac{A_b}{A_a} = \frac{A_0^b}{A_0^a} e^{\alpha_a (1 - \frac{f_b}{f_a}) x},$$

so that $\frac{A_b}{A_a}$ will decrease if $f_b > f_a$. For harmonic ratios we use the fundamental frequency for f_a and and the first harmonic for f_b and we call the ratio B/A.

Tehachapi data

The data we analyzed first are from a single shot gather in a Vibroseis reflection survey conducted by CALCRUST in the Tehachapi Mountains. We investigated the change in harmonic amplitude ratio (B/A) as a function of distance over the frequency range of the Vibroseis sweep (8 to 32 Hz) and its harmonics (up to the 62.5 Hz anti-alias filter corner frequency limitation). Because the source sweeps a range of frequencies over a period of time, the direct wave for each frequency arrives at a unique time. This source generated frequency is hereafter called the fundamental. The method used is to perform an FFT (Fast Fourier Transform) on the data in a time window centered at the arrival time of the direct wave at a particular frequency. The time is determined by summing the P-wave arrival time on the correlated trace, and the time from the beginning of the sweep to the time when that particular frequency occurs in the sweep. For the Tehachapi data, the sweep length is 32 s and the sweep rate is 1.33 s/Hz (3/4 Hz/s), beginning at 8 Hz. This means, for example, the 18 Hz fundamental is generated 13.33 s after the sweep onset, while the 18 Hz first harmonic of 9 Hz is generated only 1.33 s after sweep onset. The FFT amplitudes of the fundamental and harmonics are tabulated at each offset and harmonic ratios are taken up to the fourth harmonic. The tabulated data show that the harmonics attenuate with distance approximately the same as the fundamental (eg. Figure 2a). The behavior of the average of all fundamental amplitudes also matches that of all harmonics (Figure 3). If these harmonics are being generated at the source or in the earth material, this somewhat surprising observation implies that Q is linearly proportional to frequency, so that the amplitude ratio A_b/A_a is constant over distance for each frequency (Figures 2a-2d). Another possible explanation is that the harmonics are generated at the receiver or in recording/analysis, but this equipment has harmonic distortion ratings of about -60 db or more.

Amplitude changes that occur at specific offset sites appear to be receiver dependent for each frequency. Figure 4 shows the amplitudes at each offset of the 20 and 24 Hz fundamentals ratioed with the 20 and 24 Hz first harmonics of 10 and 12 Hz. The ratios show very similar behavior (Figure 4c). A comparison of Figures 4c and 2 shows the amplitude behavior for waves of a particular frequency

to be less variable than the behavior of harmonics and their fundamental.

The Tehachapi data do not suggest nonlinearity of the material, but rather a Q proportional to frequency (spatial attenuation factor independent of frequency). Nonlinearity is implicit in the presence of the harmonics, undoubtedly due to the inherent nonlinearity of the vibroseis source. If the earth were nonlinear, the harmonics would gain energy with continued propagation at short offsets, as more of the energy at the fundamental frequency is converted into harmonics. There is no indication of this phenomenon in the data.

NTS Walk-away

Data from a walk-away VSP were acquired at NTS. The geometry featured a stationary receiver at 400 ft depth in a borehole, recorded vibroseis sweeps from 7 source locations at offset distances of 400 ft, 600 ft, 800 ft, 1000 ft, 1200 ft, 1400 ft, and 1600 ft from the borehole. Three drive levels, 15%, 50% and 85% of maximum, were used for the vibrator at each source location, giving 3 strain levels of source for the same seismic wavefield. An 8-80 Hz, 12 s sweep produced a sweep rate of .1666 s/Hz. A variation in B/A with distance and/or drive level could be indicative of nonlinear behavior in the propagation medium. The correlated signals show that the waveforms, while quite different from shot points only 200 ft apart, are very repeatable when one shotpoint was reoccupied with a change in drive level (Figures 5a-5c).

Fourier Transforms of half-second windows incremented by eight-sample steps were computed as for the Tehachapi data (Figure 6). The data suffer from noise and spurious spectral peaks, particularly near 14 and 33 Hz (these are probably source or receiver resonances). Spectra for the 20, 40, 45, 50 Hz arrival times are shown at each offset and drive level in Figures 7a-7l. It is clear that the noise levels preclude definitive conclusions based on the harmonic amplitudes. The behavior of the harmonics with different drive levels does not suggest an effect due to elastic nonlinearity of the material along the propagation path. This experiment could be repeated with better conditions (e.g. reducing resonances and using a site with more consistent near-surface conditions) for more conclusive results.

LANL data - Harmonic generation

LANL scientists, with Halliburton Geophysical acquired in West Texas a set of test data using 6 vibroseis units in various source arrays and a receiver spread 17600 ft long with 110 ft sensor spacing. The vibrators were operated in a number of combinations intended to produce difference-frequency wave generation through nonlinear interaction of two primary monotonic wavefields. In one experiment with 20-sec mono-frequency sweeps, three of the sources used 13 Hz and the

other three used 23 Hz. The experiment was repeated with 31 and 43 Hz sweeps (Figures 8a-8c). For each offset, the FFT was calculated in a 4 -second window starting at the initial energy arrival. Frequency content vs. distance for the spread is shown in Figures 9a and 9b for true and normalized amplitudes. As for the Tehachapi data, the harmonics are strong, indicating nonlinear behavior in one or more of the source, the medium, or the acquisition system. Harmonic ratios, determined up to the fourth harmonic for the 13+23 Hz primary frequencies are fairly constant over distance for both frequencies (Figures 10 and 11). The ratio increases with distance for higher harmonics of 23 Hz, but this behavior is probably due to the decreasing signal-to-noise ratio with distance for the higher frequencies, causing background noise to dominate the high frequency spectrum. We can not see the signal when if falls below the noise floor. The harmonic ratio does generally increase at large positive distances, especially for the 13 Hz harmonics, but it is following the noise seen in Figure 9 (the red color represents noiser data).

Similar results were observed with a longer 12-second analysis window (Figure 12; first harmonic), and in the 31-43 Hz data (Figure 13). The spectral peaks in the 31+43 Hz data are clearer, because of their greater separation in frequency. The B/A ratio is fairly constant with distance, though noisy (Figure 14).

These observations are consistent with the Tehachapi data in failing to yield unambiguous evidence for nonlinear elastic phenomena in the wave propagation.

Parkfield Vibroseis

In a study of shear-wave propagation within the San Andreas fault zone at Parkfield, Ca, a horizontal (S-wave) vibrator is swept from 8 to 24 Hz at sites near the fault and recorded with a network of ten borehole 3-component receivers. We explored the possibility of monitoring temporal changes in B/A using this data, however we found it too noisy and sparse for such purposes.

Measurement of Difference frequency

Introduction

When the signals from two monofrequency sources interact in a nonlinear material, secondary waves at the sum and difference frequencies of the two primary waves can be produced. Our interest is primarily in the difference frequency wave which could be produced at very low frequencies (less than 5 Hz), well below the frequencies at which Vibroseis sources can produce coherent energy. Such a low-frequency source would have great promise in seismic imaging of deep crustal and mantle targets. Several data acquisition experiments were conducted in an effort to produce difference-frequency waves. One method used two sets of vibrators, each with a constant-frequency sweep, giving a single difference

frequency. In another method the two sets of vibrators had differing source sweeps, designed so that the difference frequencies represent a distinctive third linear sweep.

LANL 13-23 Hz and 31-43 Hz data

The plots of frequency vs. offset distance (Figure 9) show that if a sum or difference frequency exists, it has an amplitude far below that of the harmonics. As part of the experiment, independent data sets were also acquired for the vibrator sets, first recording data for the 3 sources at 13 Hz, then the other 3 vibrators at 23 Hz. These two data sets are summed and then compared to the simultaneously acquired data by taking a point-by-point ratio of the frequency vs. offset data (Figure 15). There is no clear evidence of either a sum or difference frequency, although the sum frequency (36 Hz) may be present in the relatively high energy near that frequency.

This procedure was repeated with 31 and 43 Hz. The 31-43 Hz data does show a significant amplitude peak (smaller than the harmonics) at the 74 Hz sum frequency (Figure 16). However, when the single frequency data are added a peak is found at 80 Hz, suggesting that a 74 Hz peak may be due to something other than material nonlinearity.

No difference frequency wave can be found in this data set. The low-frequency peak in Figure 15b is at 9 Hz, not at the expected 12 Hz difference frequency. The possible presence of the 74 Hz sum frequency represents some evidence for nonlinearity in the system.

NTS VSP Dual upsweeps, 25-76 Hz and 40-79 Hz

At NTS two vibrators were used to produce simultaneous upsweeps from 25 to 76 Hz and 40 to 79 Hz. The signals were recorded with a borehole geophone at approximately 700 ft depth. The purpose was to produce a 15-3 Hz difference-frequency downsweep from the nonlinearity of the earth. Spectral analysis of the vertical receiver component (Figure 17a) shows a small peak at about 15 Hz, about 20 dB and 3 dB, respectively, below the 40 Hz and the 25 Hz signals which would combine to produce it. Figure 17b shows the spectrum for the same trace low-pass filtered at 15 Hz. Most of the energy in this band is near 15 Hz. The analysis of this data included producing a time-frequency plot by stepping through the uncorrelated trace with a 1 second window and calculating an FFT in the window at each step. The result fo the entire bandwidth is shown if Figure 17c while the band of interest (0 to 20 Hz) is shown in Figure 17d. The result (Figure 17d) shows that the difference sweep indeed exists, though very weak and the amplitudes die out at about 8 Hz. The 14 Hz geophones used in the data acquisition

attenuate energy below 14 Hz at 12 dB/octave so we did not expect to see much energy below 7 or 8 Hz. During acquisition, we generated each up sweep individually and then both together. Figure 18 (a, b, and c) show the 3 data sets (each with 3 components) correlated with the two source sweeps and the difference sweep. The difference sweep was clear only on one of the horizontal receivers. When this component was correlated from 15 to 3 Hz, energy was seen at the expected P-wave arrival time, but with amplitudes just above the noise (Figure 18c).

NTS VSP dual crossing sweeps, 40-90 Hz and 90-40 Hz

Another experiment at NTS employed two vibroseis trucks with crossing sweeps from 40 to 90 Hz and 90 to 40 Hz, to produce a 50 to 0 to 50 Hz difference-frequency sweep. Processing as above, the time-frequency plots (Figures 19a and 19b) show difference frequencies visible to about 8 Hz. In this case, correlation for the difference sweep did not produce a clear arrival.

LANL dual crossing sweeps, 50-90 Hz and 90-50 Hz

During the LANL experiment, a 20-sec sweep shot gather was acquired from 6 vibrators assembled in a circle, nose to nose, with 3 sources using a 50 to 90 Hz sweep and the other three using 90 to 50 Hz. Unlike the NTS crossing sweep experiment, in this test the difference frequency (40-0-40 Hz) did not overlap the driving frequencies. The receiver spread was split, with 160 receivers on either side of the shot (maximum offset 17600 ft). The stacked shot gather was correlated for the difference frequencies of the crossing sweeps (40 to -40 Hz). The results show surface waves and body waves, including possible reflections consisting entirely of the difference frequencies (Figure 20). Most of the energy is produced from 25 to 40 Hz (Figure 21). The greatest interest would be for lower frequencies, but these results do show that nonlinearity exists somewhere in the system of source, propagation path and acquisition hardware.

All the experiments with dual sweeps involved 2 or more vibrators in close physical proximity. Vibrator interaction through the electronic-hydraulic feedback circuit is a known problem in reflection profiling (Okaya et al., 1992). It is quite possible that the difference frequencies are being created in the sources by complex interactions of the vibrators and their feedback systems. A definitive experiment for nonlinear elastic wave propagation must account for source and acquisition system nonlinearities.

Conclusions

We conducted the analyses described in this report because we had various data sets which we felt might show evidence of nonlinear elasticity. Our hope was to find results which could be logically tied to wave-propagation in the earth rather than data-acquisition equipment. In particular, we were (and still are) excited by the prospect of generating controlled-source, very low frequency (less than 5 Hz) seismic sources for use in deep crustal imaging. However, these initial searches for evidence of nonlinear elastic wave propagation yielded mixed results, results which warrant further experimentation, but do not provide conclusive evidence of nonlinear elasticity at strain amplitudes used in seismic exploration.

The B/A studies described here find large harmonic distortion, but the ratios do not increase with distance as they would in a nonlinear media. We conclude that the harmonics are produced at the source and propagate linearly in the subsurface material or that the harmonics are generated by the receiver or recording system after propagation. The extreme signal variation seen with receiver site raises strong doubts about any similar study using a limited number of receiver locations (e.g. Beresnev, et. al., 1986). If the harmonics are generated by the source, we find evidence for Q increasing linearly with frequency in the 8-80 Hz range. If this observation for seismic Q is true, it would contradict standard theory.

The studies searching for generation of a difference frequency give the most promising results, yet they are still inconclusive. Difference frequencies are clearly seen on the dual source crossing-sweep data from two separate experiments, but not at all on the constant-frequency data. The generation of difference-frequency sweeps is exactly the observation we would hope for since it gives us a controllable low frequency source. However the lack of difference-frequency energy from mono-frequency sources suggests that the effect may be caused by the vibrator feedback mechanism, since this feedback circuitry would be fairly passive when operating in a mono-frequency mode. These studies searching for generation of a difference frequency give the most promising results, yet they are still inconclusive since source effects may explain the difference frequency results. Practically speaking, this could be immaterial, since the results still yield a low-frequency energy source. Whatever the cause of the difference-frequency sweeps, further studies, will require use of sensors which have better response in the 0.1 to 10 Hz band.

Future investigations of nonlinear elastic wave propagation will be based more on the theoretical expectations of nonlinear elastic effects. However, the probable large nonlinear component at the source must be either eliminated or quantified before the nonlinearity in wave propagation can be extracted. We are currently exploring a range of experiments that have promise of more precise definition of elastic nonlinearity in the earth.

Acknowledgments

The authors would like to thank Don Lippert for help with acquisition of the NTS and Parkfield data, Eleni Karageorgi for help with analysis of Parkfield and Tehachapi data, and Paul Johnson for ideas and for providing the LANL vibroseis data. This work was supported by the Director, Office of Energy Research, Office of Basic Energy Sciences, Engineering and Geosciences Division of the U.S. Department of Energy under Contract No. DE-AC03-76SF00098.

References

Beresnev, I. A., A. V. Nikolayev, V. S. Solov'yev and G. M. Shalashov, *Nonlinear Phenomena in Seismic Surveying Using Periodic Vibrosignals,* Izvestiya, Earth Physics, v22, 10, 1986.

Johnson, P. A., T. J. Shankland, R. J. O'Connell and J. N. Albright, *Nonlinear Generation of Elastic Waves in Crystalline Rock* Journal of Geophysical Research, v92, B5, 1987.

Johnson, P. A. and T. J. Shankland, *Nonlinear Generation of Elastic Waves in Granite and Sandstone: Continuous Wave and Travel Time Observations,* Journal of Geophysical Research, v94, B12, 1989.

Jones, G. L., and D. R. Kobett, *Interaction of Elastic Waves in an Isotropic Solid,* Journal of the Acoustical Society of America, v35, 1, 1963.

Muir, T. G., and J. G. Willette, *Parametric Acoustic Transmitting Arrays,* Journal of the Acoustical Society of America, v52, 5, 1972.

Nikolaev, A. V., *Scattering and Dissipation of Seismic Waves in the Presence of Nonlinearity,* Pure and Applied Geophysics, v131, 4, 1989

Westervelt, P. J., *Scattering of Sound by Sound,* Journal of the Acoustical Society of America, v29, 2, 1957.

Westervelt, P. J., *Parametric Acoustic Array,* Journal of the Acoustical Society of America, v 35, 4, 1963.

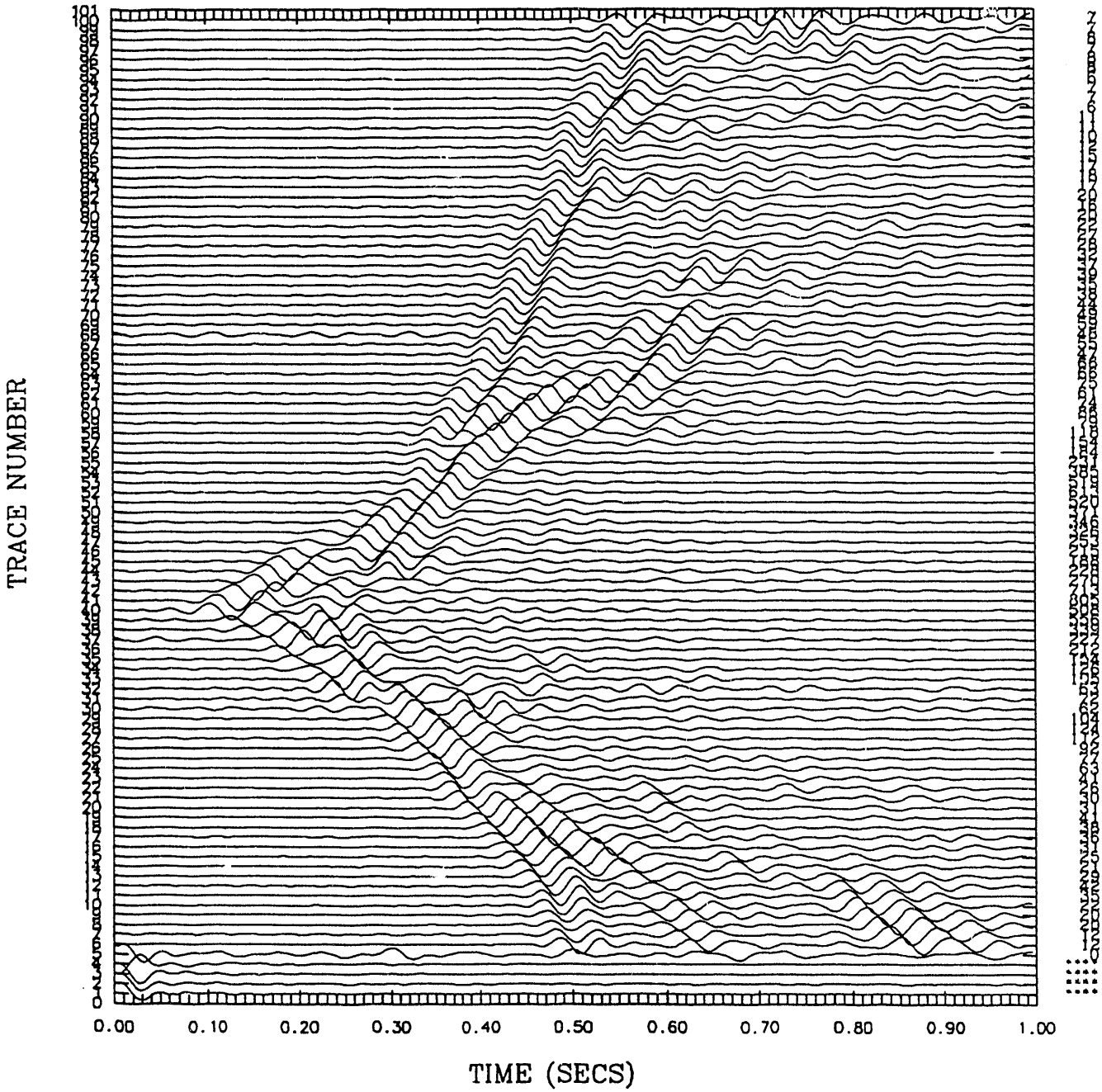

Figure 1. Correlated data traces from the Tehachapi Mountains seismic reflection profile. Each trace is plotted such that its maximum amplitude is one trace spacing. The relative maximum amplitude is printed at the end of each trace. The first 5 traces are not data.

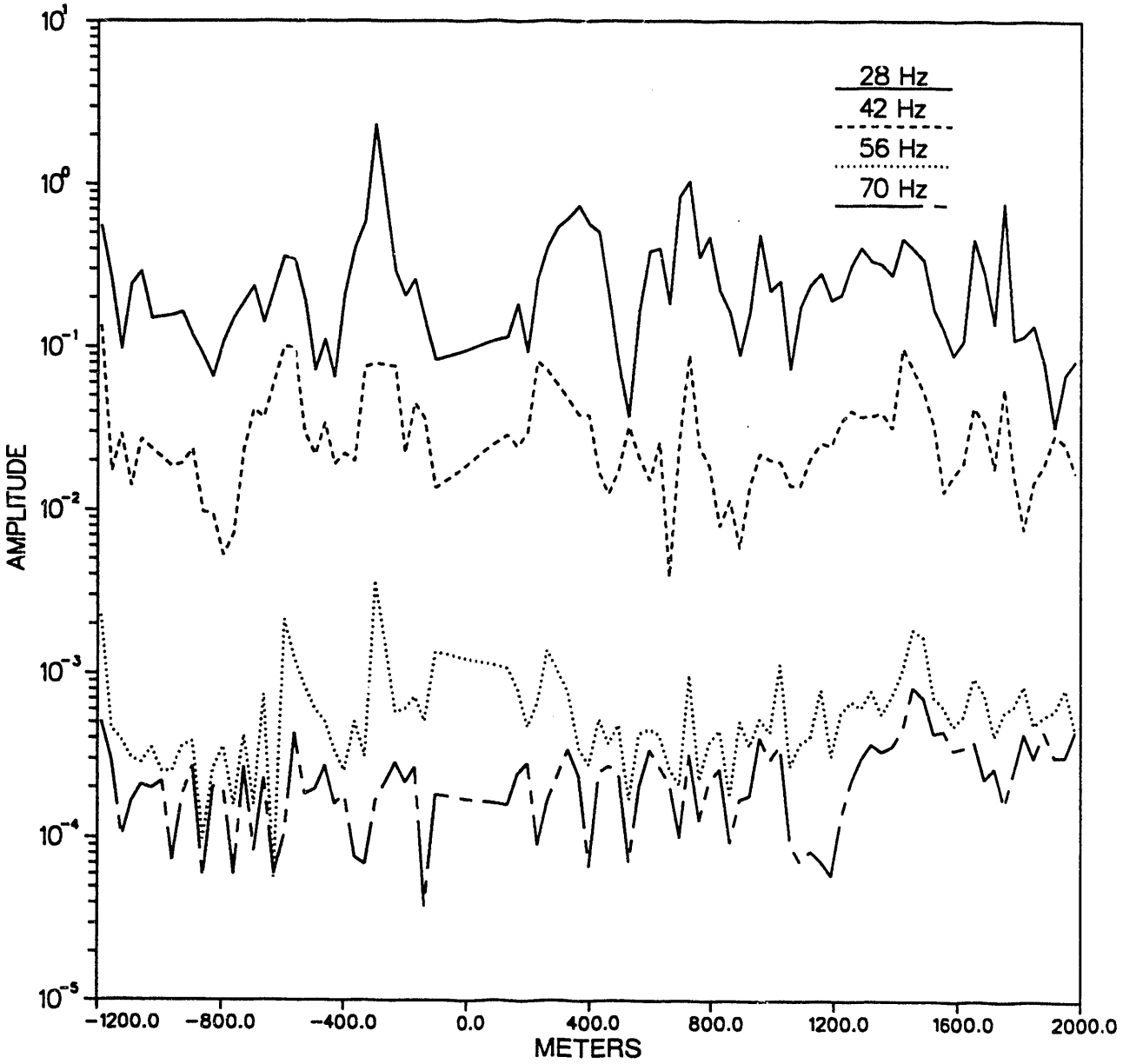

Figure 2a. Tehachapi vibroseis data. Offset distance in meters. Ratio of harmonic amplitude to 14 Hz fundamental amplitude for the first four harmonics as a function of offset distance. There does not appear to be any increase in the ratio with distance. This means that no energy is being converted from the fundamental to the harmonics as the wave propagates.

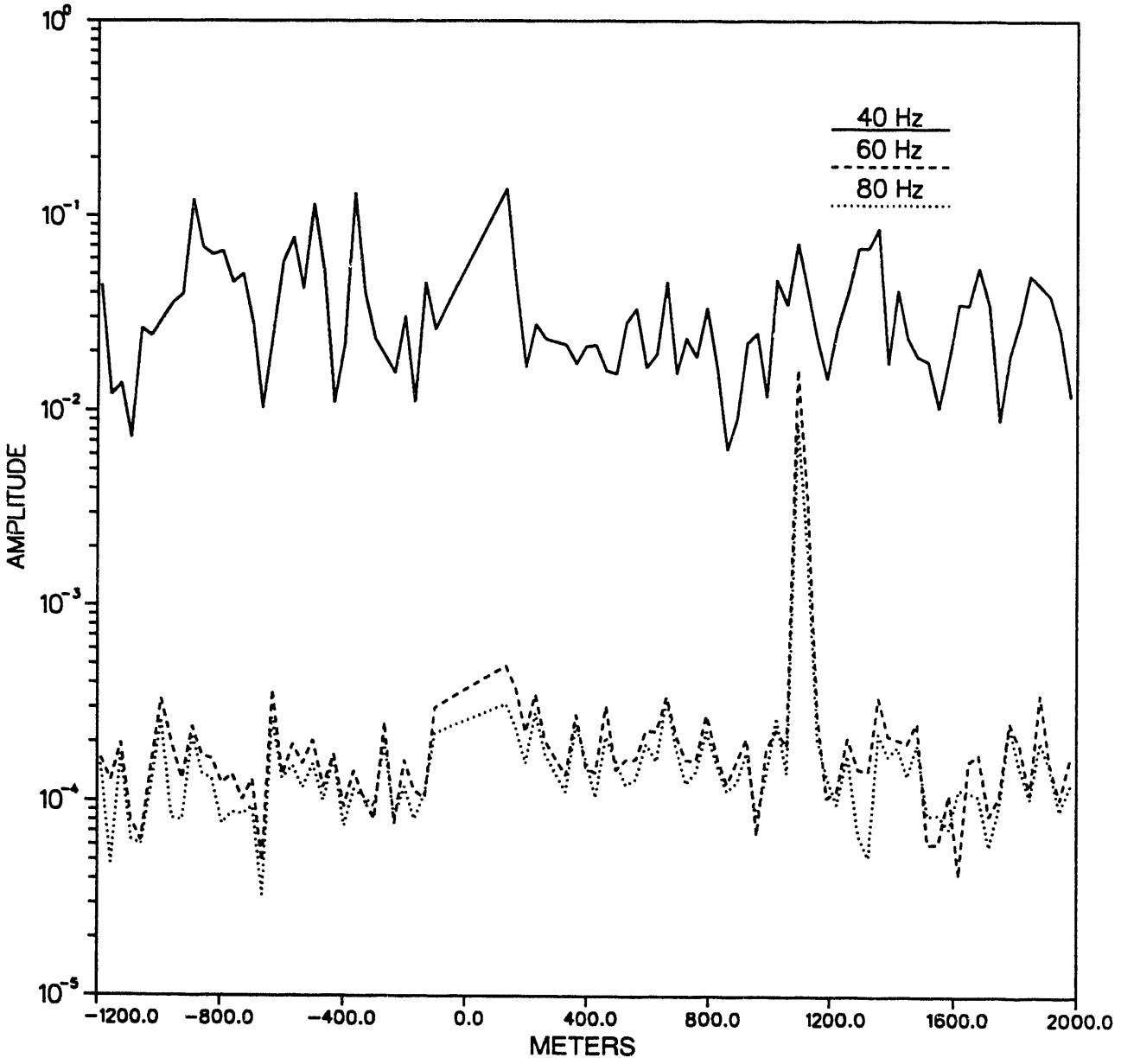

Figure 2b. Tehachapi vibroseis data. Offset distance in meters. Ratio of harmonic amplitude to 20 Hz fundamental amplitude for the first three harmonics. There does not appear to be any increase in the ratio with distance. This means that no energy is being converted from the fundamental to the harmonics as the wave propagates.

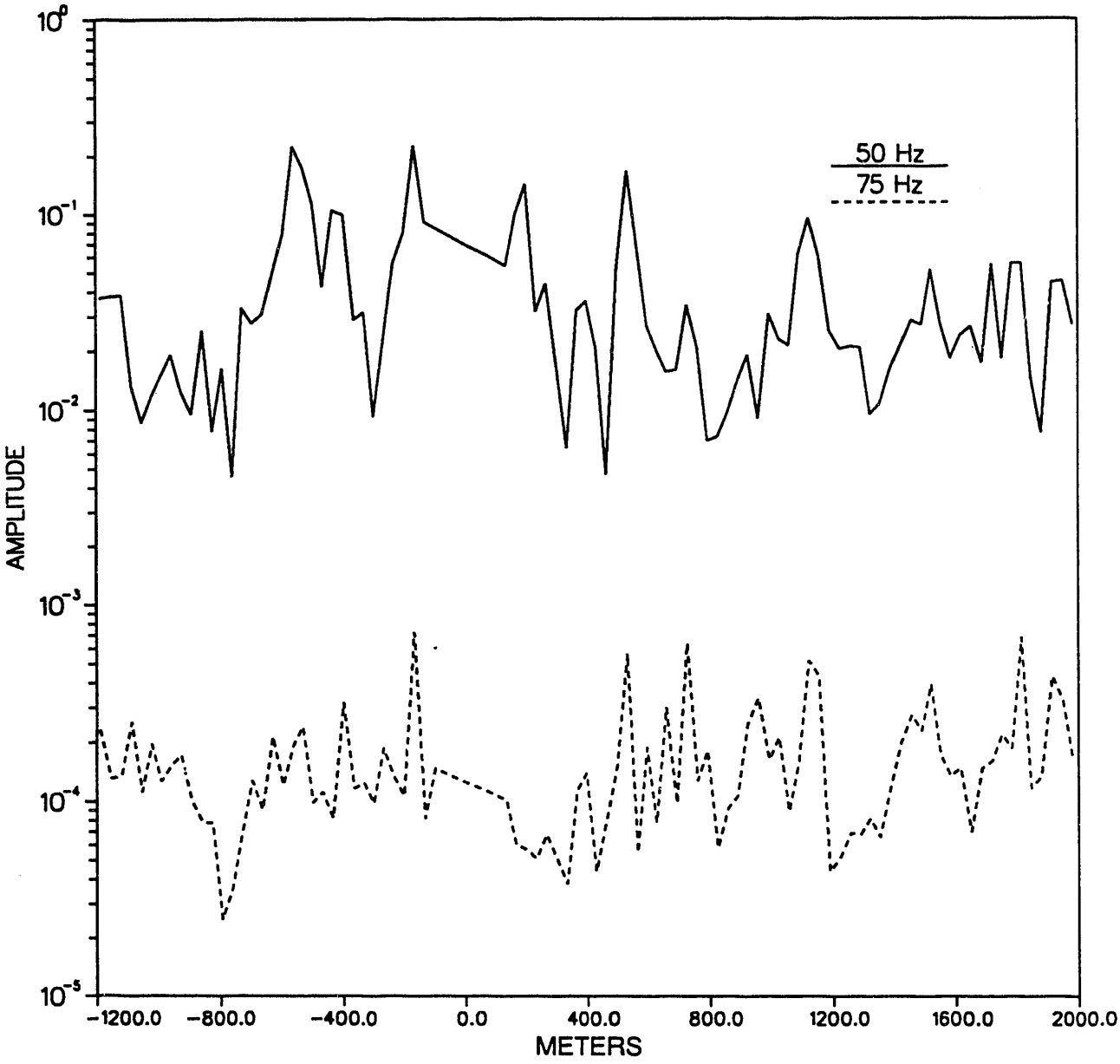

Figure 2c. Tehachapi vibroseis data. Offset distance in meters. Ratio of harmonic amplitude to 25 Hz fundamental amplitude for the first two harmonics. There does not appear to be any increase in the ratio with distance. This means that no energy is being converted from the fundamental to the harmonics as the wave propagates.

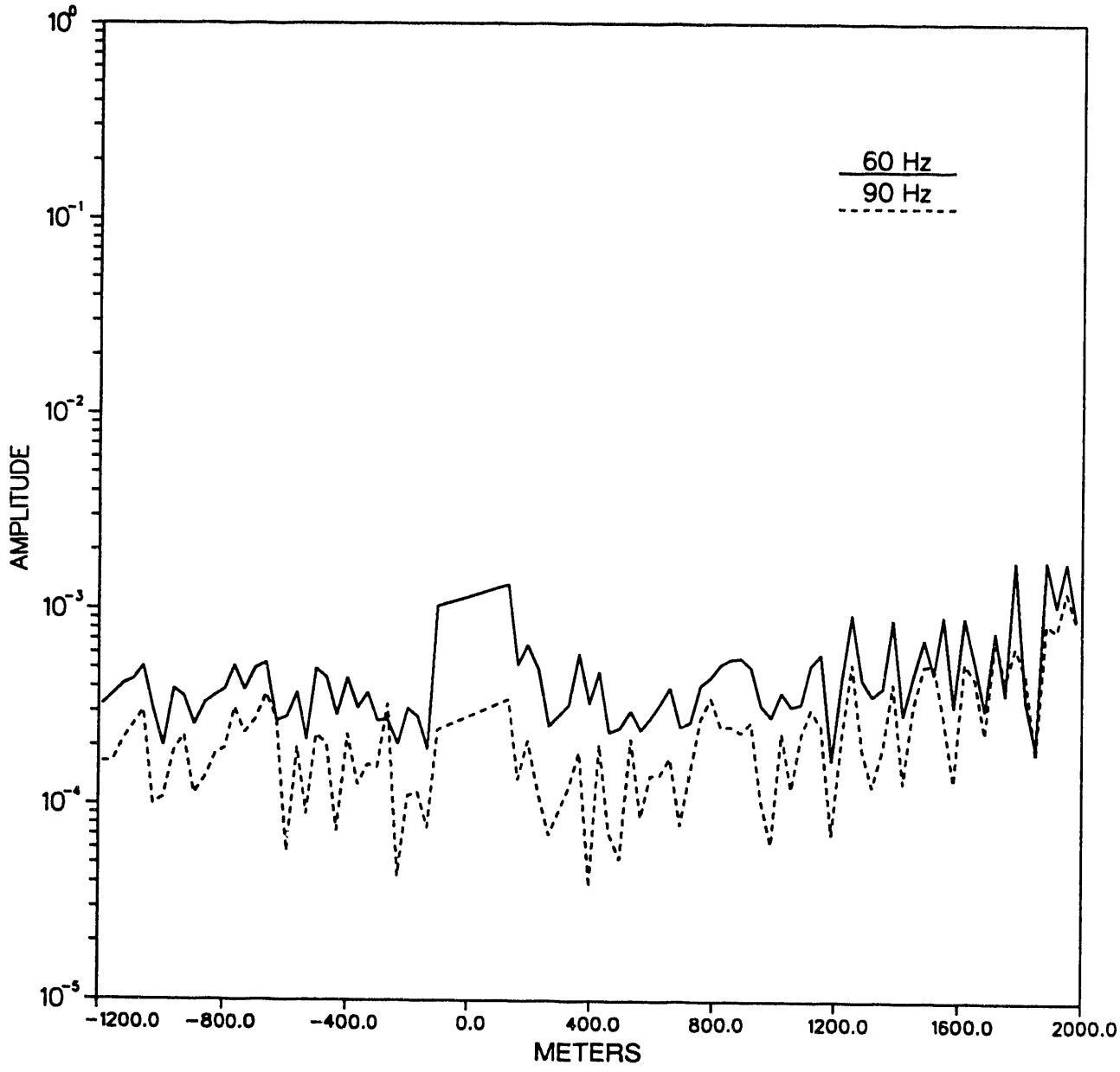

Figure 2d. Tehachapi vibroseis data. Offset distance in meters. Ratio of harmonic amplitude to 30 Hz fundamental amplitude for the first two harmonics. There does appear to be an increase in the ratio with positive distance, however we interpret this to be a result of background noise rather than non-linear propagation (see text).

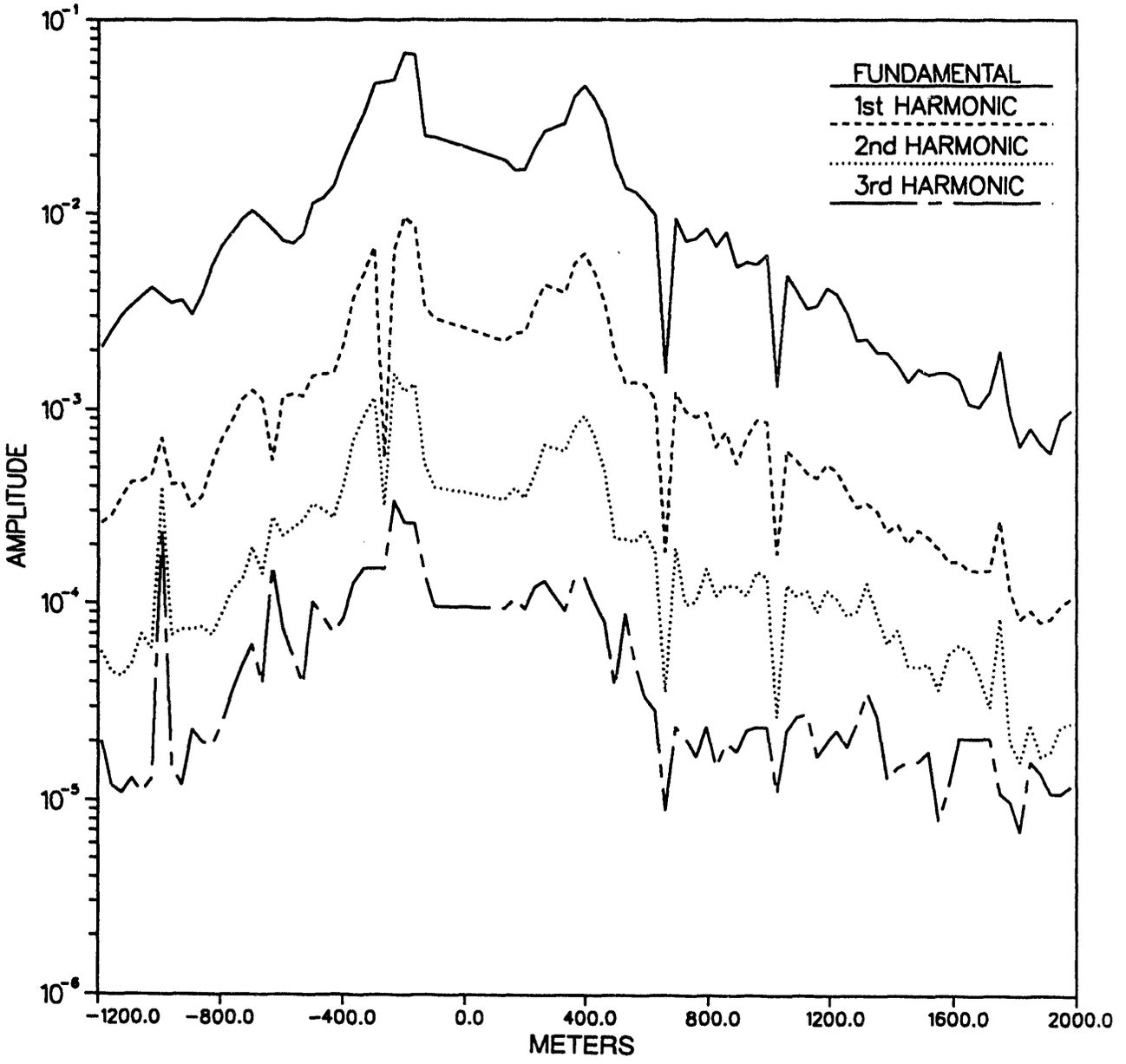

Figure 3. Tehachapi vibroseis data. Offset distance in meters. Ratio of harmonic amplitude to fundamental amplitude, averaged for the data in Figures 2a, 2b, 2c and 2d. Note the consistent spectral character as a function of distance for each curve. There does not appear to be any increase in the ratio with distance. This means that no energy is being converted from the fundamental to the harmonics as the wave propagates.

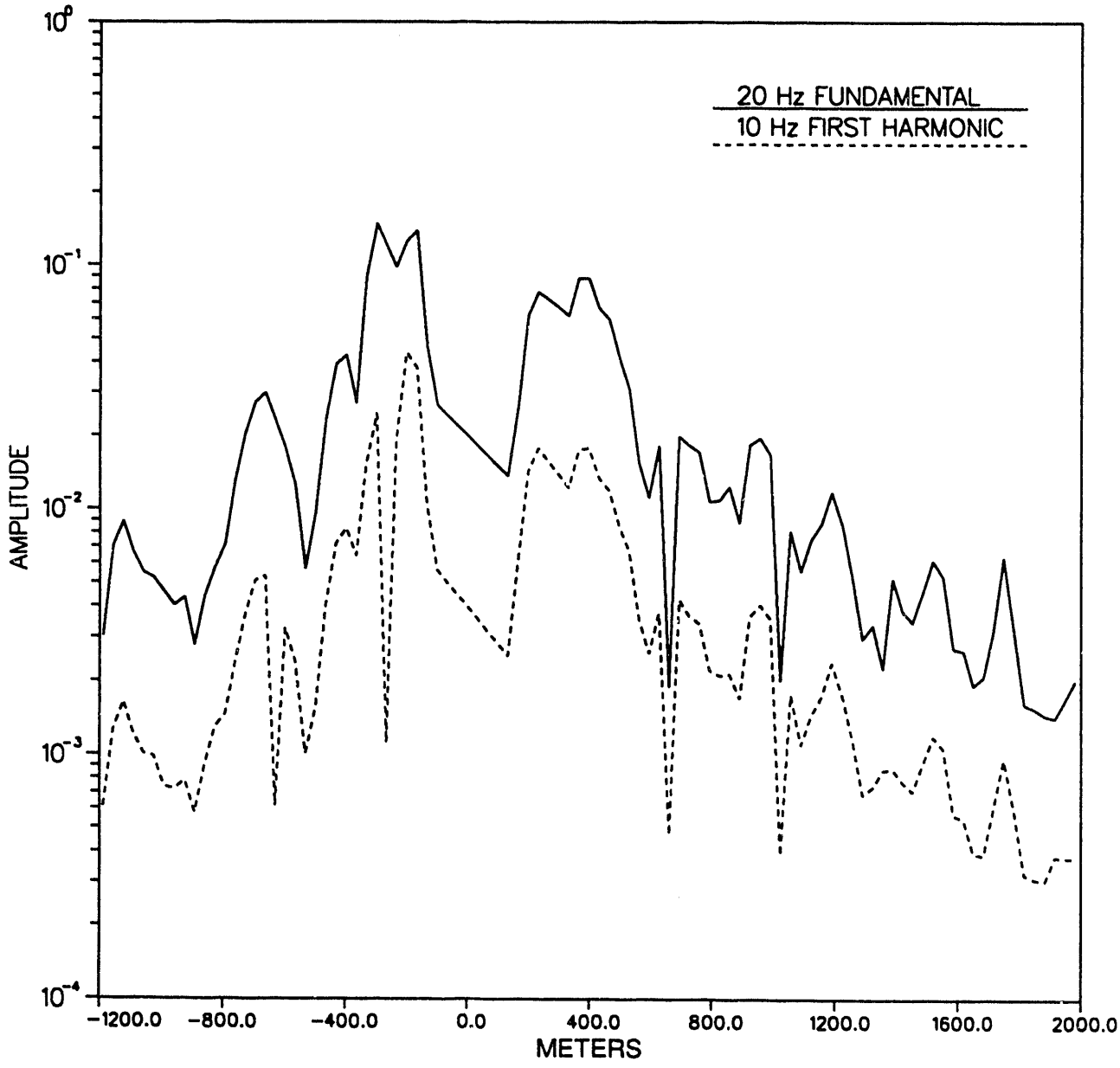

Figure 4a. Tehachapi vibroseis data. Offset distance in meters. Amplitude versus distance for the 20 Hz fundamental (20 Hz generated by the vibrator) and for the 20 Hz harmonic of the 10 Hz fundamental (10 Hz generated by the vibrator). These two 20 Hz signals show nearly identical curves, indicating that the receiver site response is the dominant effect.

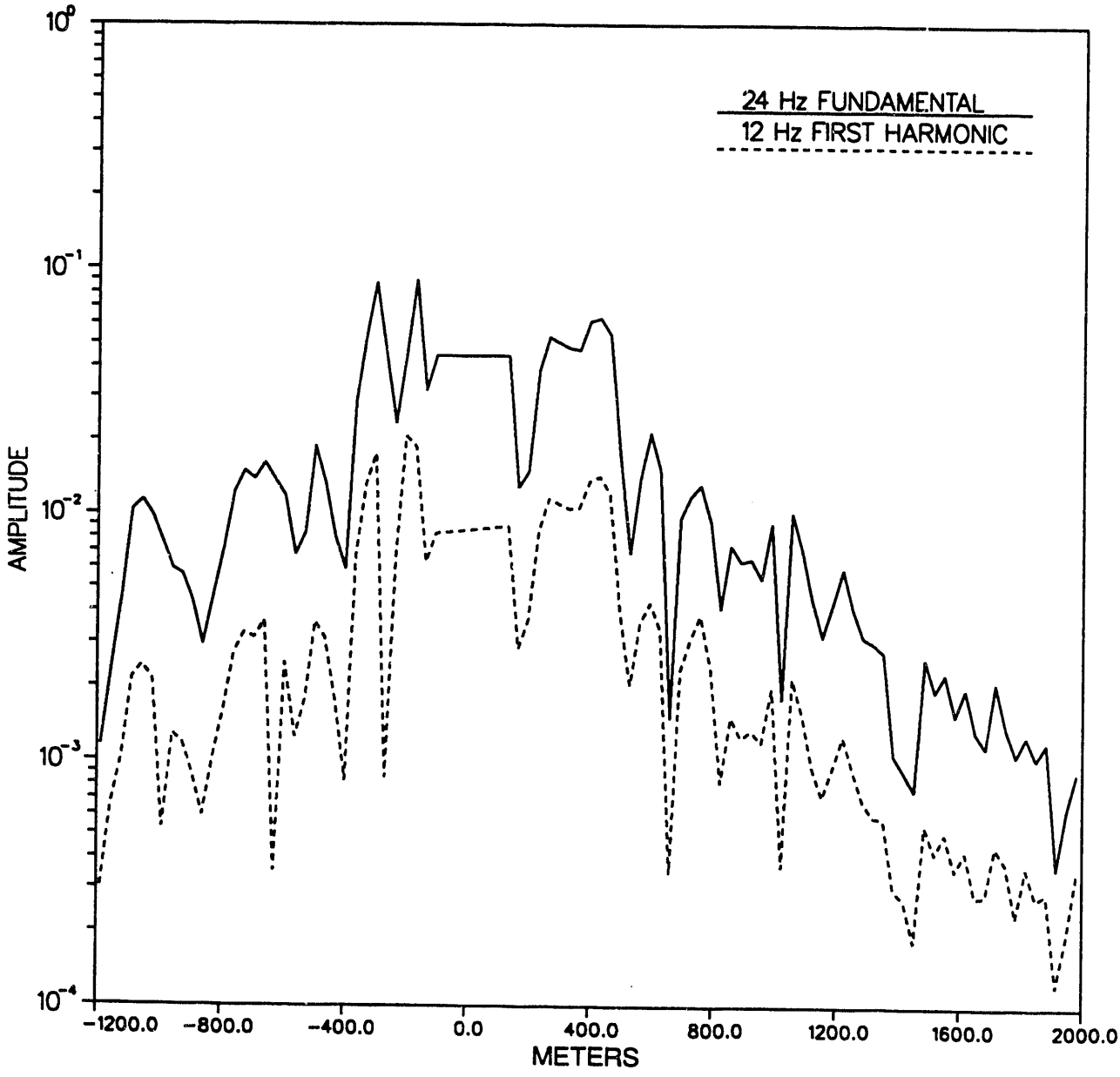

Figure 4b. Tehachapi vibroseis data. Offset distance in meters. Amplitude versus distance for the 24 Hz fundamental (24 Hz generated by the vibrator) and for the 24 Hz harmonic of the 12 Hz fundamental (12 Hz generated by the vibrator). These two 24 Hz signals show nearly identical curves, indicating that the receiver site response is the dominant effect.

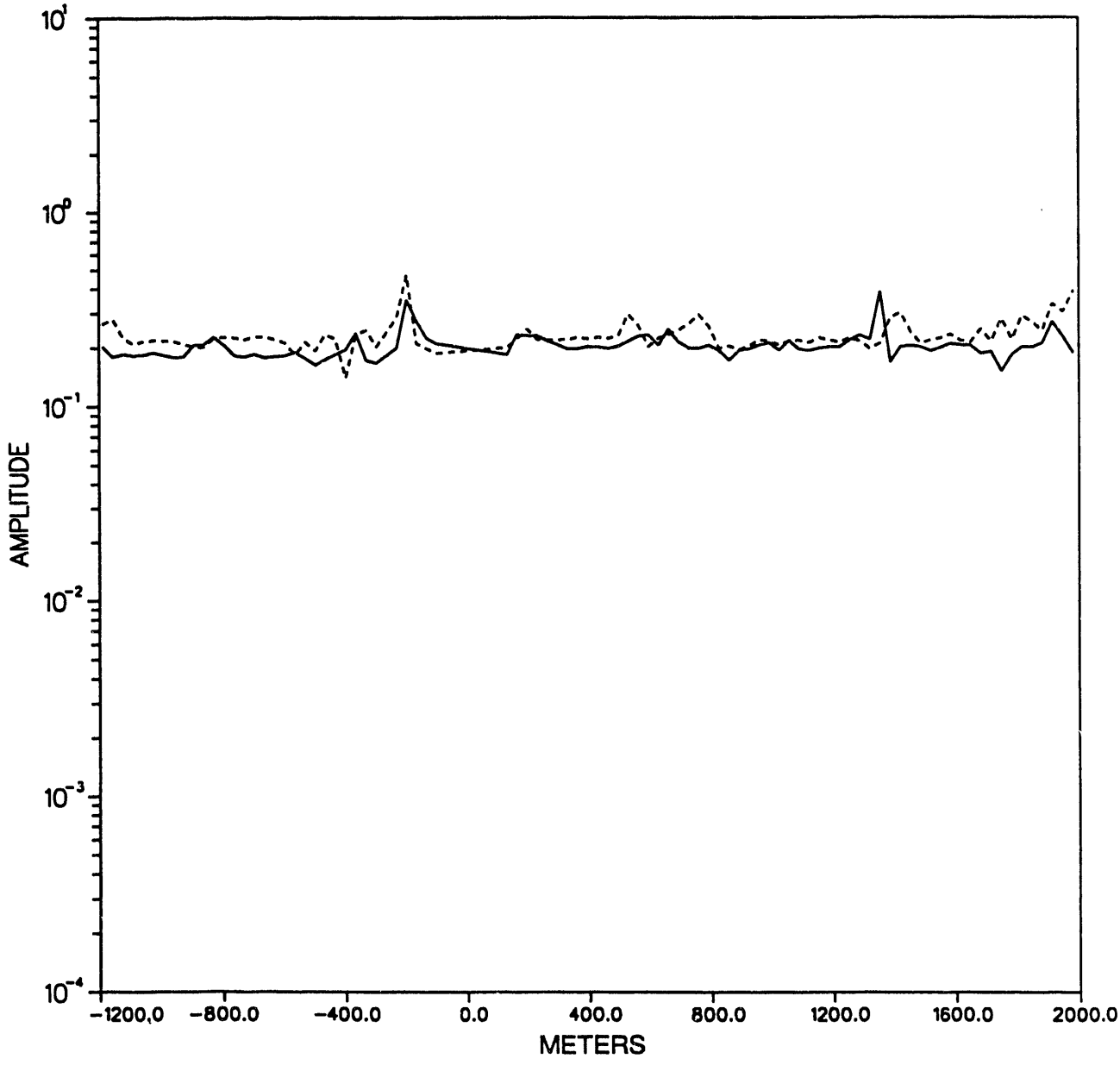

Figure 4c. Tehachapi vibroseis data. Offset distance in meters. Amplitude ratio of 20 Hz fundamental to 20 Hz harmonic of 10 Hz fundamental (solid line), and the ratio of 24 Hz fundamental to the 24 Hz harmonic of 12 Hz fundamental (dashed line). Note that the ratio with does not change with offset distance, indicating that the harmonics do not gain energy with propagation.

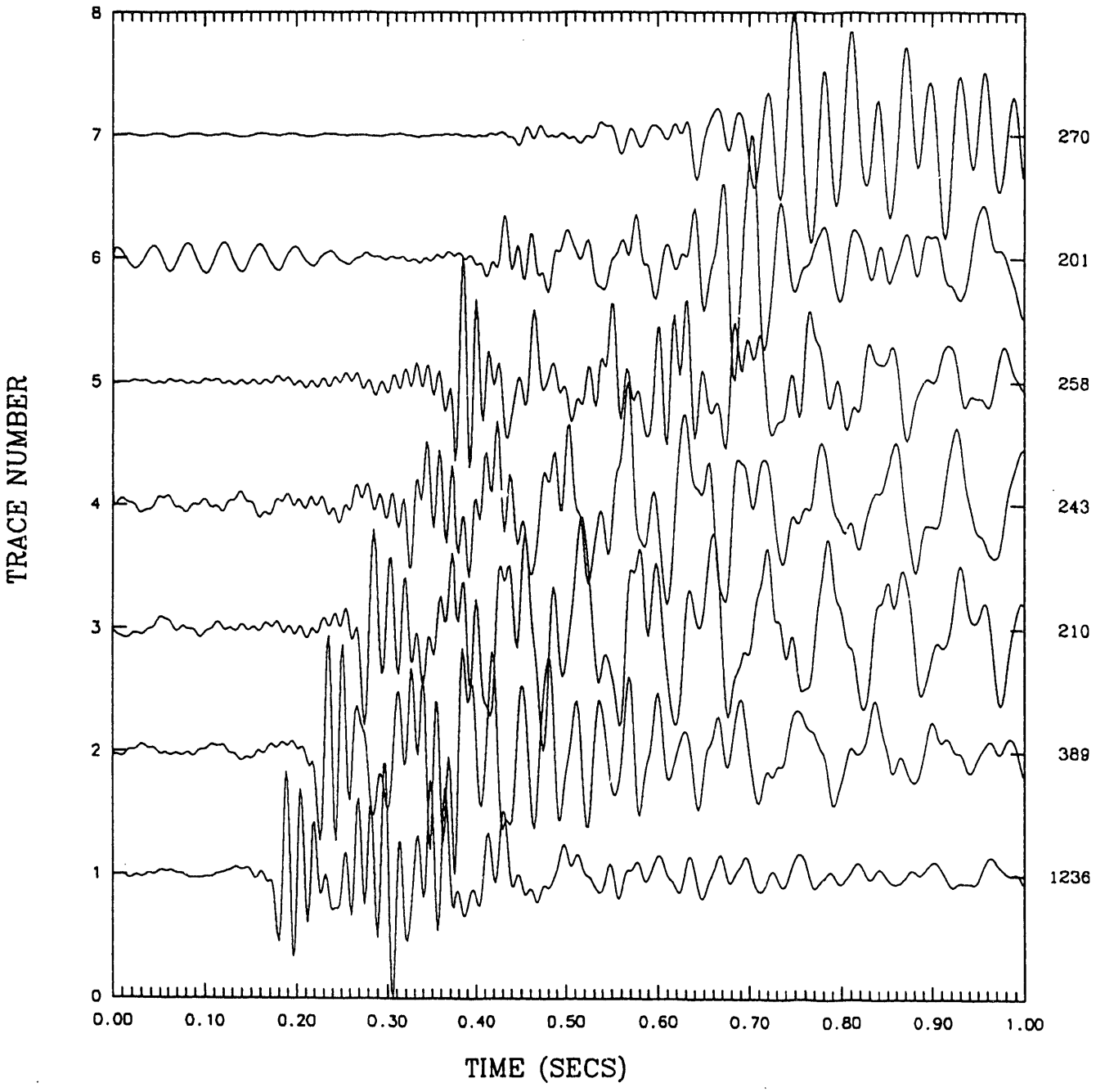

Figure 5a. Correlated data traces from the NTS walk-away VSP experiment. The vibrator was at 85% output. Traces 1 through 7 are, respectively, 400 to 1600 ft source offset at 200 ft increment. The traces are plotted with the maximum amplitude having the same height for each trace. The relative amplitudes are written at the end of each trace. The receiver was at 400 ft depth. Note the variation in waveform with increasing offset.

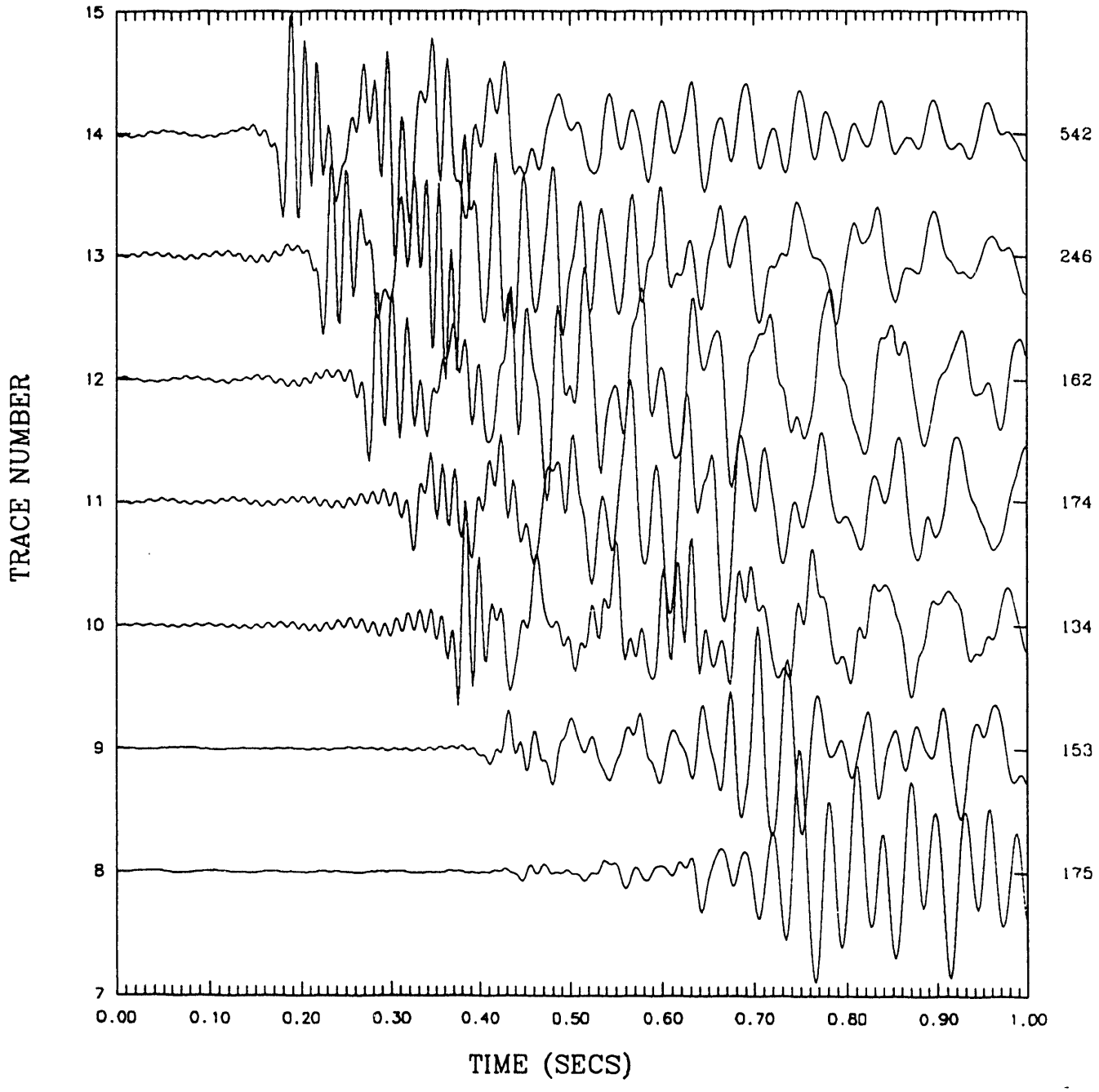

Figure 5b. Correlated data traces from the NTS walk-away VSP experiment. The vibrator was at 50% output. Traces 8 through 14 are, respectively, 1600 ft to 400 ft source offsets at 200 ft increment. The traces are plotted with the maximum amplitude having the same height for each trace. The relative amplitudes are written at the end of each trace. The receiver was at 400 ft depth. Note the variation in waveform with increasing offset.

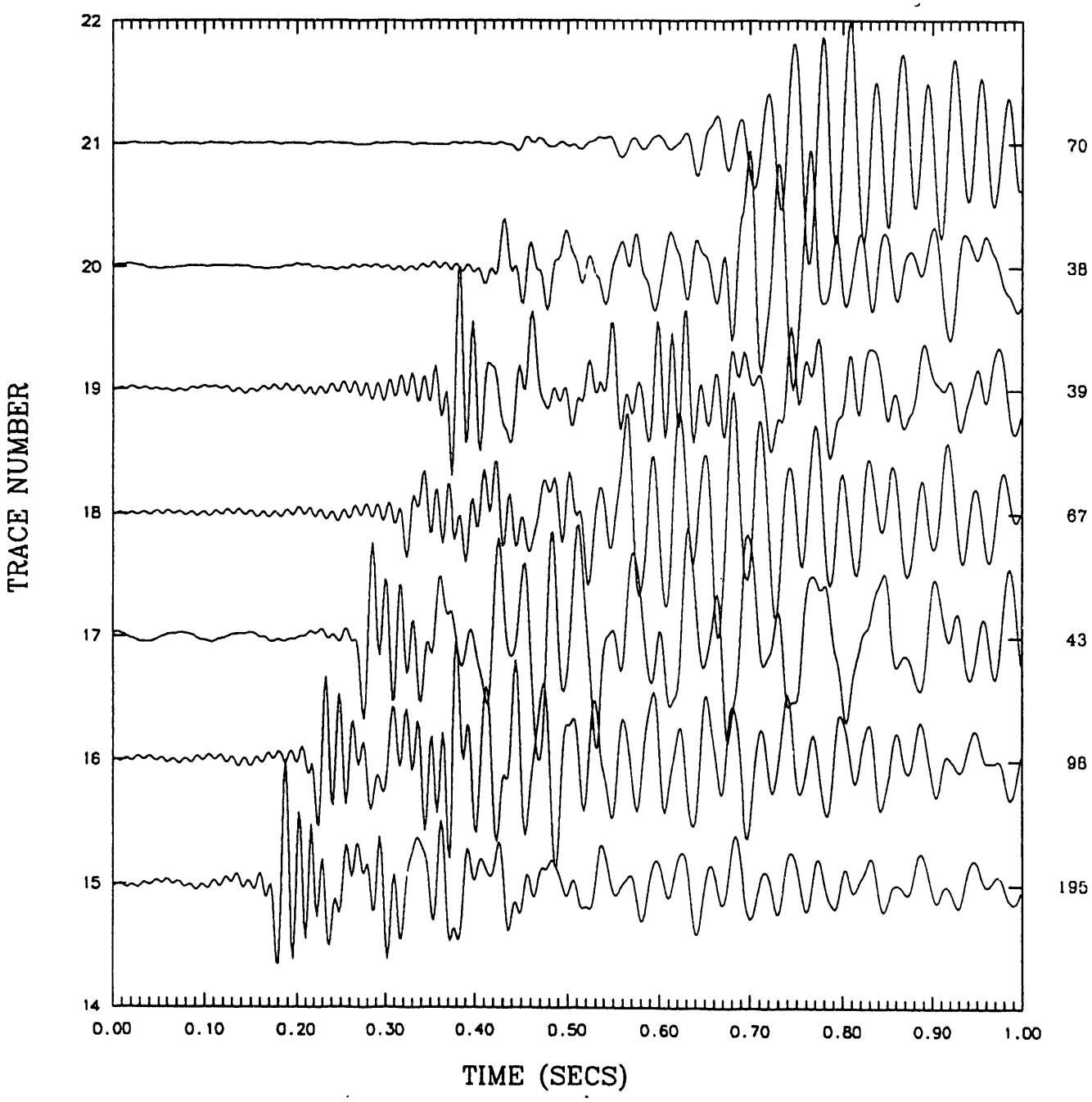

Figure 5c. Correlated data traces from the NTS walk-away VSP experiment. The vibrator was at 15% output. Traces 15 through 21 are 400 ft to 1600 ft source offset at 200 ft increment. The traces are plotted with the maximum amplitude having the same height for each trace. The relative amplitudes are written at the end of each trace. The receiver was at 400 ft depth. Note the variation in waveform with increasing offset. By comparing 5a, 5b and 5c, we see that source location has a larger effect on waveform than source strength.

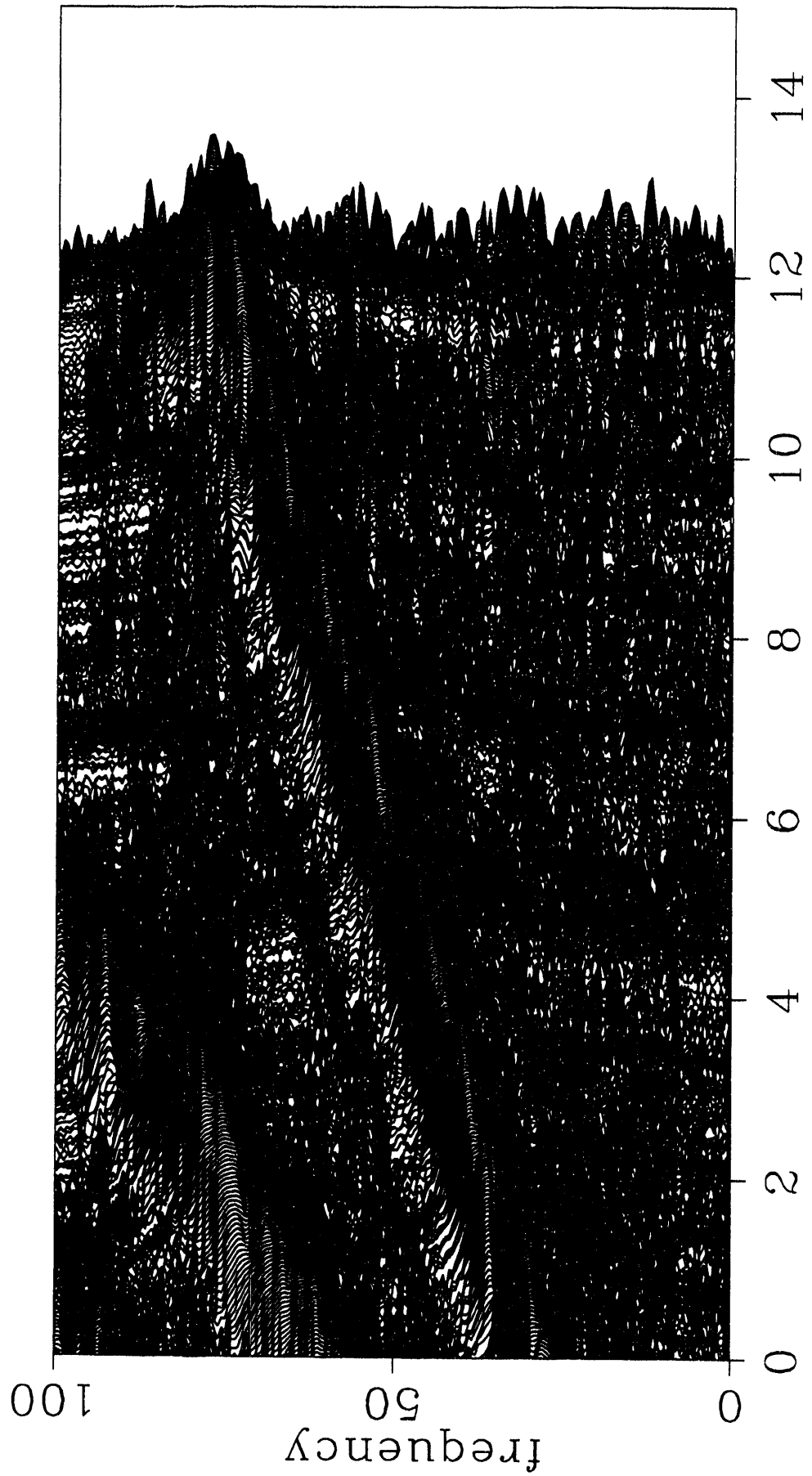

Figure 6. NTS VSP data. Plot of spectral amplitude versus time for the vertical component. A trace is plotted at each time step with the trace amplitude being the spectral amplitude for each frequency. The high amplitude peak from 0 to 12 sec increasing in frequency and time is the vibrator sweep, at higher frequency the first harmonic is seen from 0 to 5 sec where it leaves our analysis band.

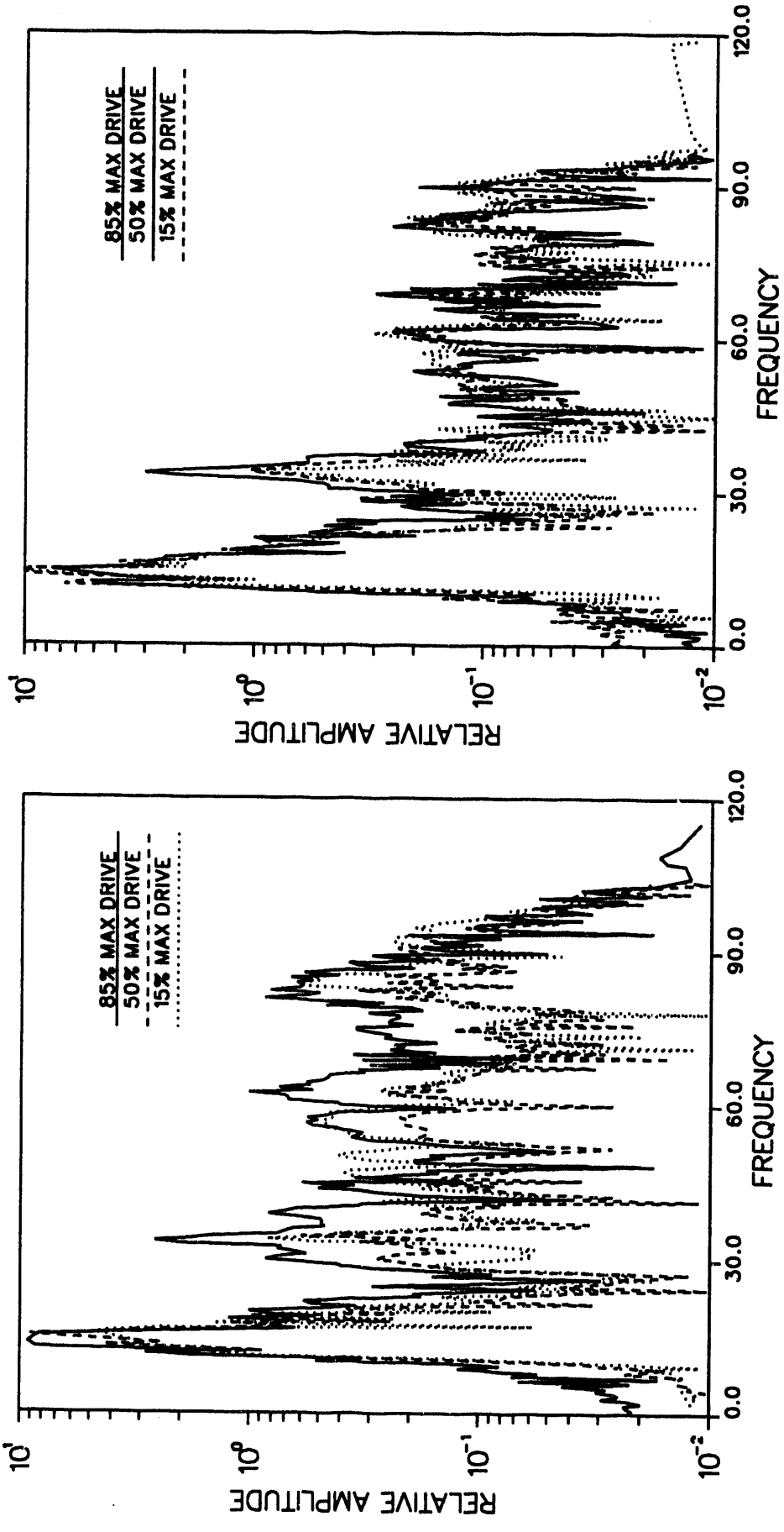

Figure 7a. NTS VSP data. Plots of spectral amplitude for the 20 Hz direct arrival at three drive levels (15%, 50% and 85%). The left side plot is for a 400 ft source offset and the right side plot is for a 600 ft source offset.

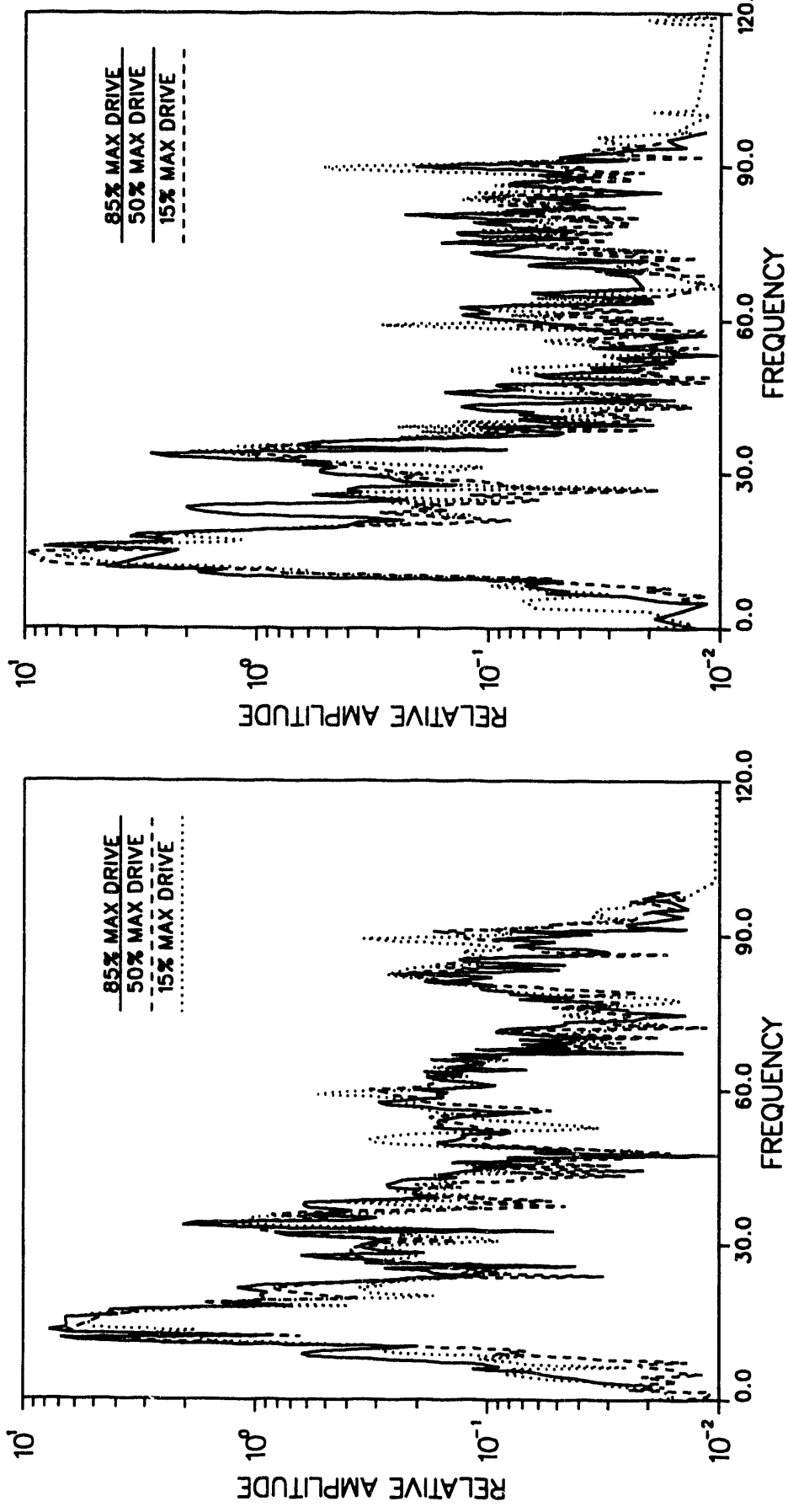

Figure 7b. NTS VSP data. Plots of spectral amplitude for the 20 Hz direct arrival at three drive levels (15%, 50% and 85%). The left side plot is for a 800 ft source offset and the right side plot is for a 1000 ft source offset.

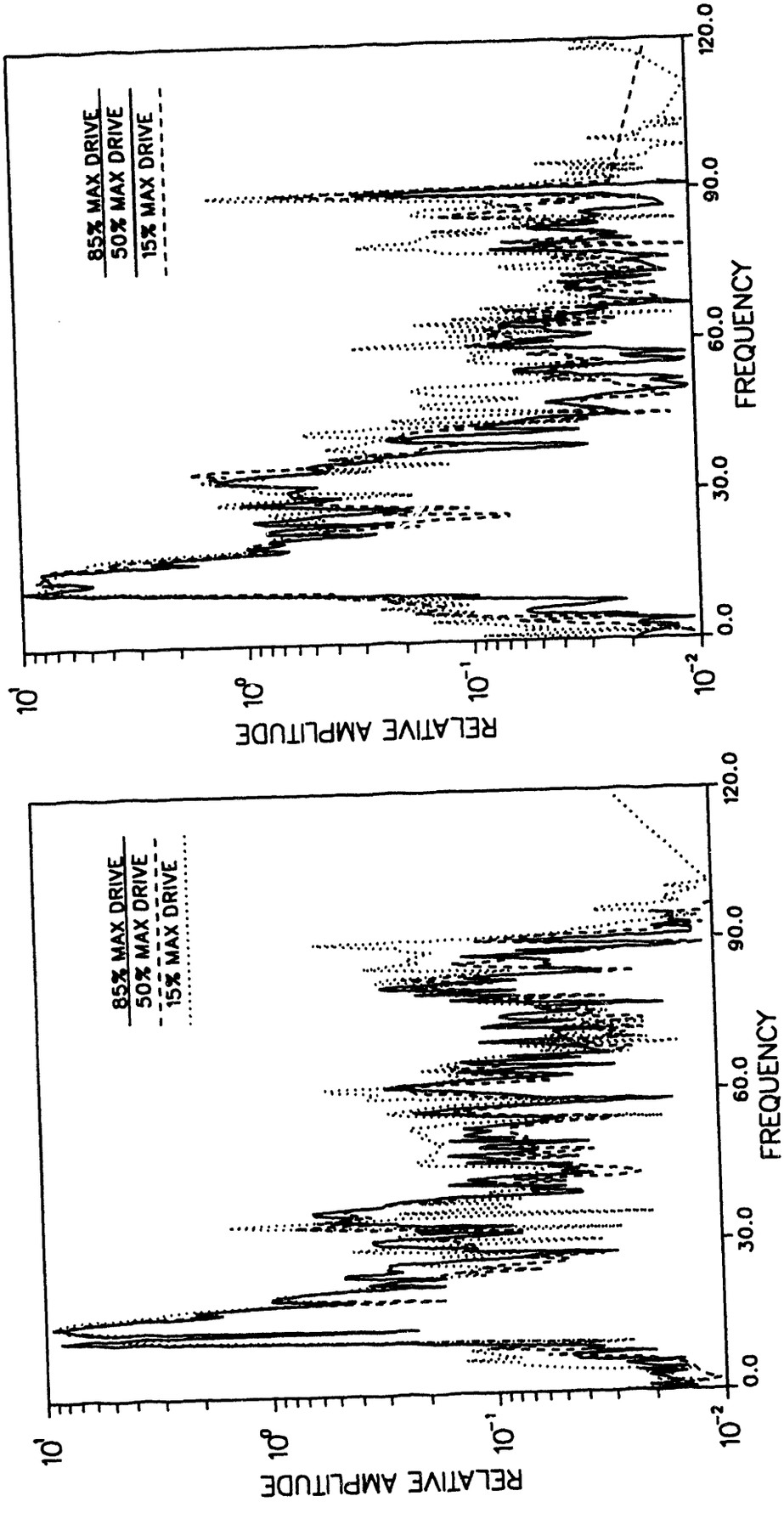

Figure 7c. NTS VSP data. Plots of spectral amplitude for the 20 Hz direct arrival at three drive levels (15%, 50% and 85%). The left side plot is for a 1200 ft source offset and the right side plot is for a 1400 ft source offset.

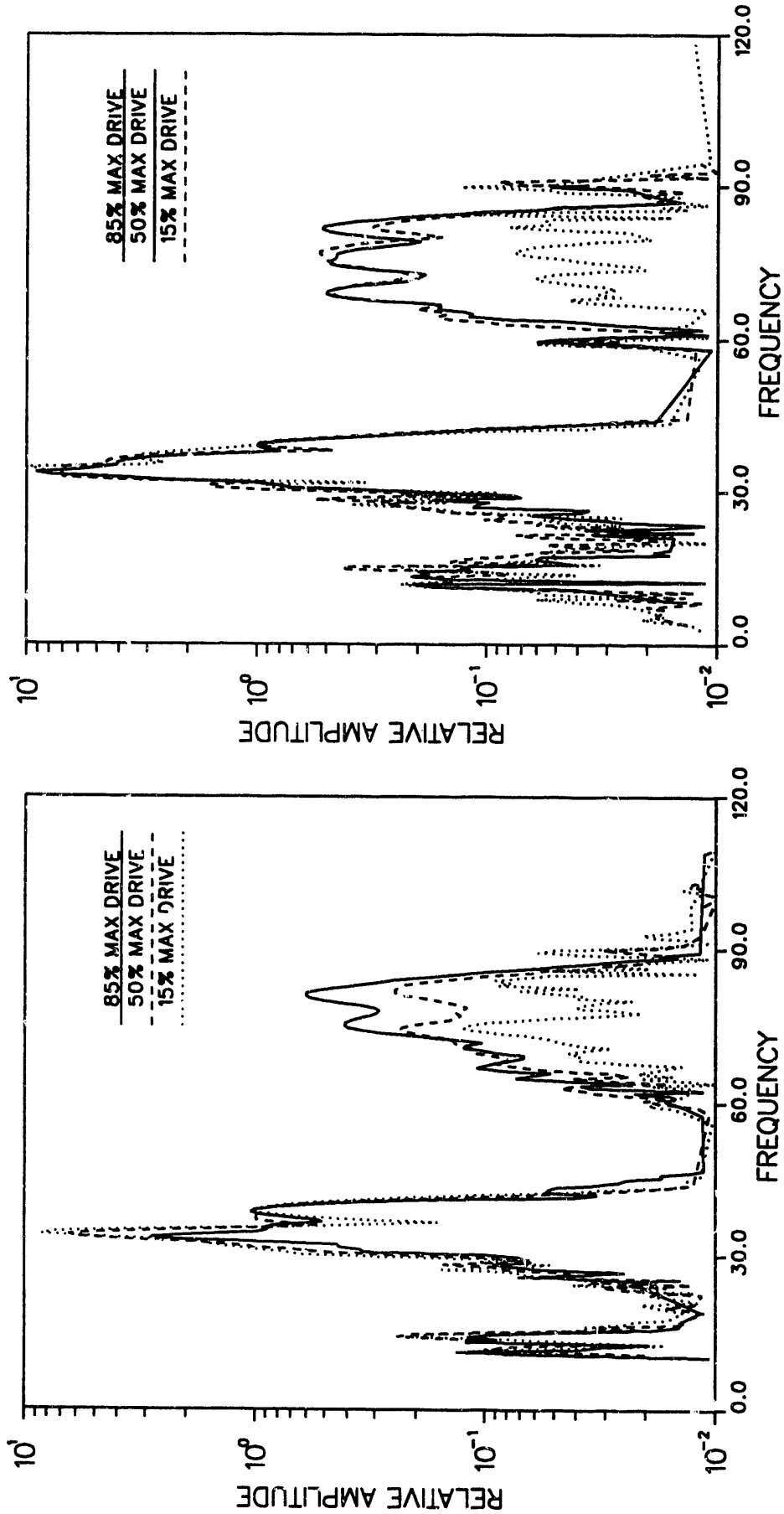

Figure 7d. NTS VSP data. Plots of spectral amplitude for the 40 Hz direct arrival at three drive levels (15%, 50% and 85%). The left side plot is for a 400 ft source offset and the right side plot is for a 600 ft source offset.

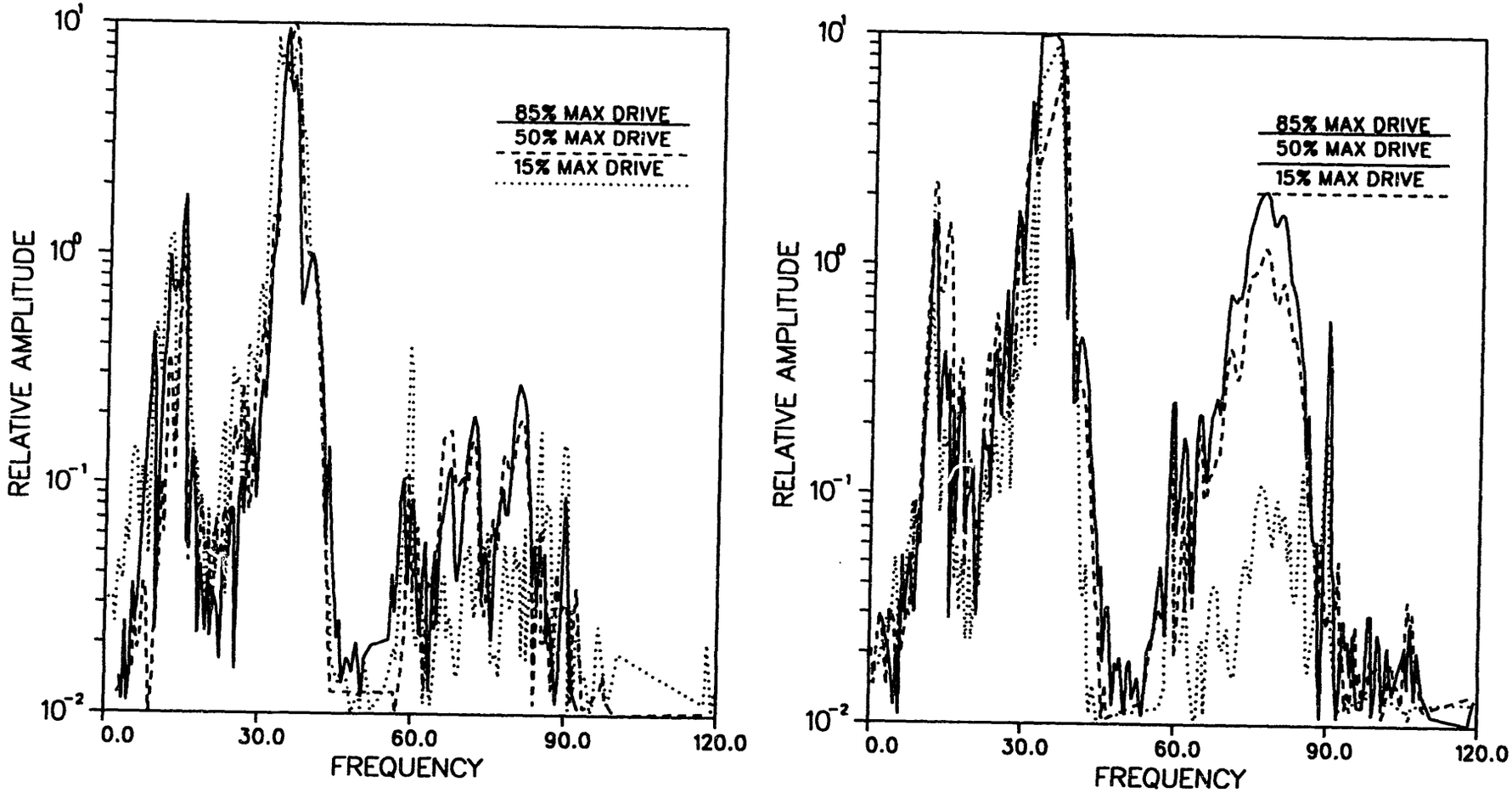

Figure 7e. NTS VSP data. Plots of spectral amplitude for the 40 Hz direct arrival at three drive levels (15%, 50% and 85%). The left side plot is for a 800 ft source offset and the right side plot is for a 1000 ft source offset.

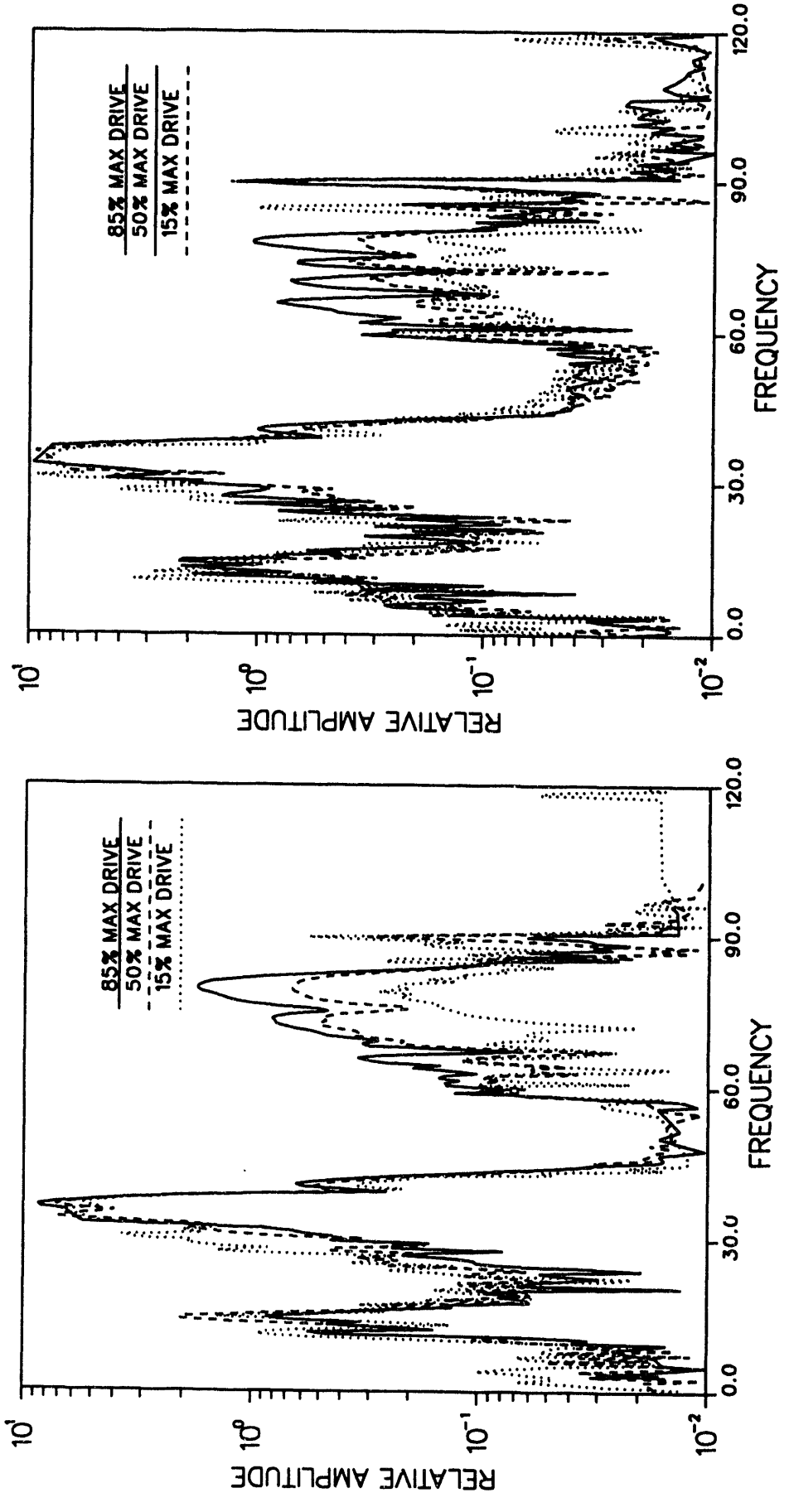

Figure 7f. NTS VSP data. Plots of spectral amplitude for the 40 Hz direct arrival at three drive levels (15%, 50% and 85%). The left side plot is for a 1200 ft source offset and the right side plot is for a 1400 ft source offset.

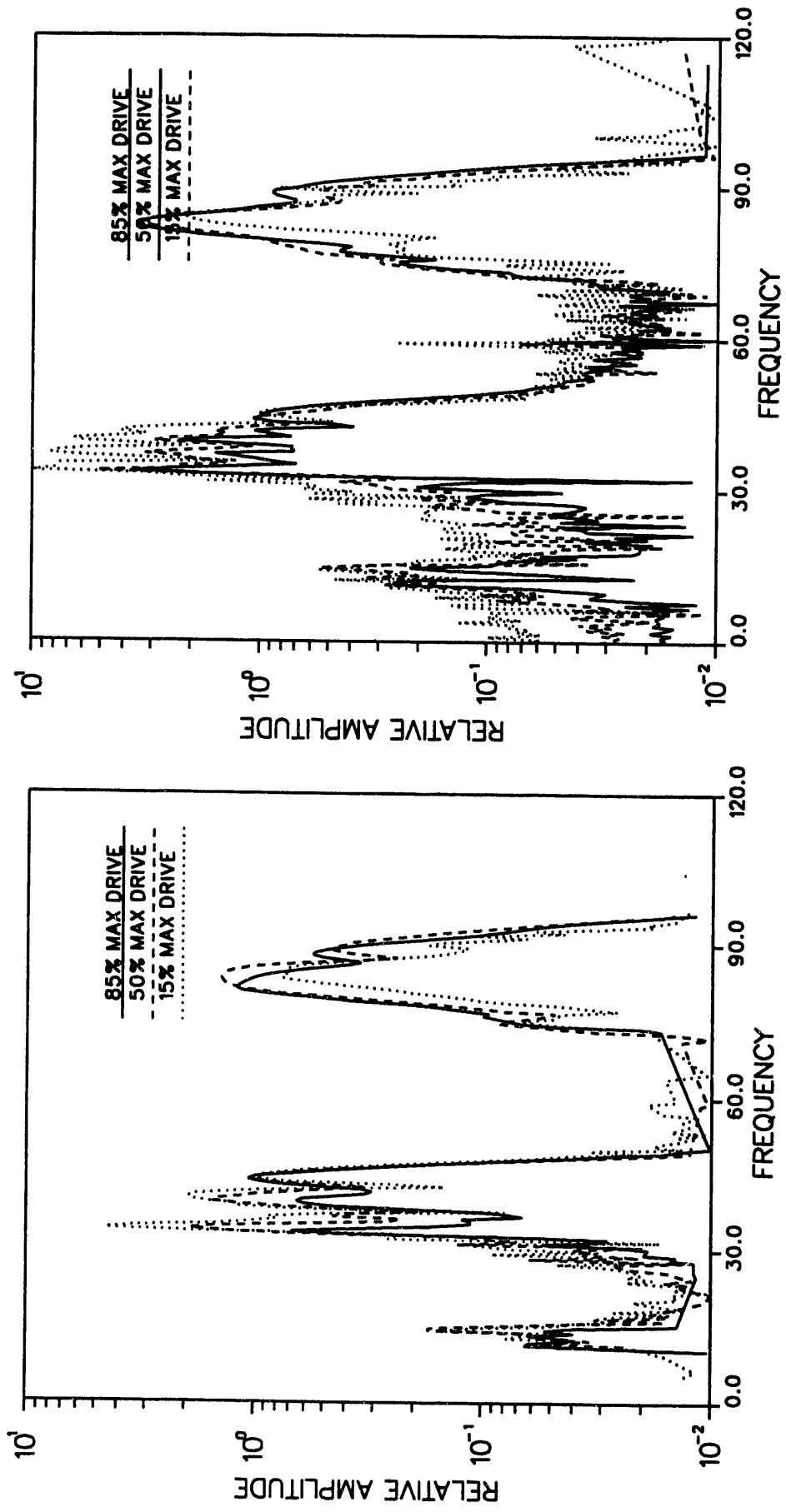

Figure 7g. NTS VSP data. Plots of spectral amplitude for the 45 Hz direct arrival at three drive levels (15%, 50% and 85%). The left side plot is for a 400 ft source offset and the right side plot is for a 600 ft source offset.

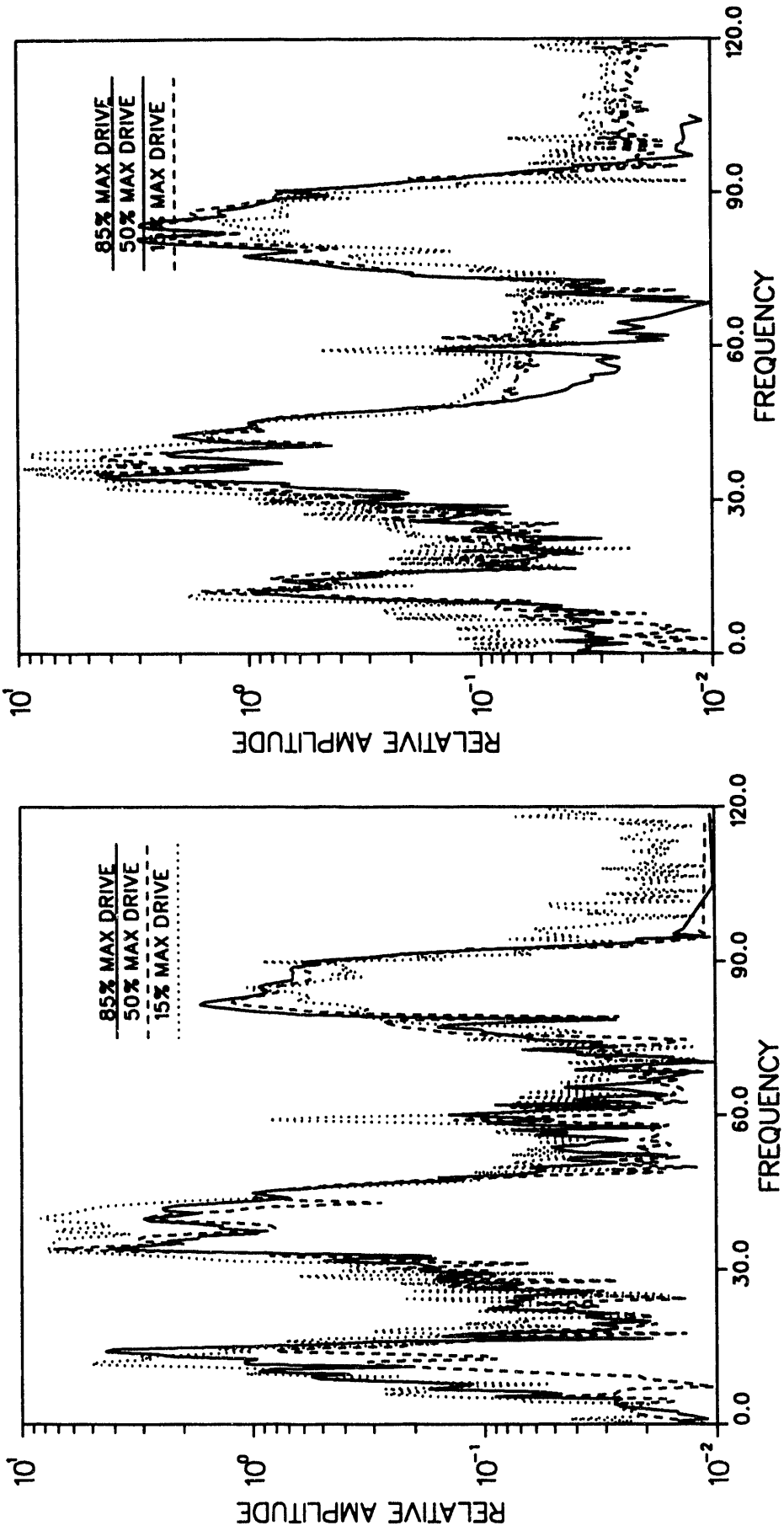

Figure 7h. NTS VSP data. Plots of spectral amplitude for the 45 Hz direct arrival at three drive levels (15%, 50% and 85%). The left side plot is for a 800 ft source offset and the right side plot is for a 1000 ft source offset.

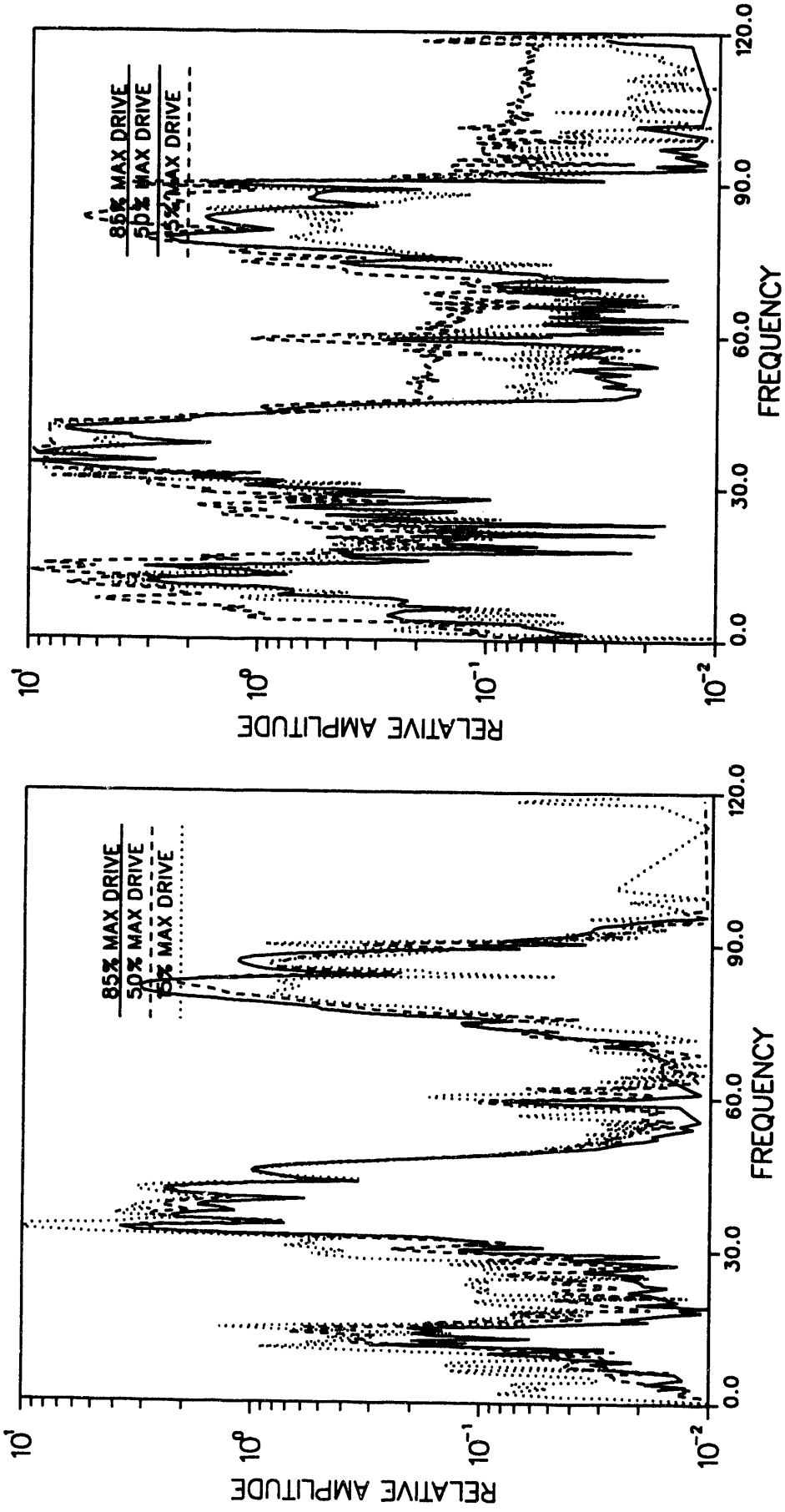

Figure 7i. NTS VSP data. Plots of spectral amplitude for the 45 Hz direct arrival at three drive levels (15%, 50% and 85%). The left side plot is for a 1200 ft source offset and the right side plot is for a 1400 ft source offset.

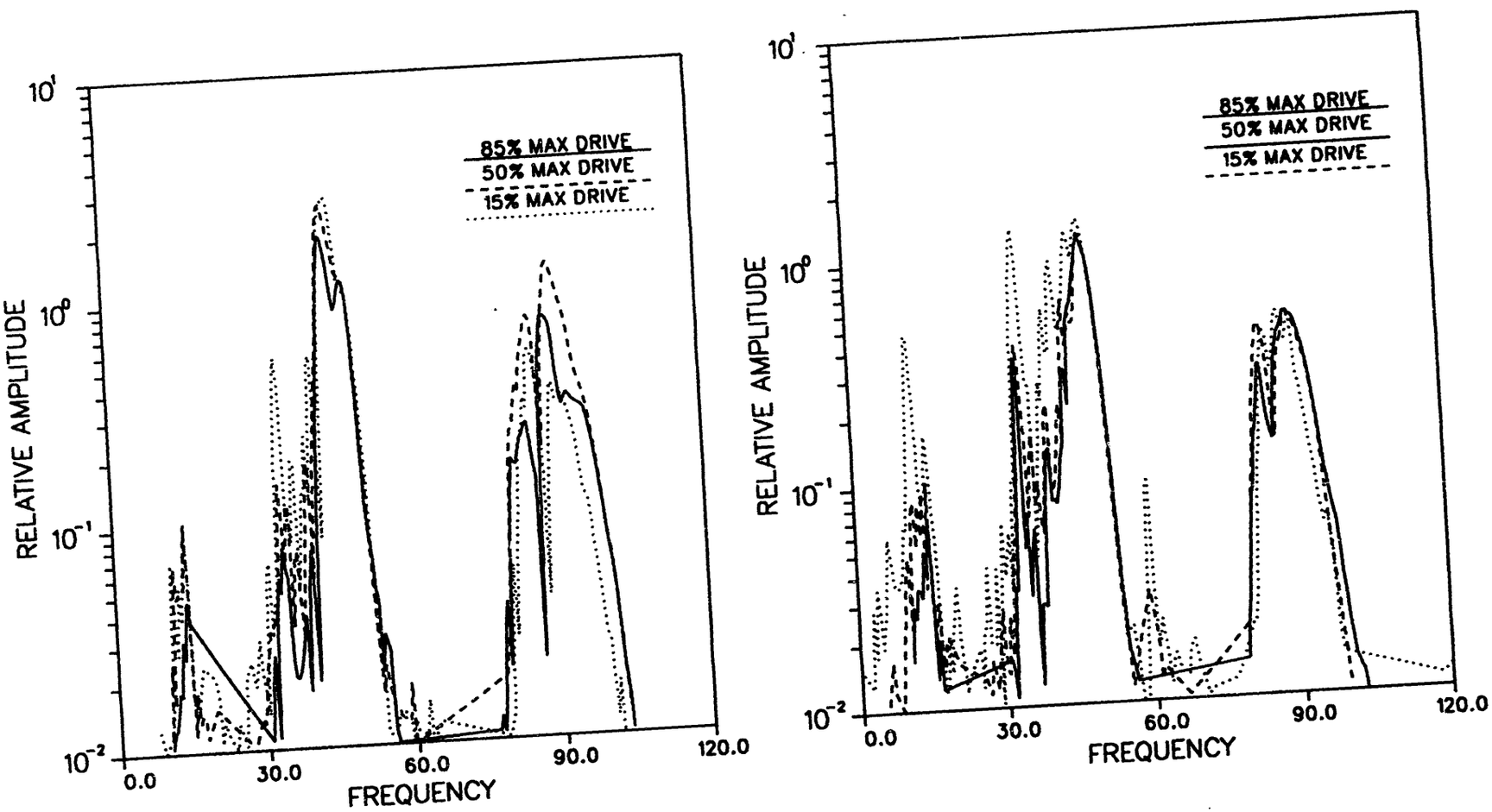

Figure 7j. NTS VSP data. Plots of spectral amplitude for the 50 Hz direct arrival at three drive levels (15%, 50% and 85%). The left side plot is for a 400 ft source offset and the right side plot is for a 600 ft source offset.

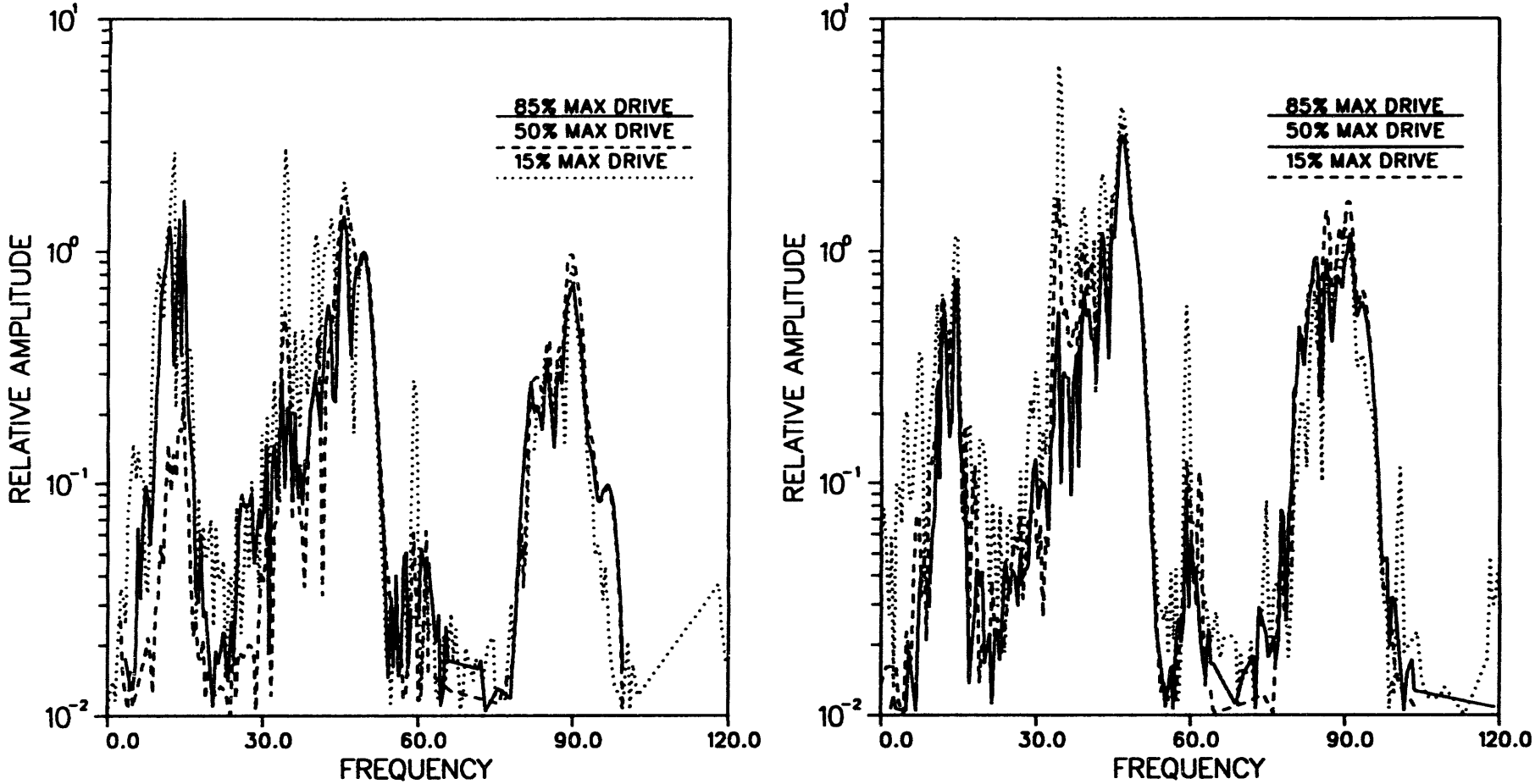

Figure 7k. NTS VSP data. Plots of spectral amplitude for the 50 Hz direct arrival at three drive levels (15%, 50% and 85%). The left side plot is for a 800 ft source offset and the right side plot is for a 1000 ft source offset.

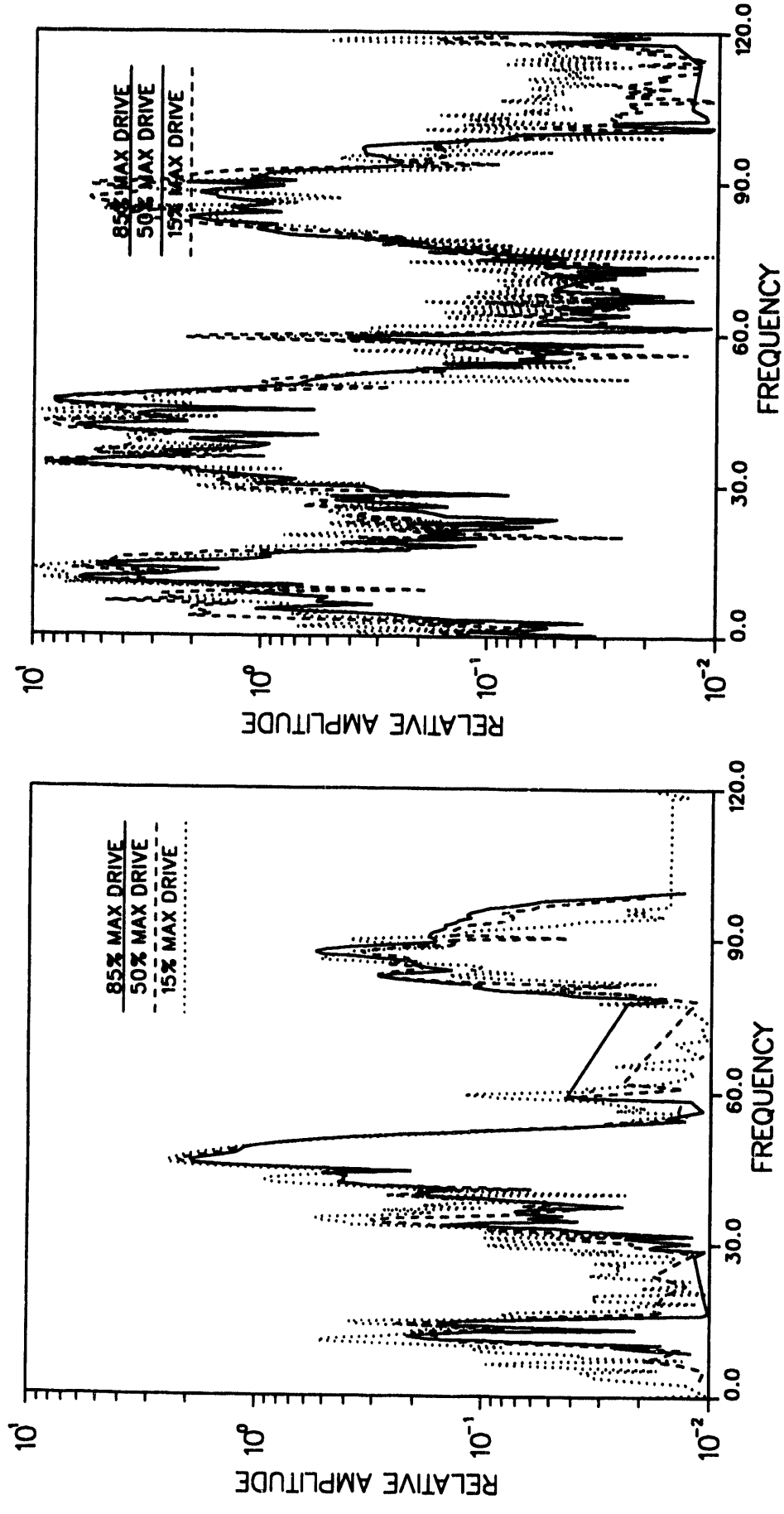

Figure 71. NTS VSP data. Plots of spectral amplitude for the 50 Hz direct arrival at three drive levels (15%, 50% and 85%). The left side plot is for a 1200 ft source offset and the right side plot is for a 1400 ft source offset.

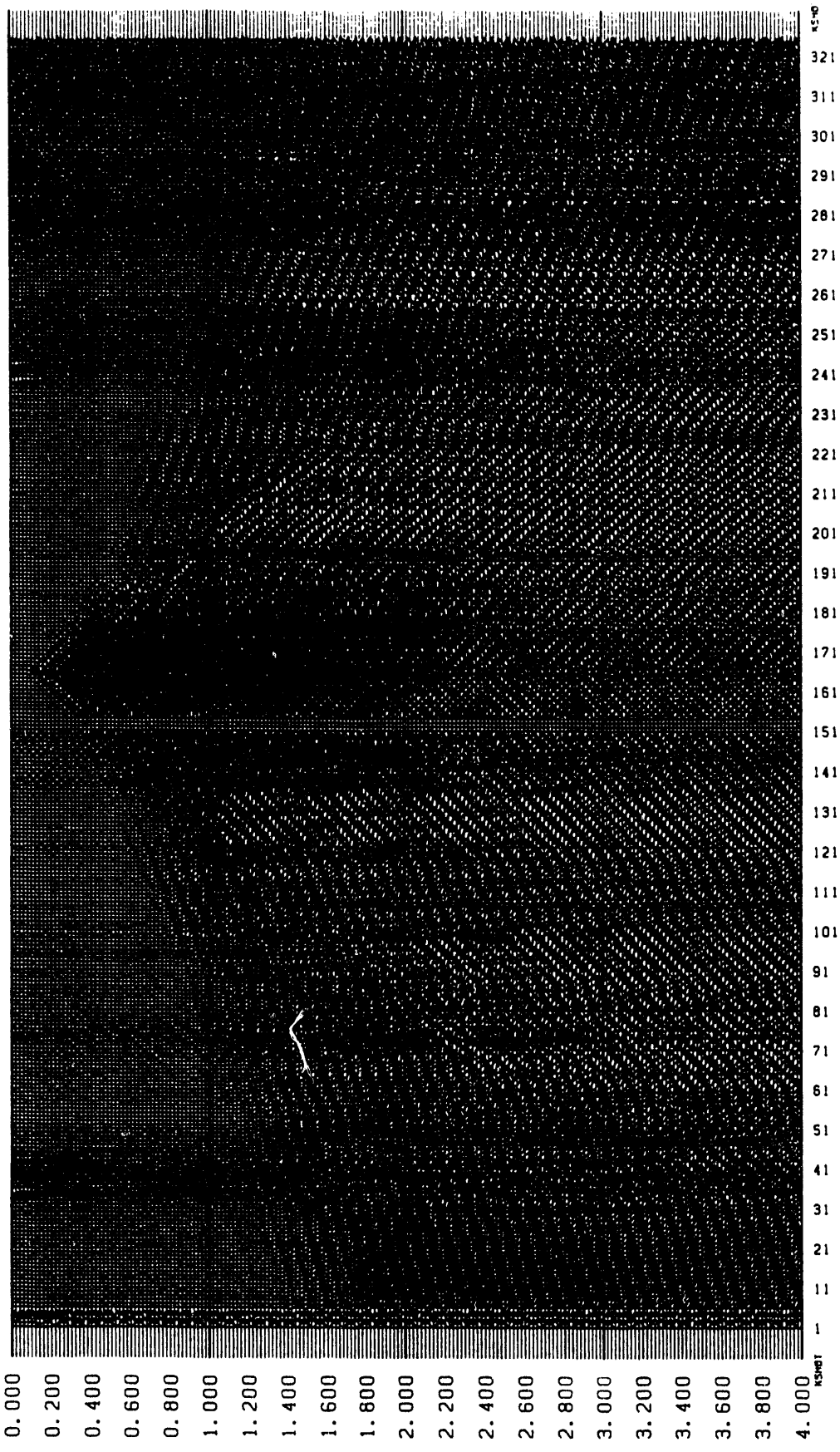

Figure 8a. Data traces from LANL experiment showing one shot gather for three vibrators shaking at 13 Hz. Note the P-wave and surface wave arrivals.

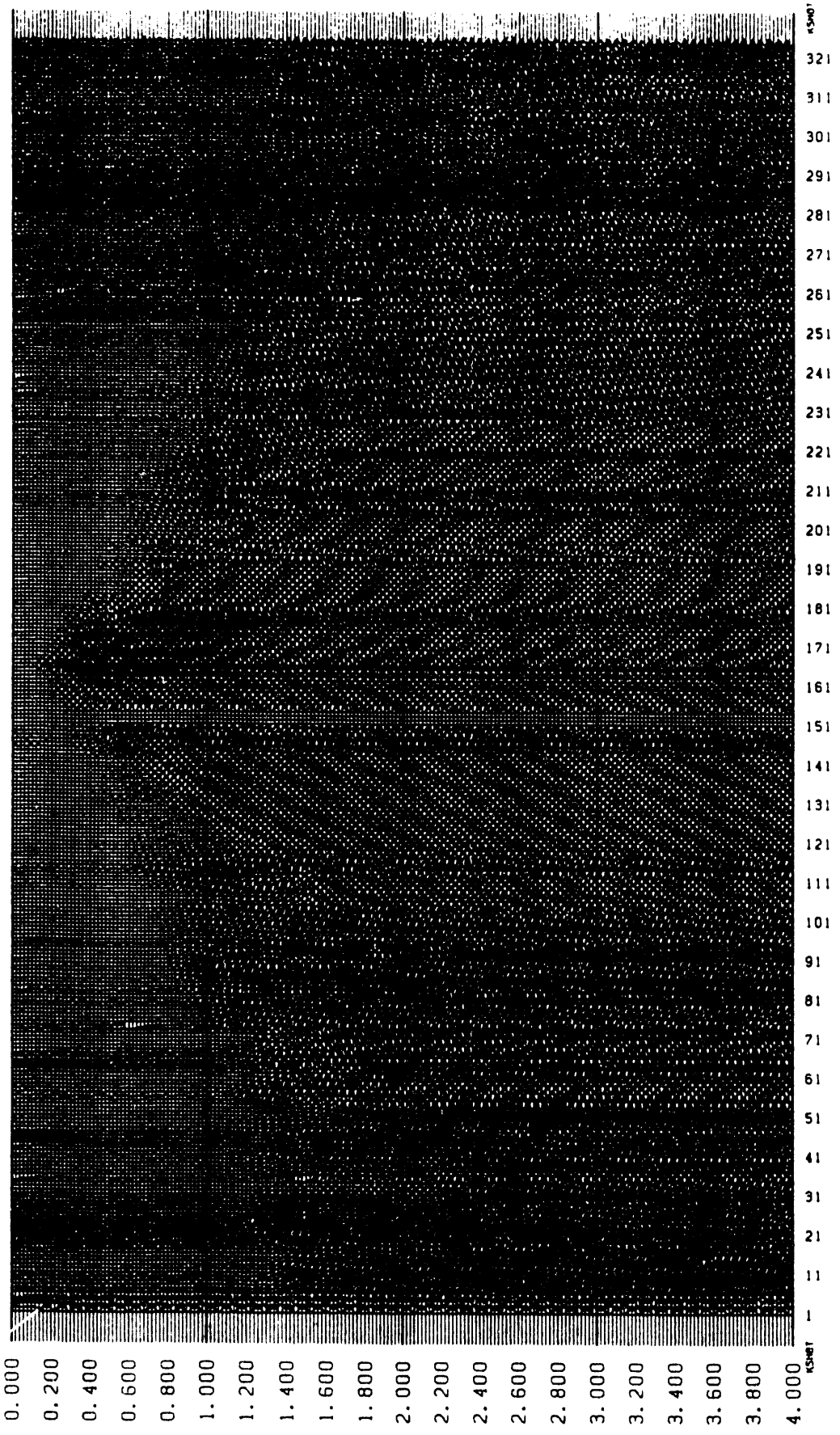

Figure 8b. Same as Figure 8a, with vibrators shaking at 23 Hz.

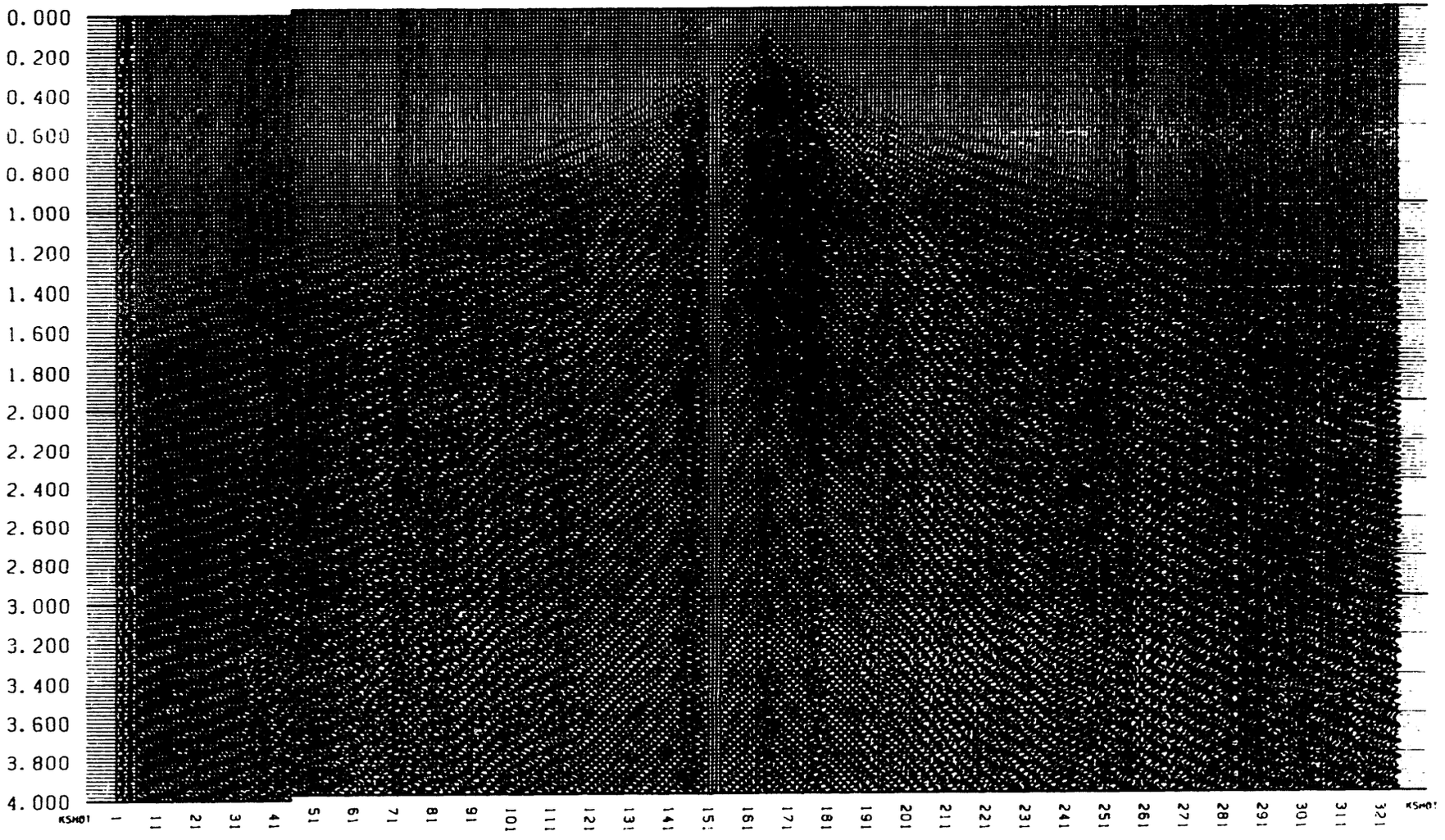

Figure 8c. Data traces from LANL experiment showing a shot gather for simultaneous sweeping of 13 Hz and 23 Hz by three vibrators each.

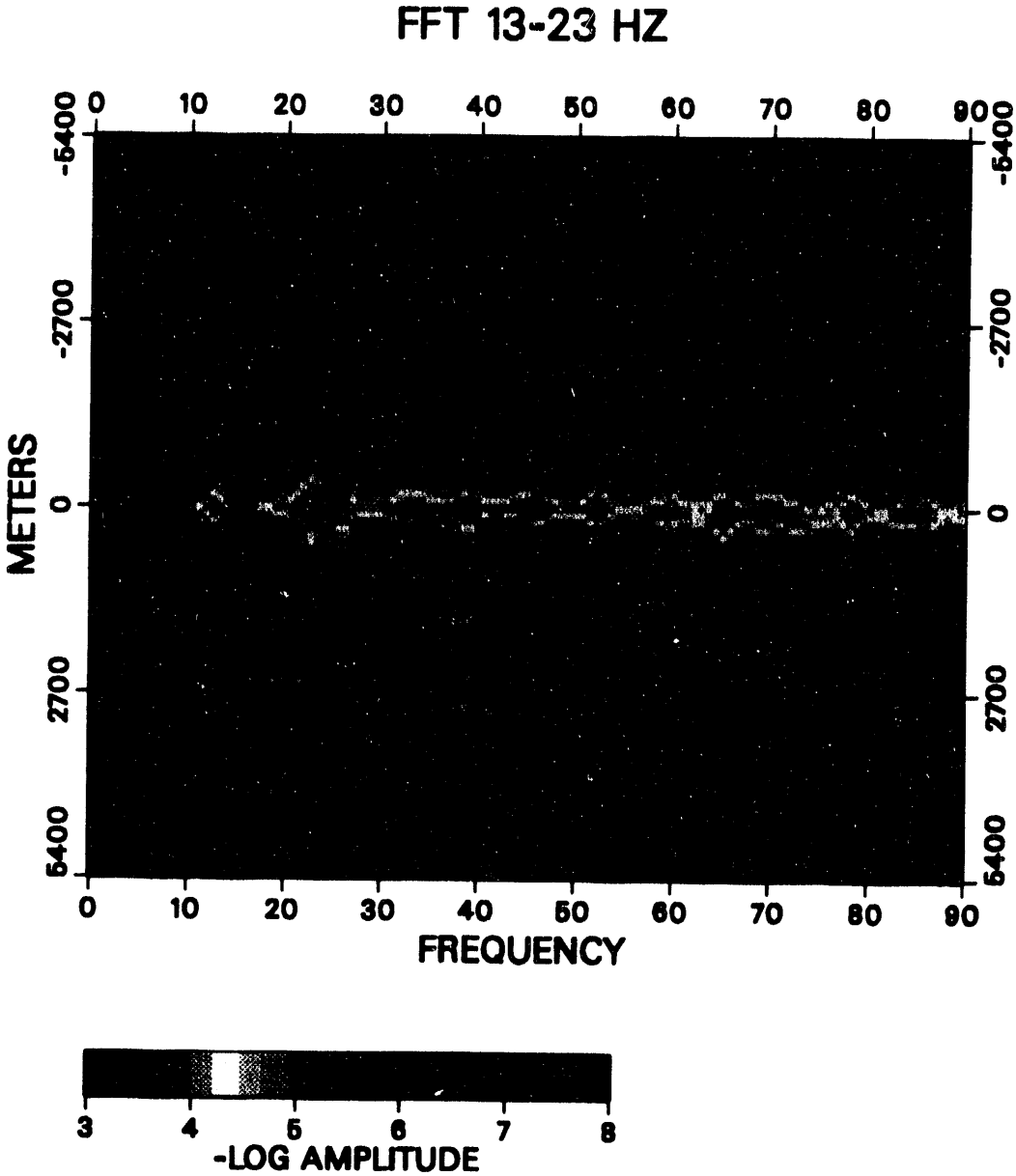

Figure 9a. Spectral amplitude versus offset for simultaneous 13 and 23 Hz data from Figure 8c.

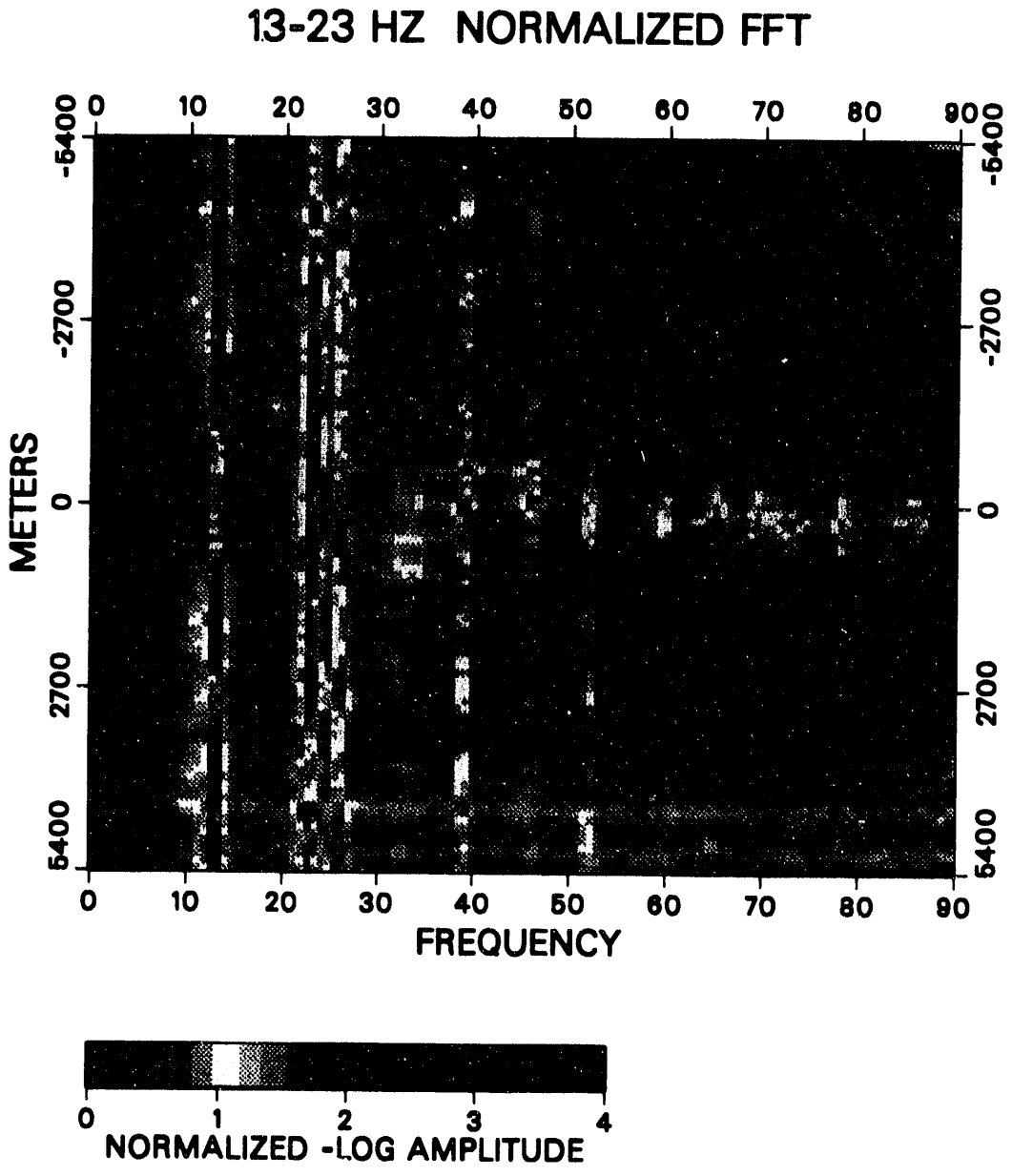

Figure 9b. Same data as Figure 9a, but with amplitude normalized to the maximum of each trace.

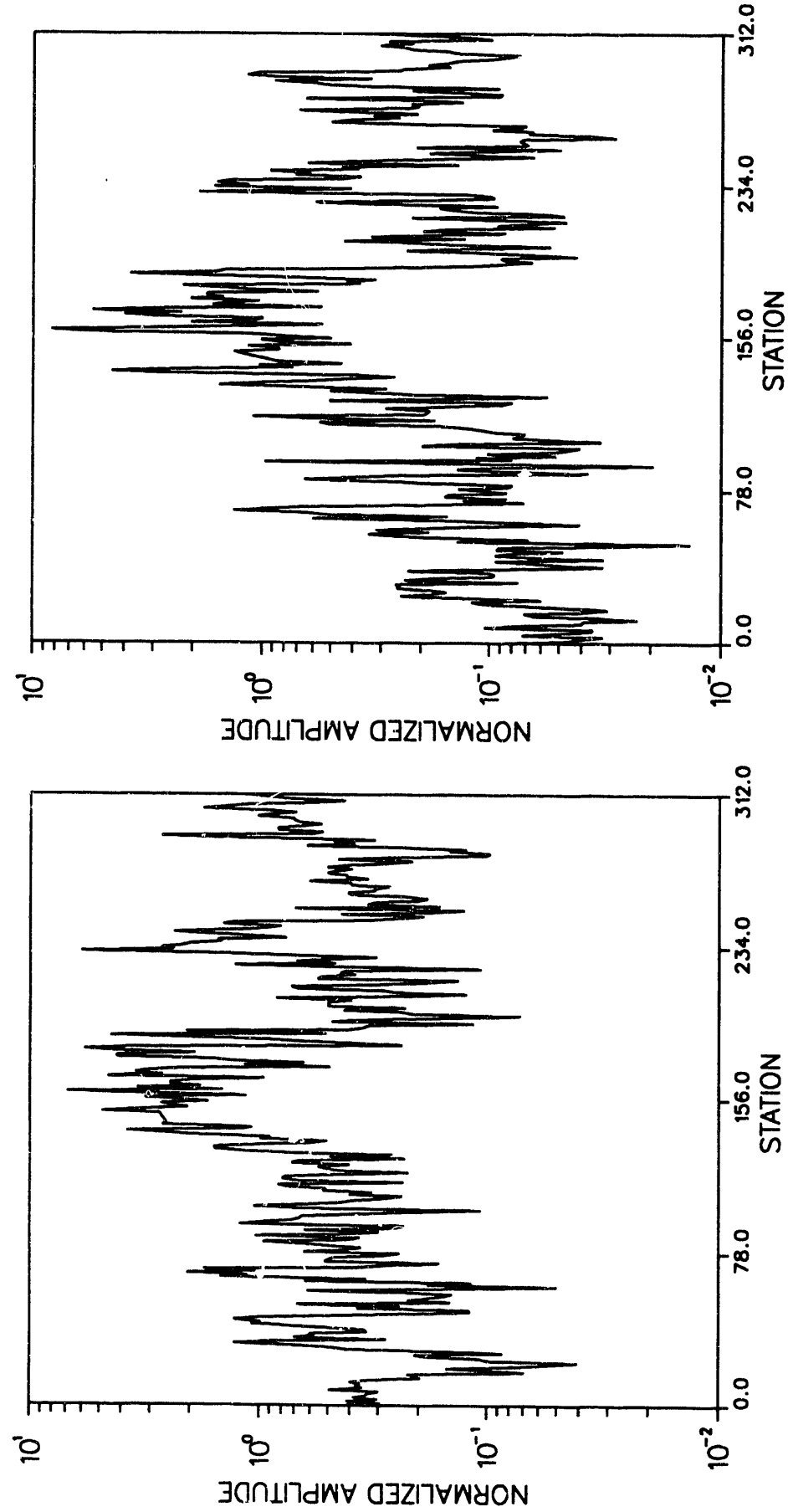

Figure 10a. Spectral amplitude ratio versus offset for first (left) and second (right) harmonic of the 13 Hz LANL data (Figure 8a). The station spacing is 110 ft. The source is at station 165.

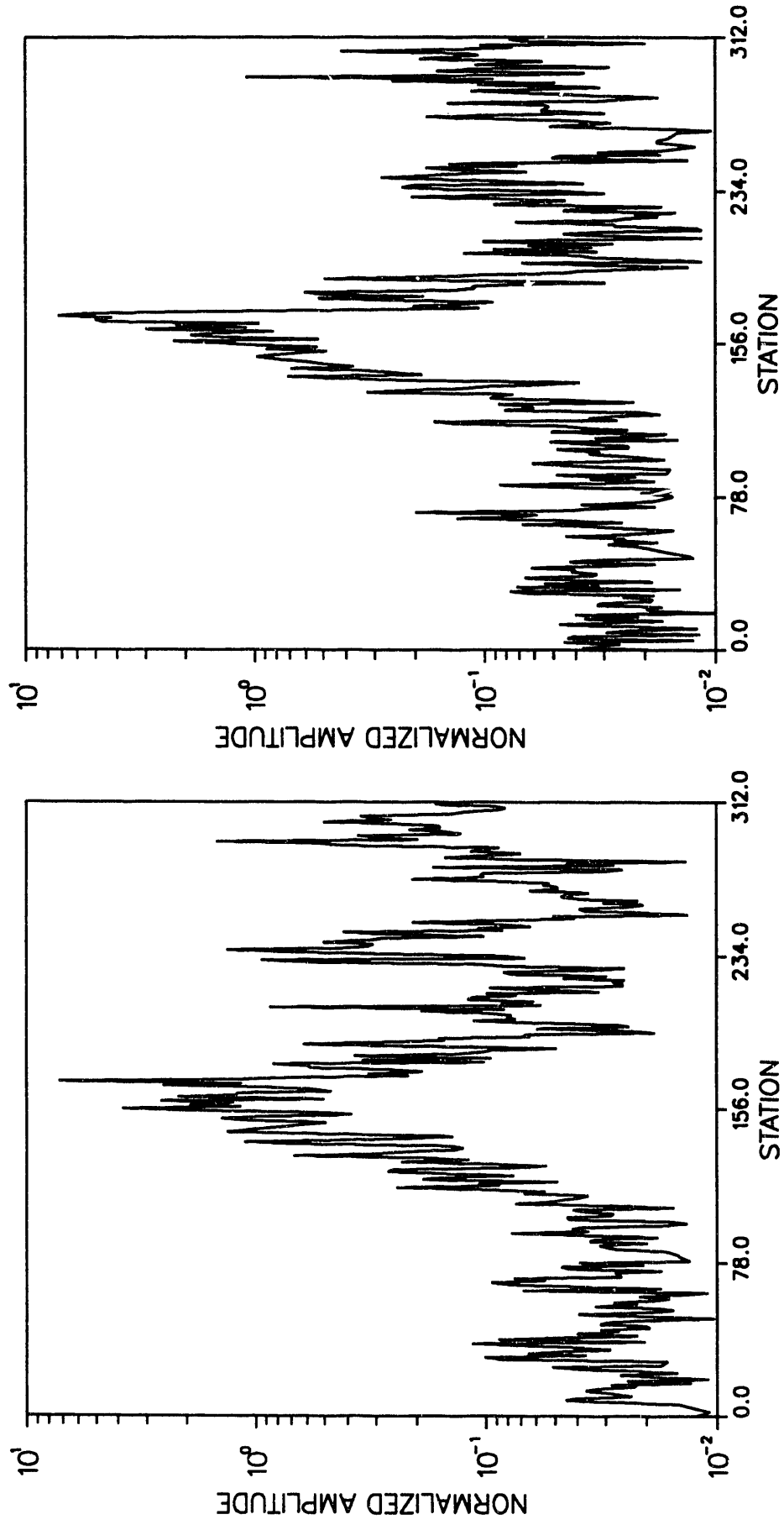

Figure 10b. Spectral amplitude ratio versus offset for third (left) and fourth (right) harmonic of the 13 Hz LANL data (Figure 8a). The station spacing is 110 ft. The source is at station 165.

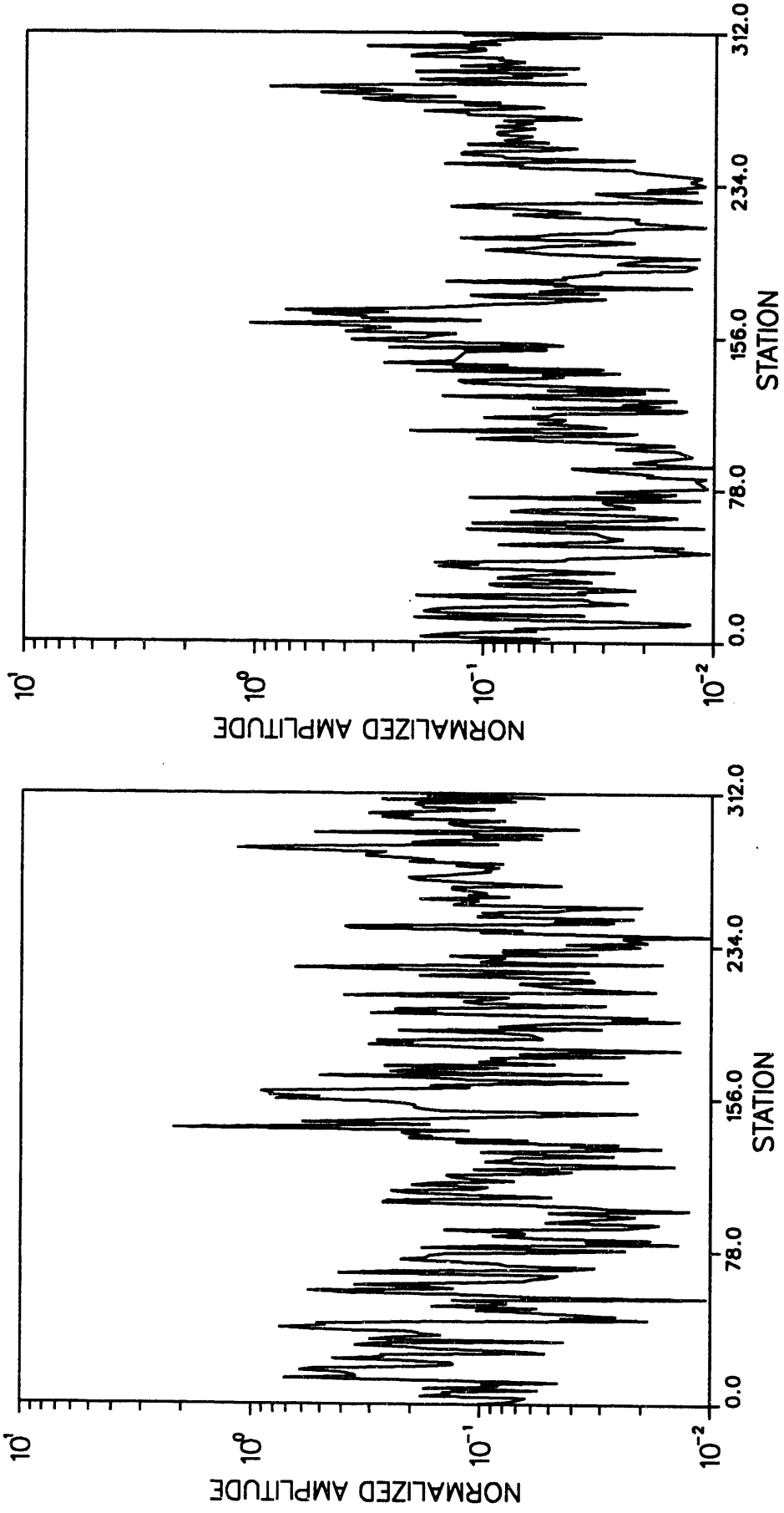

Figure 11a. Spectral amplitude ratio versus offset for first (left) and second (right) harmonic of the 23 Hz LANL data (Figure 8b). The station spacing is 110 ft. The source is at station 165.

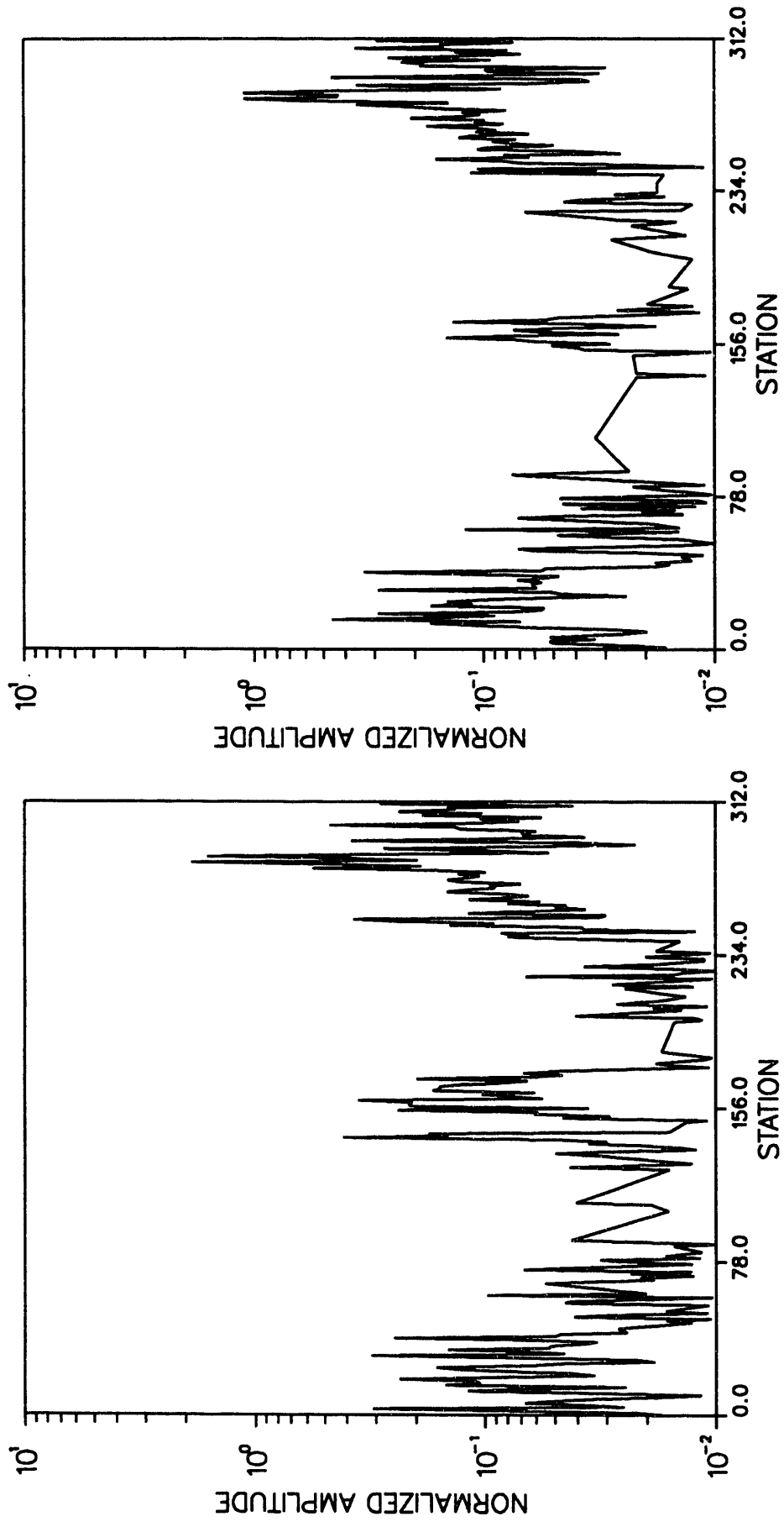

Figure 11b. Spectral amplitude ratio versus offset for third (left) and fourth (right) harmonic of the 23 Hz LANL data (Figure 8b). The station spacing is 110 ft. The source is at station 165.

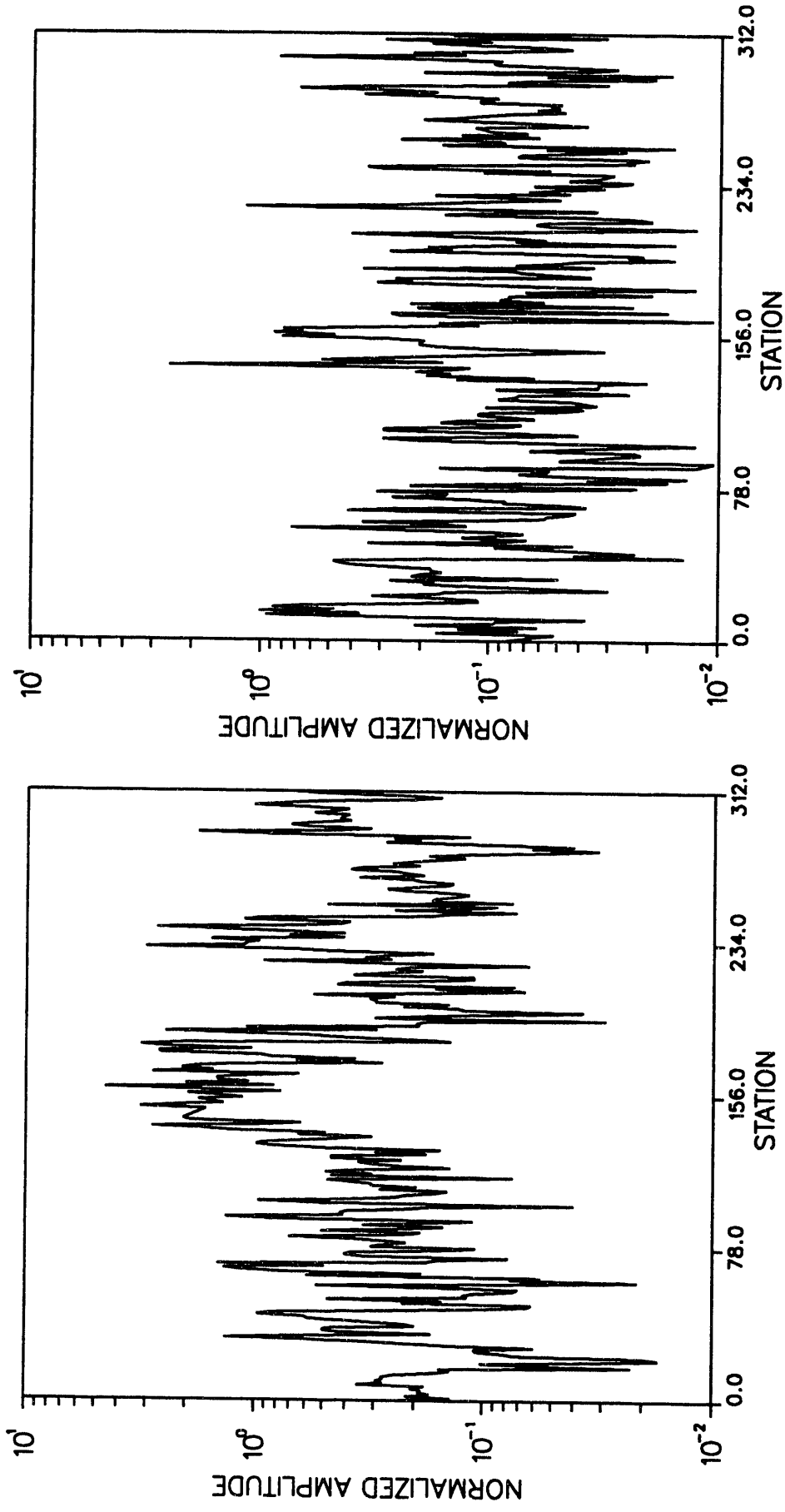

Figure 12. Spectral amplitude ratio versus offset using 12 seconds of LANL data. Left side is first harmonic of 13 Hz, right side is first harmonic of 23 Hz data. The station spacing is 110 ft. The source is at station 165. LANL.

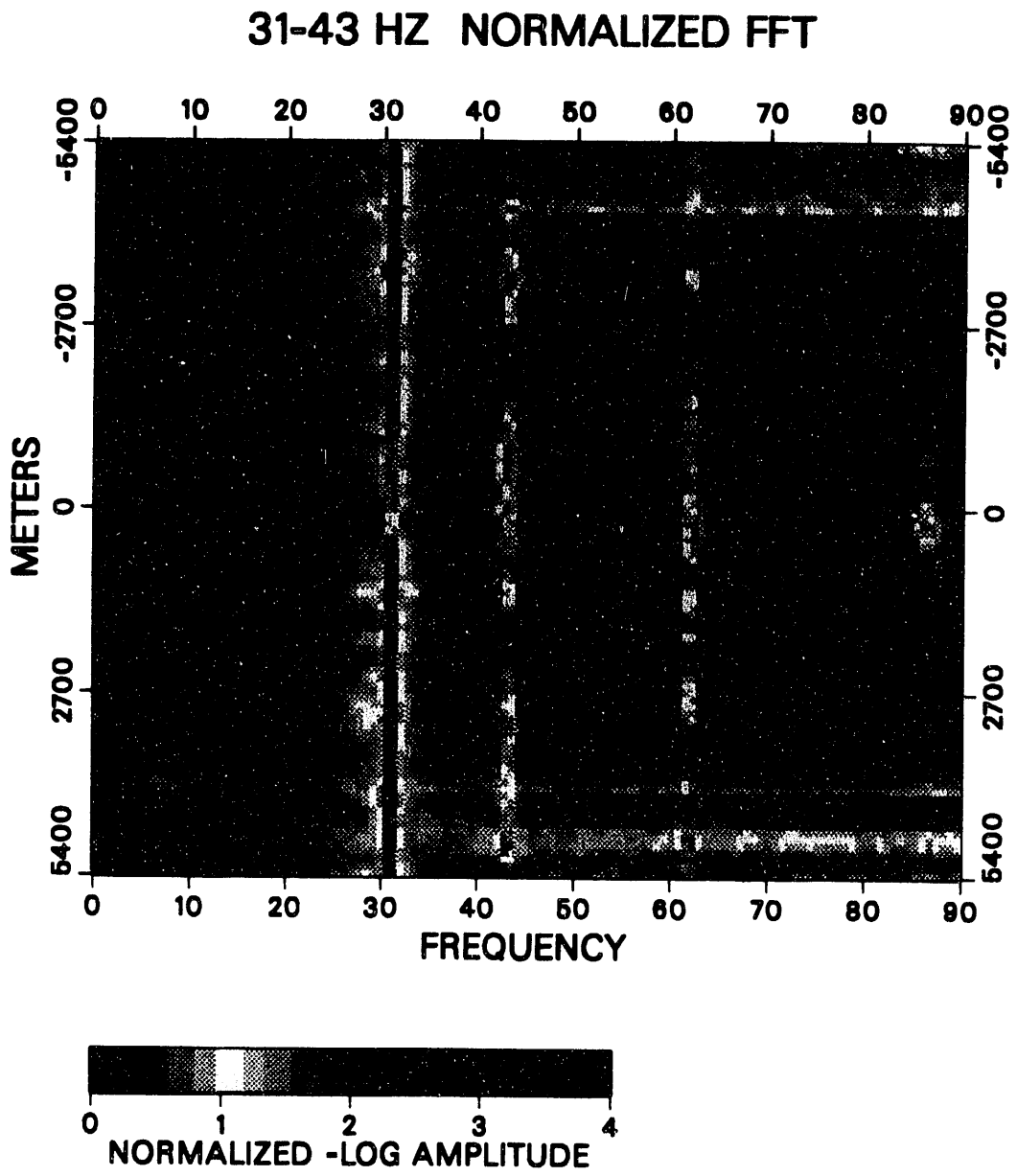

Figure 13. Spectral amplitude versus offset using 12 seconds of LANL data with simultaneous 31 and 43 Hz sources. Amplitude of spectra at each offset is normalized to the maximum for that offset.

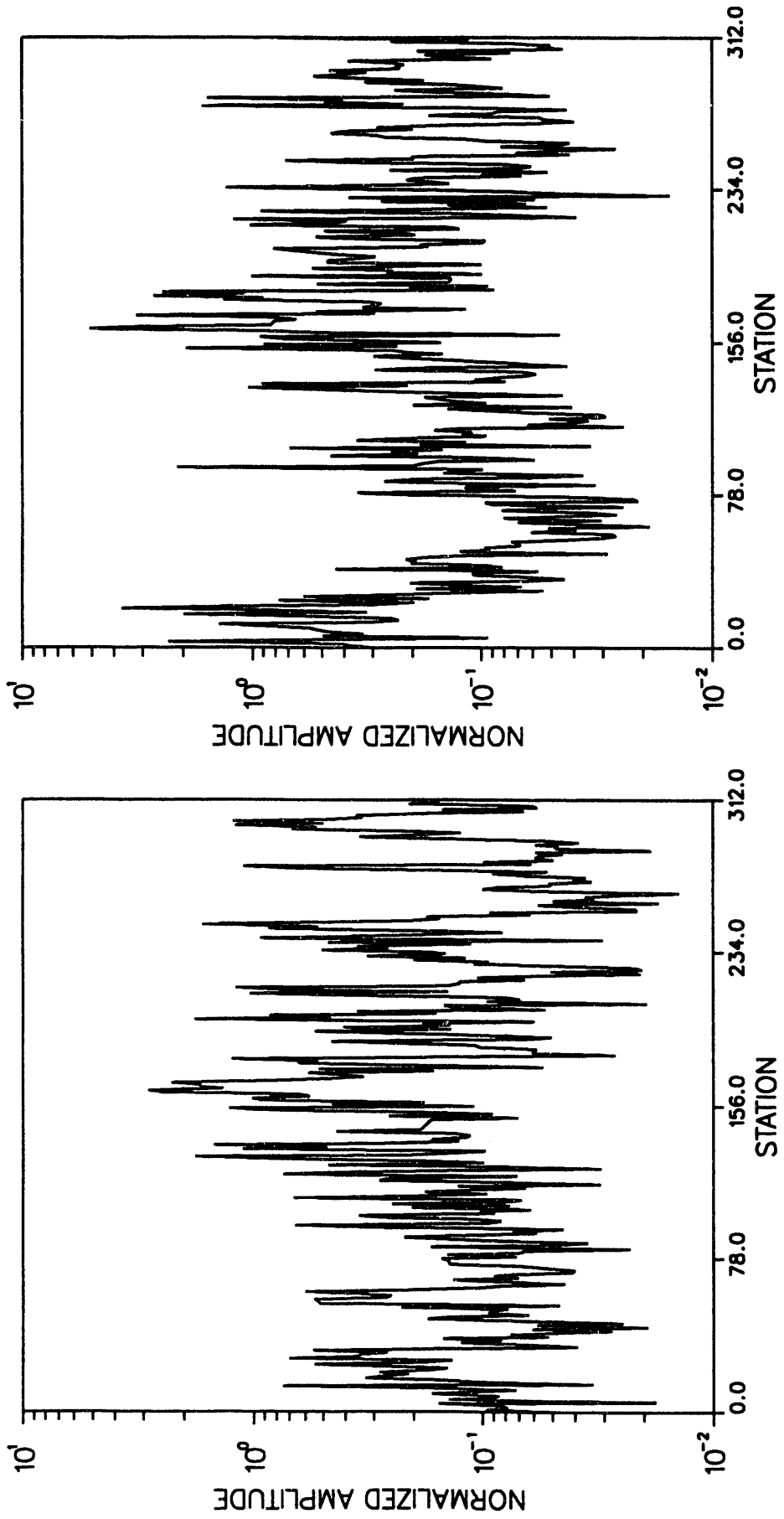

Figure 14. LANL data. Spectral amplitude ratio versus offset for the first harmonic of 31 Hz data (left) and 43 Hz data (right). The station spacing is 110 ft. The source is at station 165.

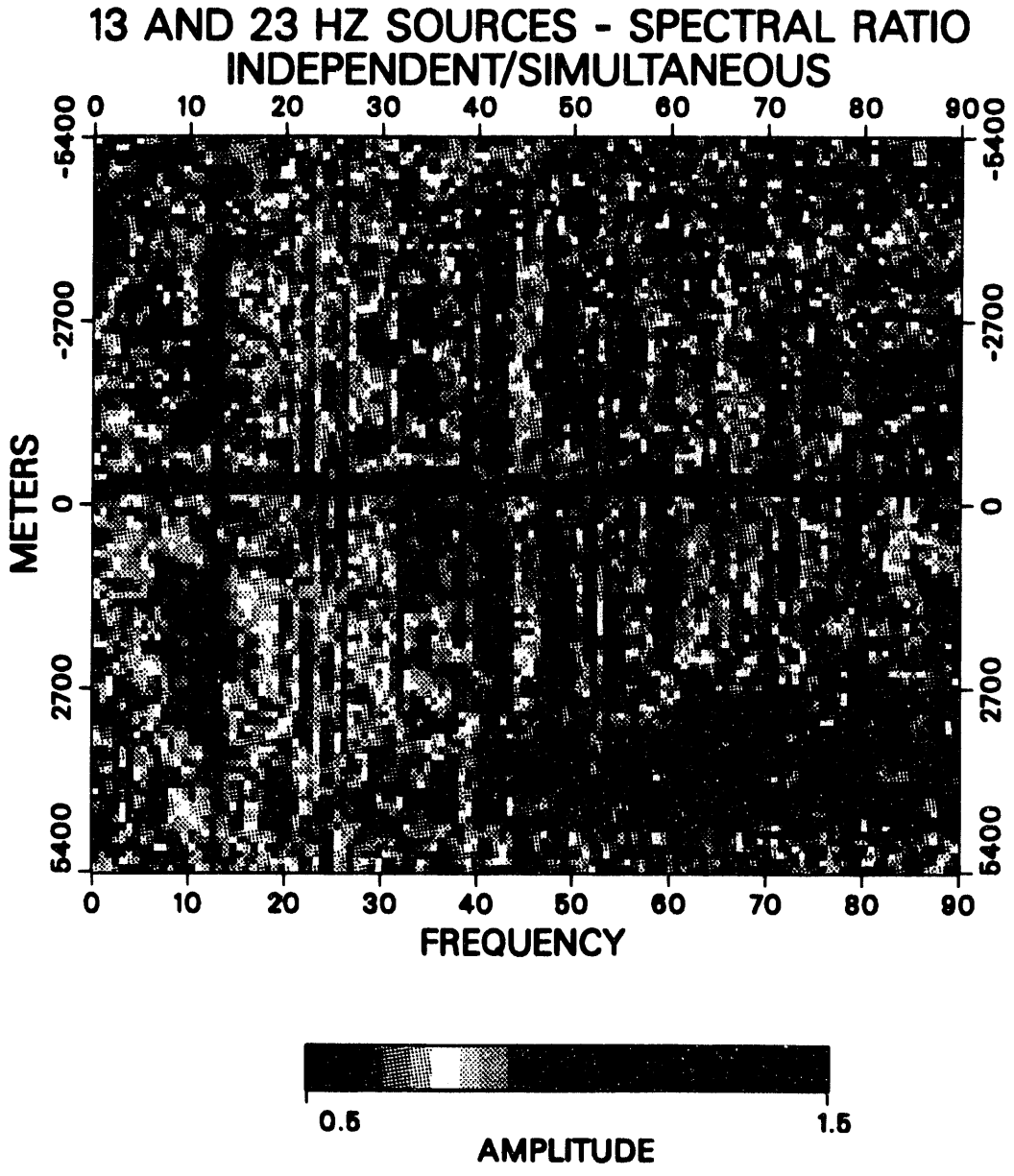

Figure 15a. The spectral ratios of two data sets are displayed as a function of offset. The numerator is the sum of 13 Hz and 23 Hz data sets. The denominator is the spectra for the simultaneous sweeping of 13 and 23 Hz.

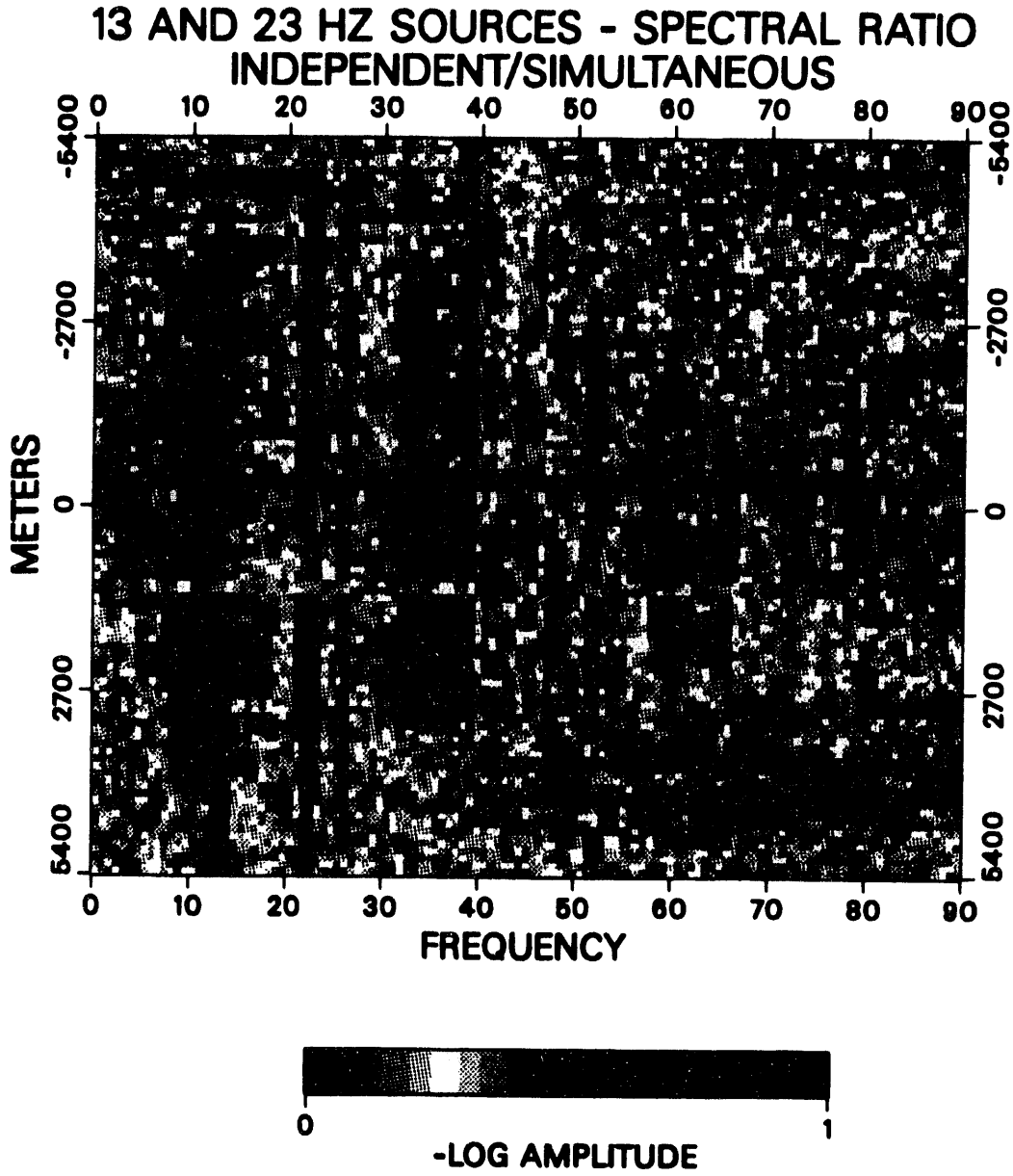

Figure 15b. Same as 15a, but with -log(amplitude) used for spectral amplitude.

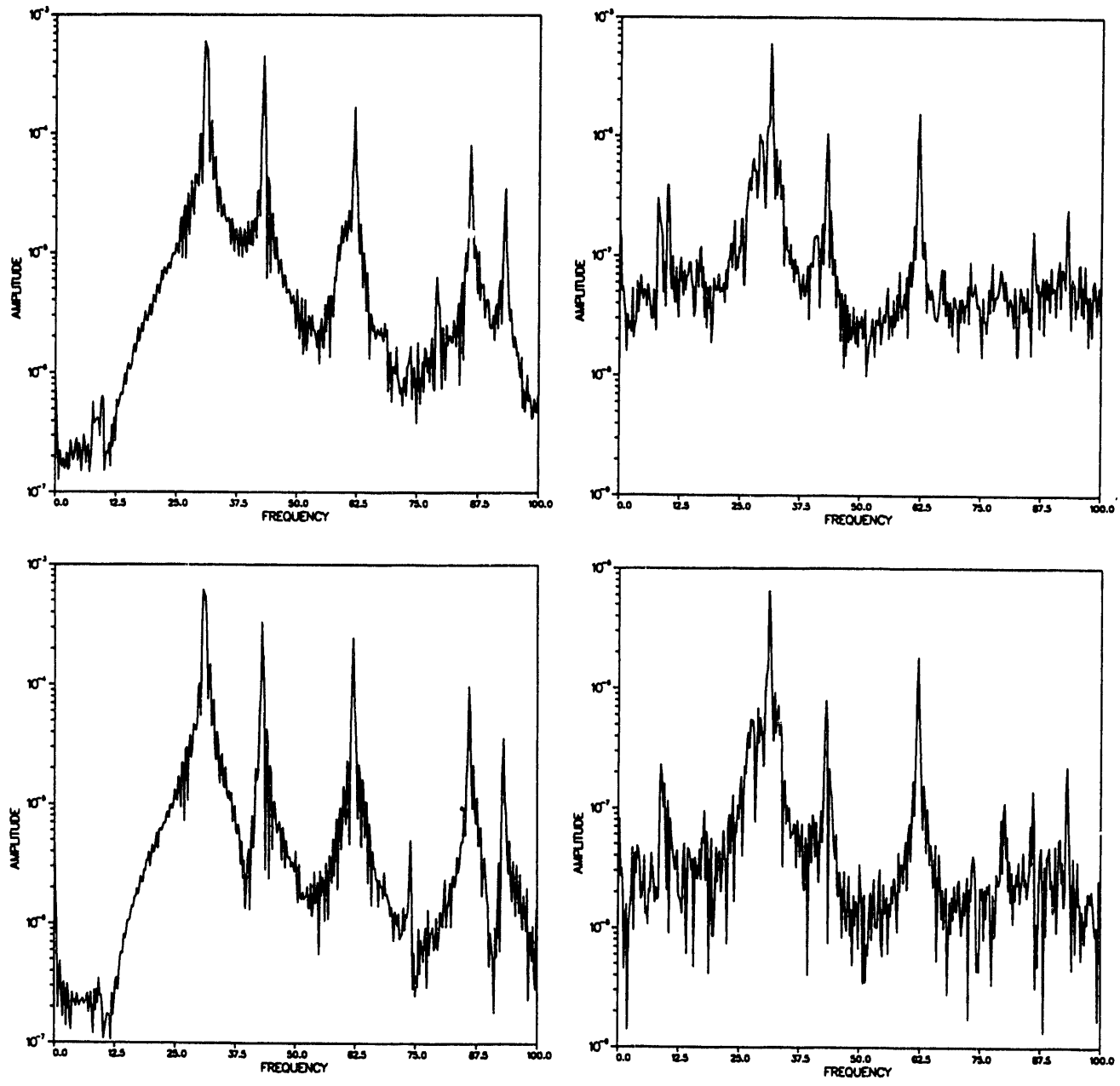

Figure 16. LANL data. Spectral amplitude for two individual traces, #150 (left top and bottom) and #95 (right top and bottom). The top two spectra are for 31 and 43 Hz sources sweeping simultaneously. The bottom two spectra are for 31 and 43 Hz sources recorded separately and added by computer. If the non-linear propagation is occurring there should be higher harmonic energy in the top two spectra (see text).

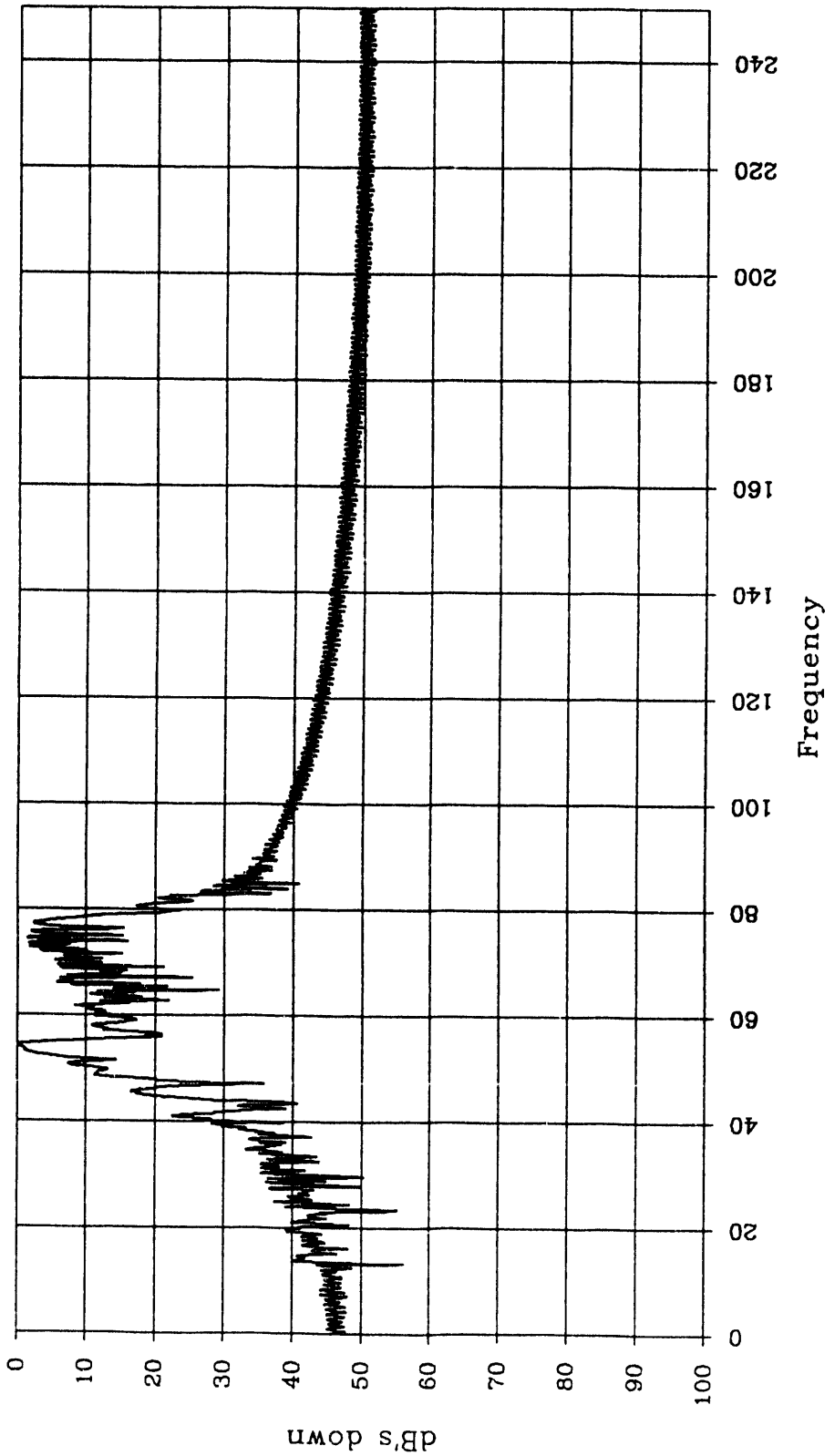

Figure 17a. Spectra for the vertical component of the NTS dual sweep experiment with a stack of 10 sweeps. While the most energy is from 50 to 80 Hz, there is a peak at ~15 Hz.

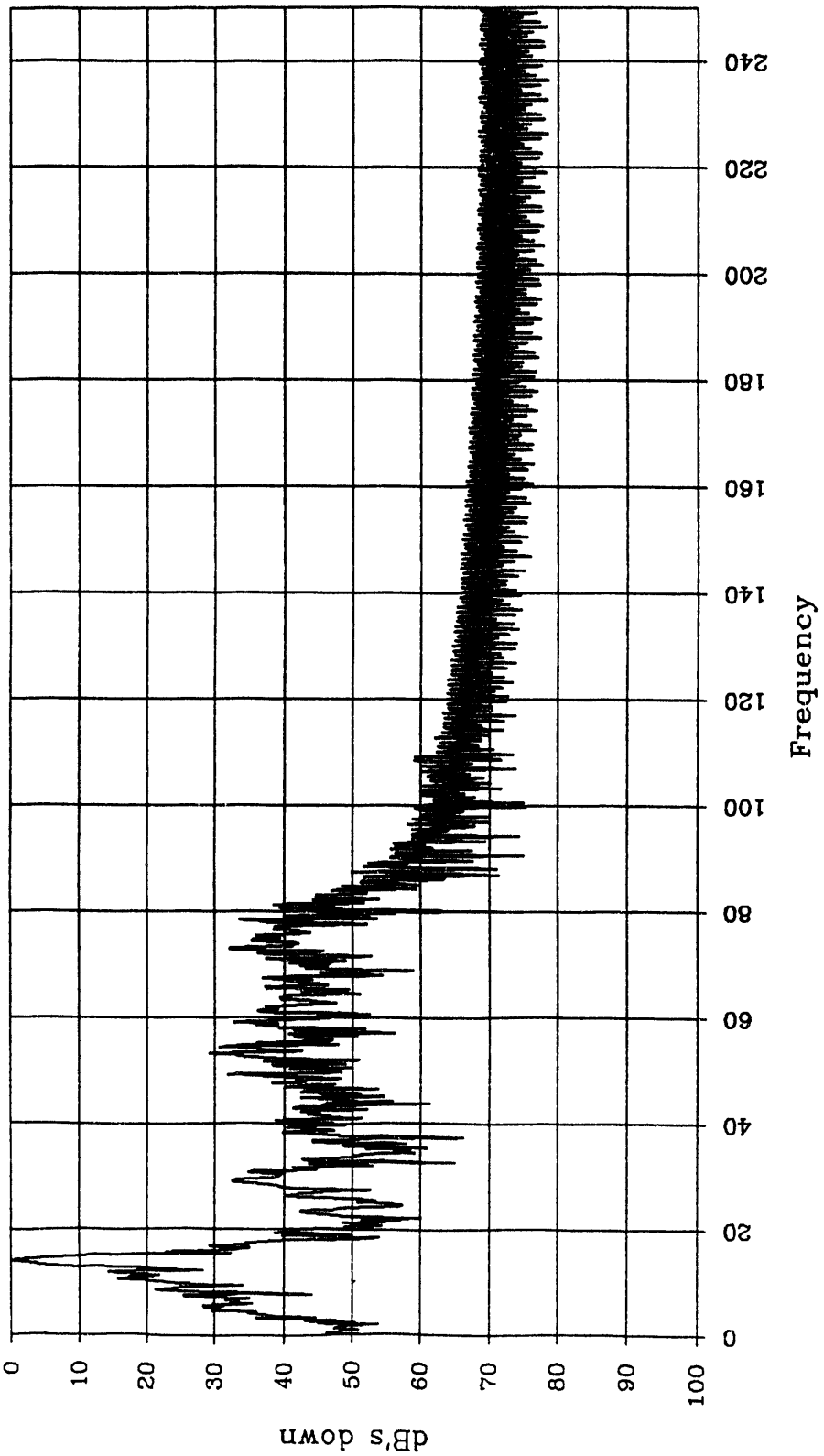

Figure 17b. Same data as 17a, but with a 3 to 15 Hz bandpass filter applied. We see a peak at about 14 Hz.

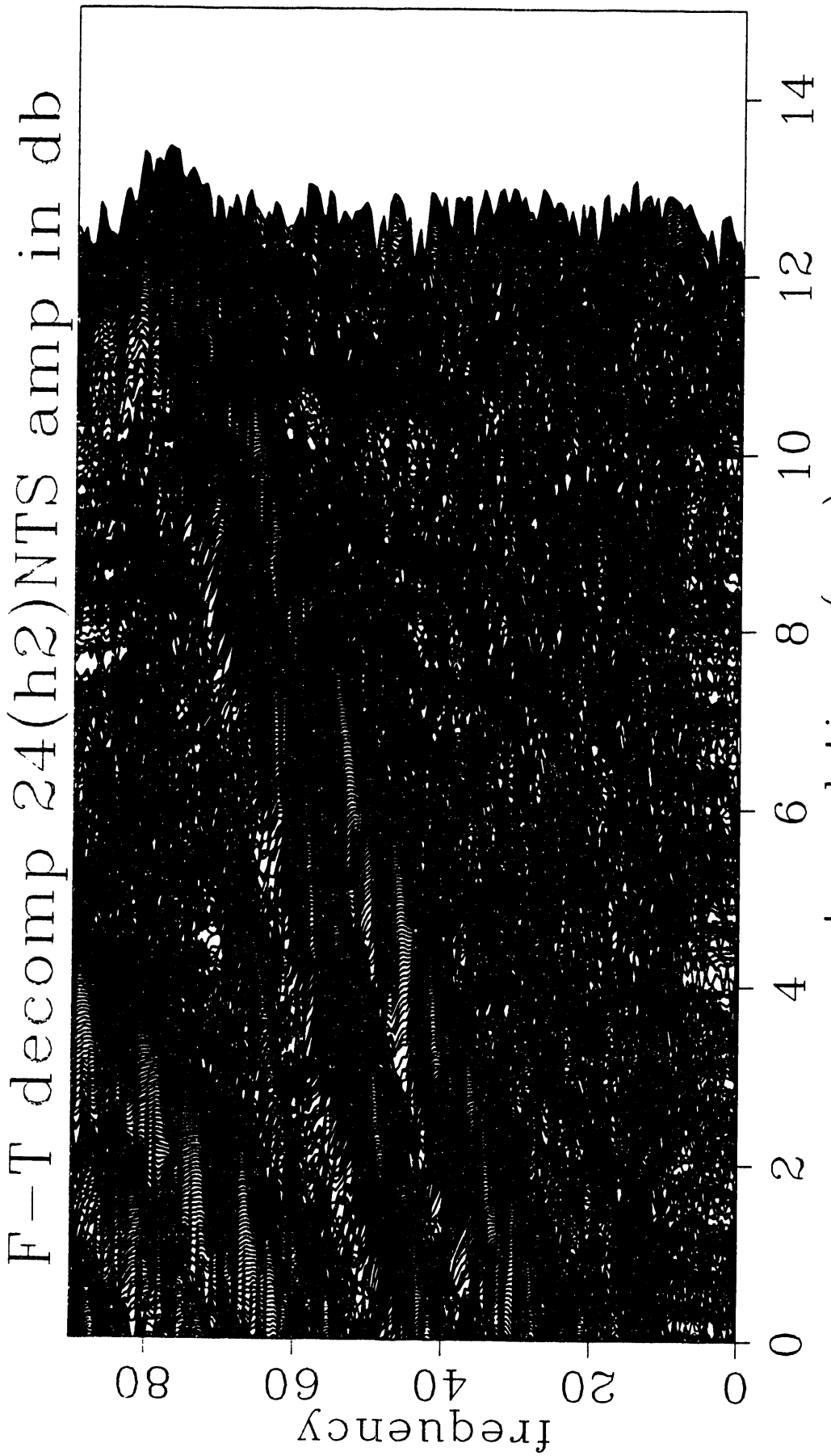

Figure 17c. Frequency vs time decomposition of horizontal component for the NTS dual upsweep data. Amplitude in db. The two upsweeps, 25 to 76 Hz and 40 to 79 Hz, can be seen.

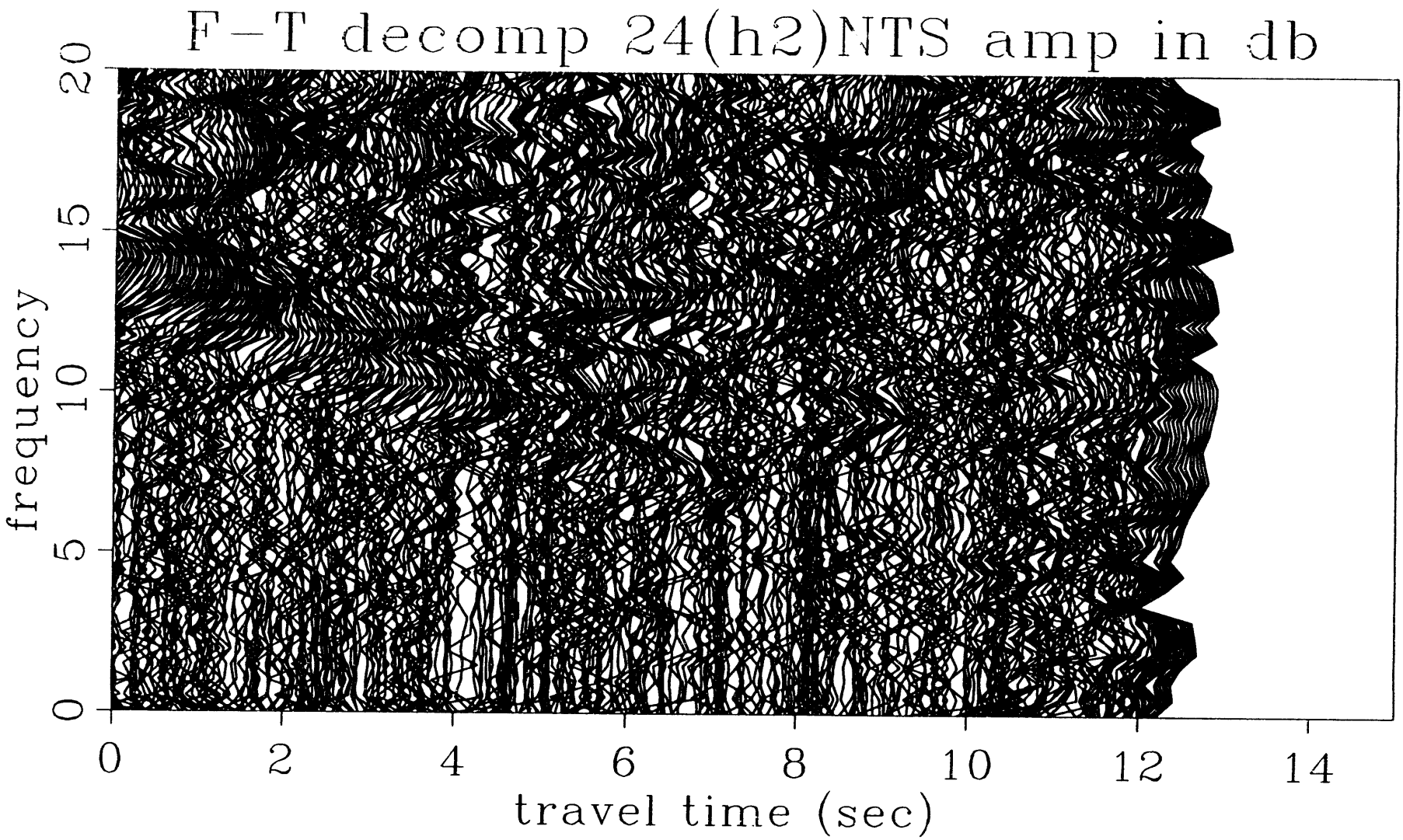

Figure 17d. Frequency vs time decomposition of the NTS dual upsweep data. The downsweeping energy (15 to 3 hz in 12 s) is seen strongest in the 15 to 8 Hz band. Amplitudes in db.

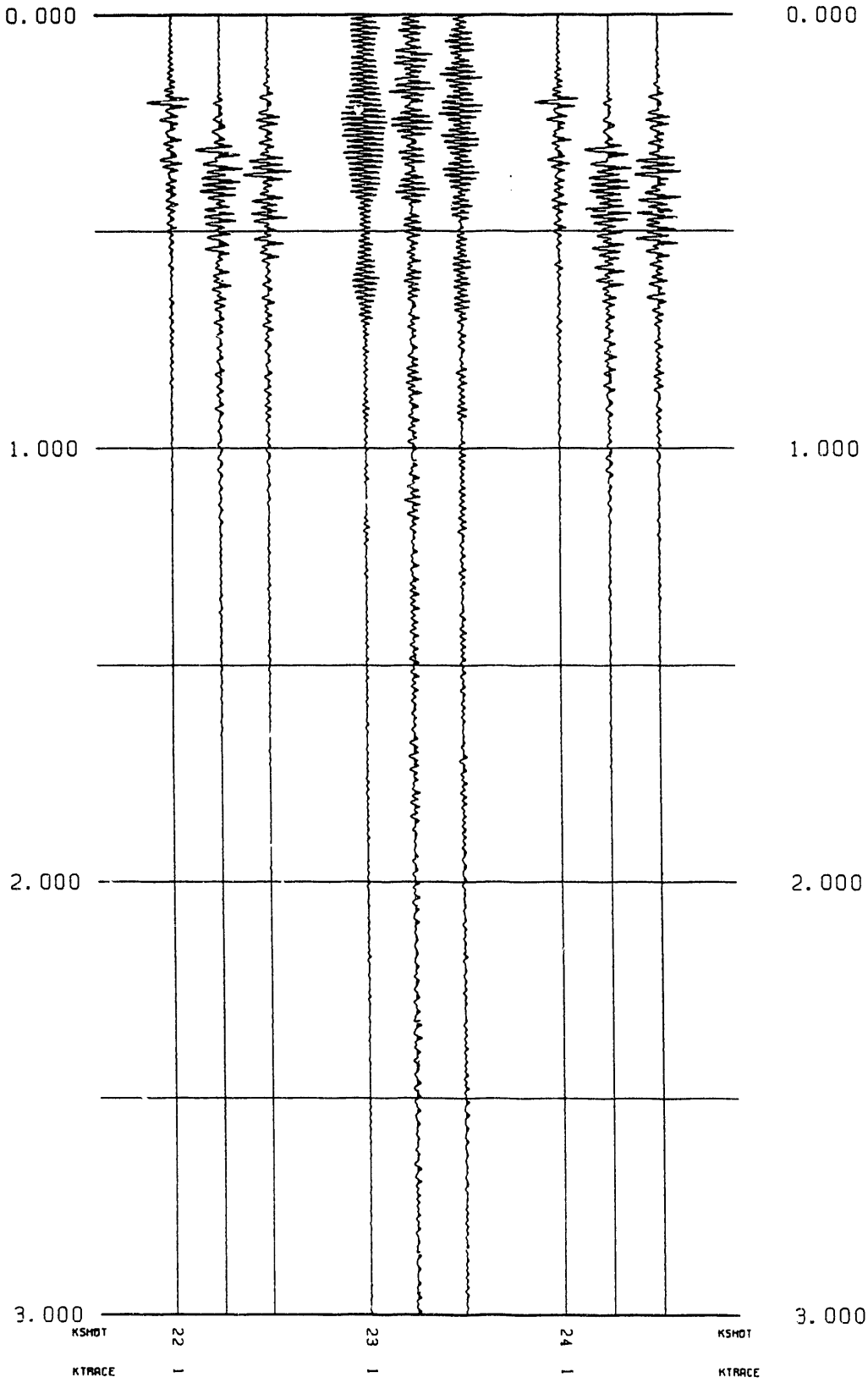

Figure 18a. Dual sweep NTS data correlated with a 25 to 75 Hz sweep. The three sets of three-component data had, left to right, a source with 25 to 75 Hz sweep, a source with 40 to 79 Hz sweep, and both sources simultaneously.

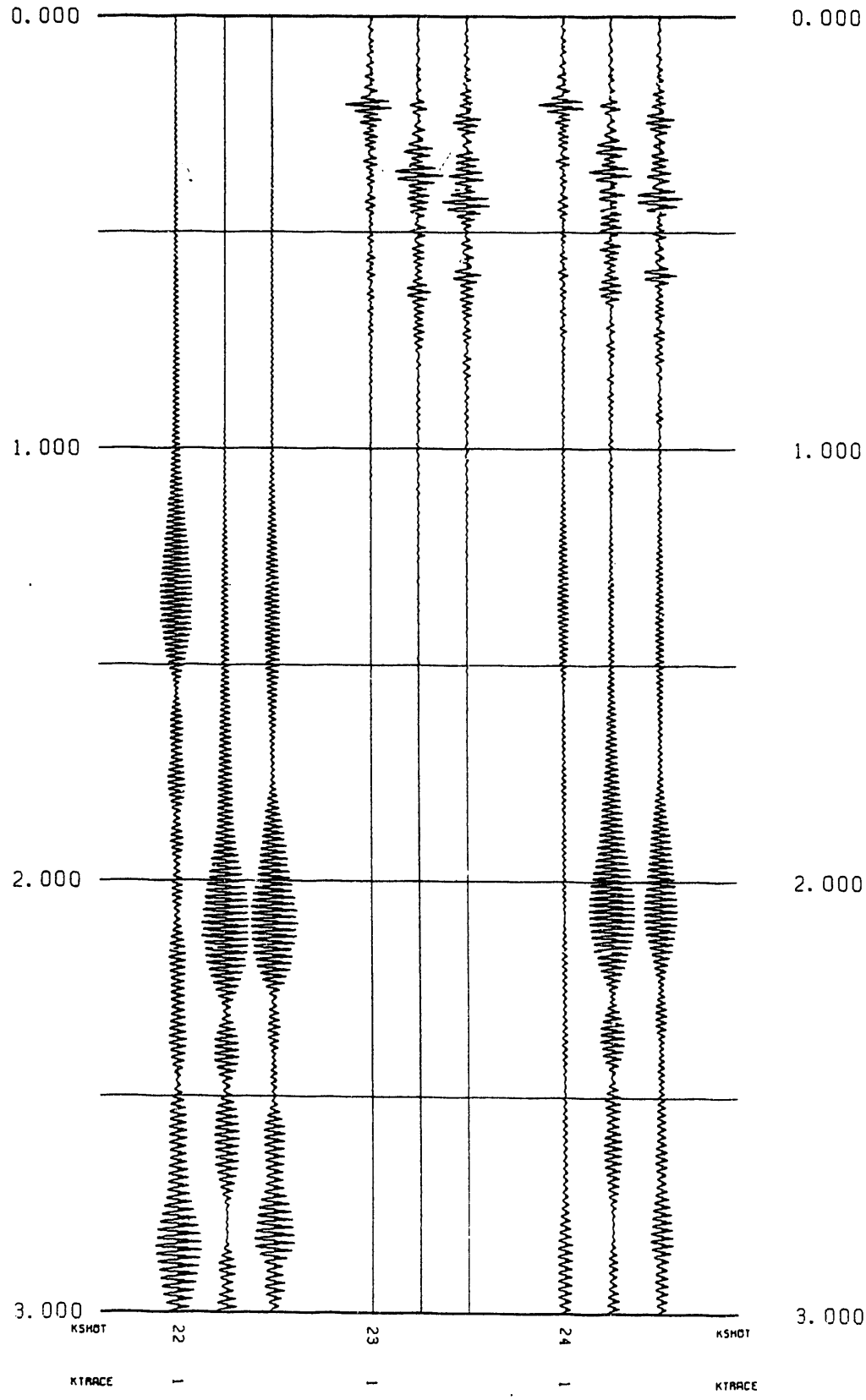

Figure 18b. Dual sweep NTS data correlated with a 40 to 79 Hz sweep. The three sets of three-component data had, left to right, a source with 25 to 75 Hz sweep, a source with 40 to 79 Hz sweep, and both sources simultaneously.

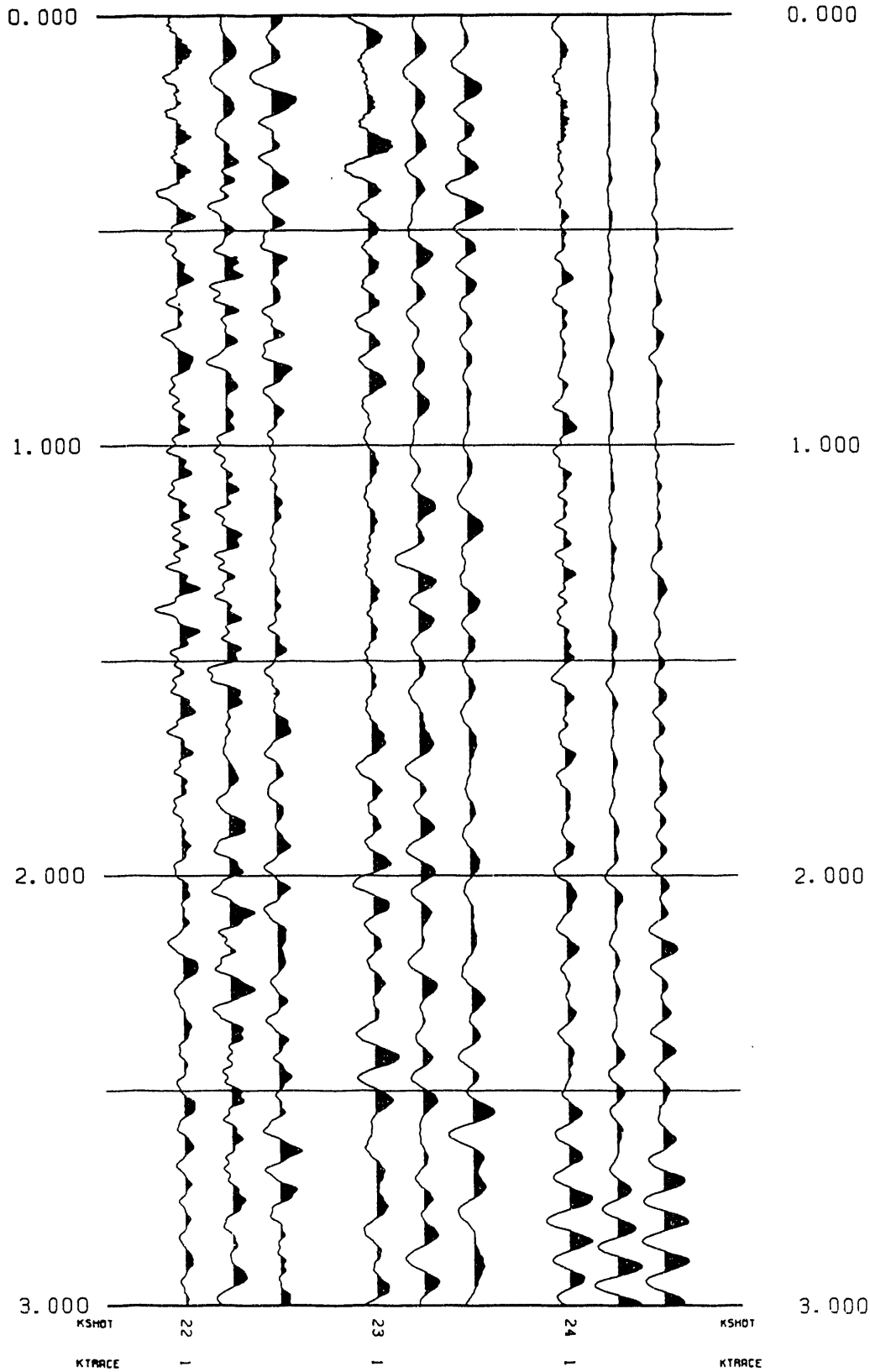

Figure 18c. Dual sweep NTS data correlated with a 15 to 3 Hz sweep. The three sets of three-component data are, left to right, 25 to 75 Hz, 40 to 79 Hz, and both simultaneously.

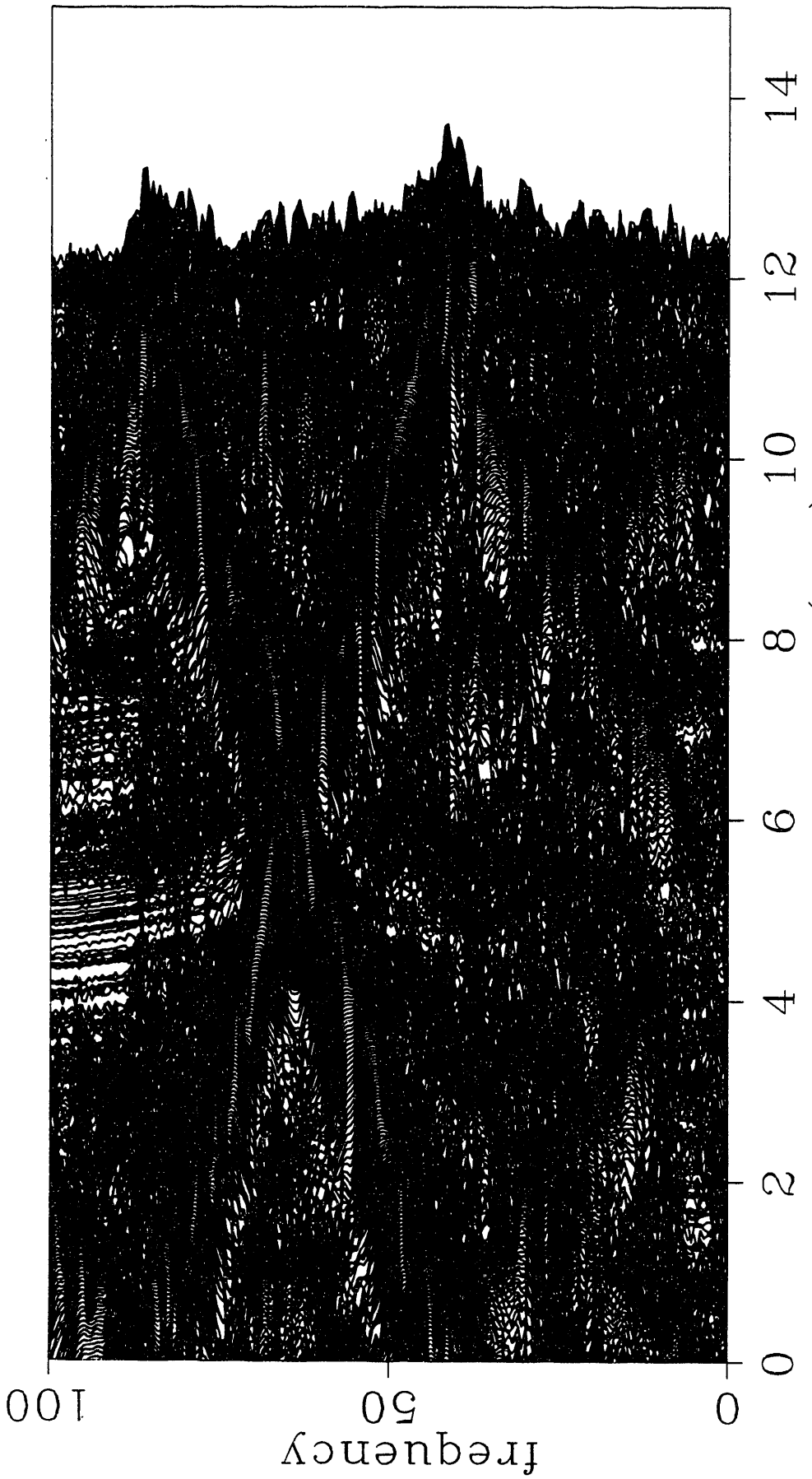

Figure 19a. Frequency vs time decomposition of a horizontal component for the NTS crossing sweep data 0 to 100 Hz. Amplitudes in db.

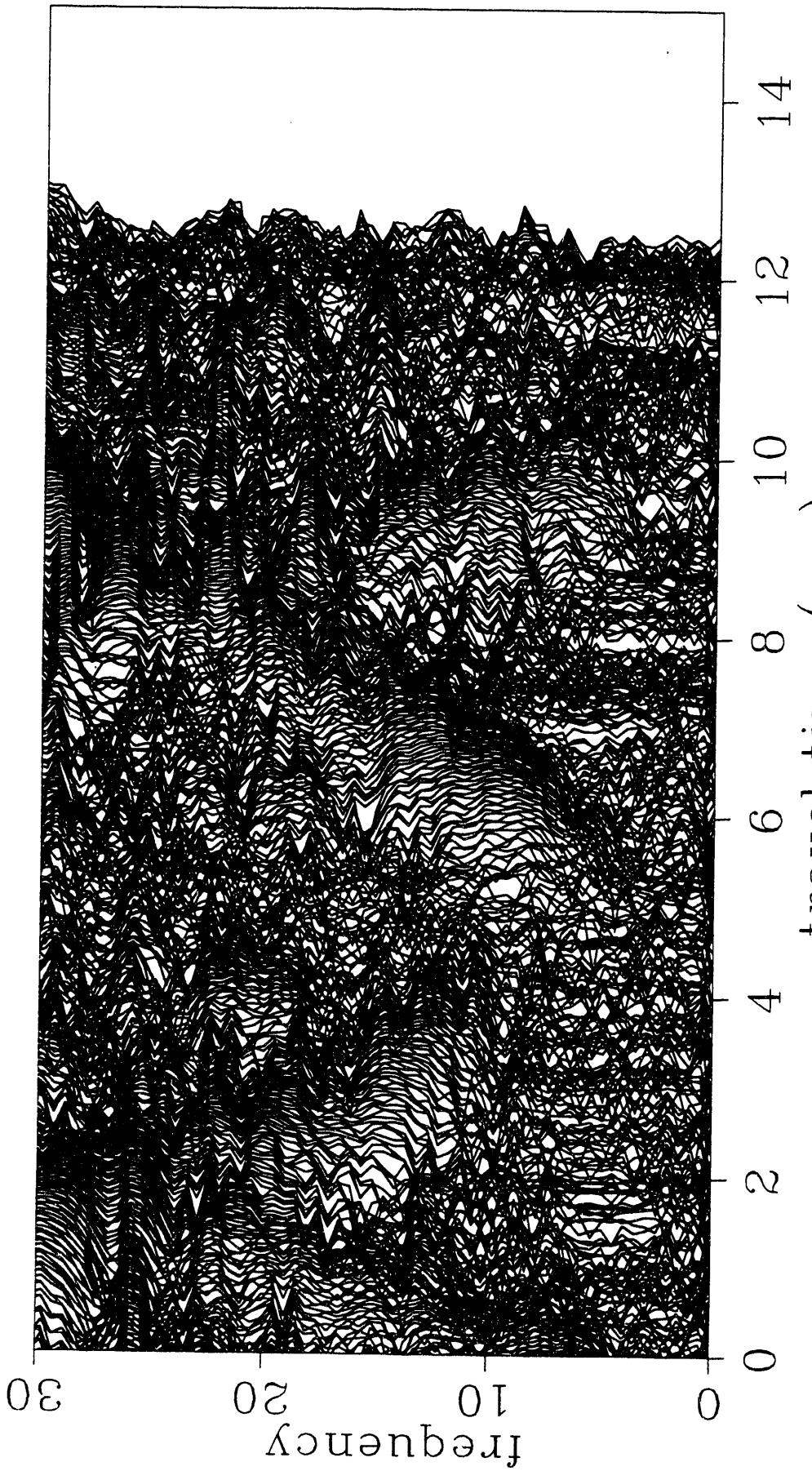

Figure 19b. Frequency vs time decomposition of the data in Figure 19a for 0 to 30 Hz. Amplitudes in db. The subharmonics below the crossing sweeps are evident in this bandwidth.

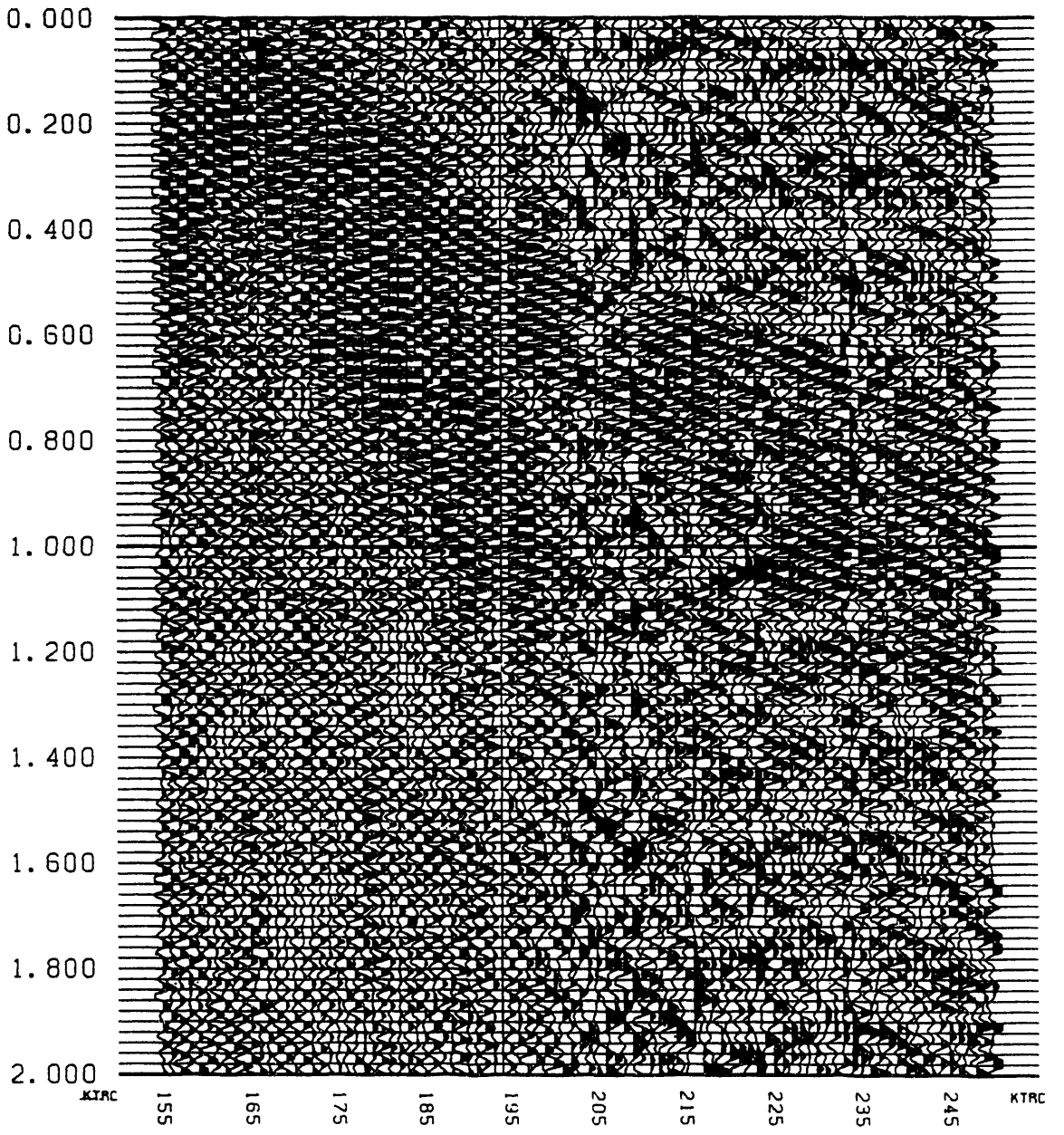

Figure 20. Crossing sweep LANL data correlated with the difference sweep, 40 to 0 to 40 Hz (actual sweep was -40 to 40 Hz). The first P-wave arrival can be clearly seen, and possible reflections are at later times.

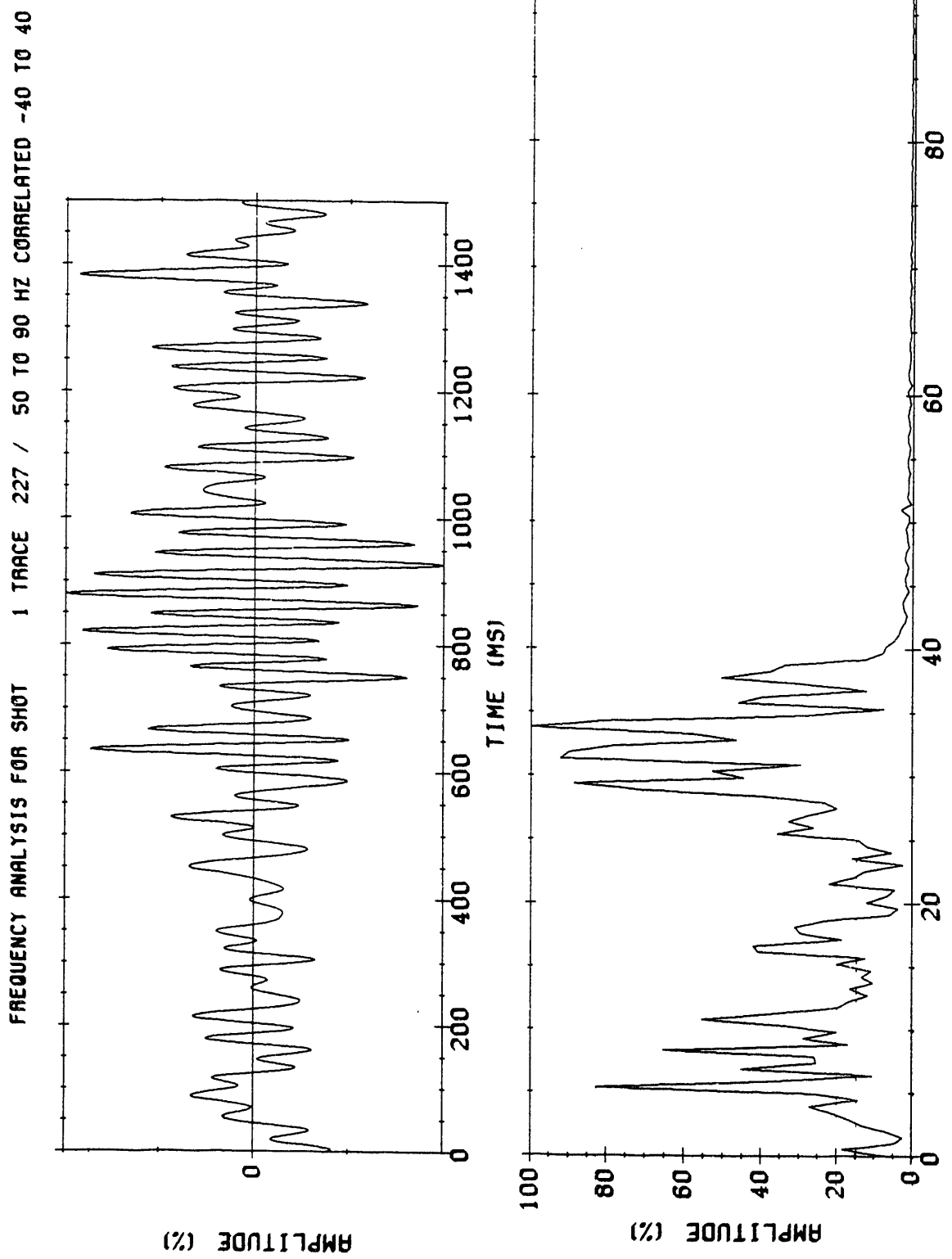

Figure 21. Time series (top) and spectra (bottom) for one trace from the data in Figure 20. The main energy is from 25 to 40 Hz, although there is measurable energy below 10 Hz.

END

DATE FILMED

8/26/93